

✓

FOR REFERENCE ONLY

21 APR 1999

40 0680268 8



ProQuest Number: 10183029

All rights reserved

INFORMATION TO ALL USERS

The quality of this reproduction is dependent upon the quality of the copy submitted.

In the unlikely event that the author did not send a complete manuscript and there are missing pages, these will be noted. Also, if material had to be removed, a note will indicate the deletion.



ProQuest 10183029

Published by ProQuest LLC (2017). Copyright of the Dissertation is held by the Author.

All rights reserved.

This work is protected against unauthorized copying under Title 17, United States Code
Microform Edition © ProQuest LLC.

ProQuest LLC.
789 East Eisenhower Parkway
P.O. Box 1346
Ann Arbor, MI 48106 – 1346

**An Experimental & Analytical Investigation of
Screen Printing Process Fundamentals**

M.C. Mitchell

A thesis submitted in partial fulfilment of the
requirements of The Nottingham Trent University
for the degree of Doctor of Philosophy
August 1998

Acknowledgements

I would like to thank everybody who contributed in some way whilst I undertook to complete this thesis. My friends and family have been supporting me for what must seem to them to be an eternity.

The staff of the Department of Mechanical & Manufacturing Engineering have been terrific, with no support task being too much of an effort. I would particularly like to thank J. Keeling, R. Potter, R. James and A. Maides.

For the academic guidance, support and friendship of Prof. Richard Gentle and Dr. Martin Howarth I am especially grateful, as without their supervision this thesis simply could never have been.

Many thanks to Tony Sackfield and Ray Tew for their patience and advice on experimental and mathematical techniques.

To Pressac I should like to express special thanks for allowing me the flexibility to attend the university during working hours and also for the financial assistance.

Last, but not least, I would like to thank my husband, Tim Randall. I would like him to know that in that enchanted place on top of the Forest, a little girl and her Bear will always be playing.

Abstract

The screen printing process has been around for centuries dating back to its use in ancient China for producing patterned silks. The same principle is used today to manufacture a diverse range of products from different areas of industry, including electronics, textiles, pharmaceuticals, packaging and graphics. Despite its age, the screen printing process is difficult to control because it is poorly understood at a fundamental level. Several attempts to model the process over the last 30 years have been reviewed here and it is concluded that, to date, none has successfully described the process and that further work is required to provide parameter relationships.

The complex nature of screen printing is confirmed in this thesis using factorial analysis to examine just a few of the many variables involved in the process. The findings are that factorial experimentation contributes minimal benefit when trying to establish process control.

As a consequence, the basic fundamentals of the process related only to filling of the screen mesh have been researched here. For the first time, the pressure required for flow through the mesh to occur has been experimentally established and this has shown that existing process models are lacking or wrong. In addition, the assumption that the screen printing process is governed by hydrodynamic lubrication theory is brought into debate, because the hydrodynamic pressure generated within the ink roll is recorded to be a factor of 25 smaller than the pressure required to ensure flow through the mesh.

This work has proposed that an adaptation of elastohydrodynamic lubrication (EHL) theory is a viable alternative on which to base a screen printing process model. Predictions of the minimum speed required to achieve the first acceptable print for a given set of parameters including mesh, squeegee and ink characteristics have been provided. This theory has been evaluated experimentally for two different squeegee types. The results show excellent agreement between theory and experiment for the softer squeegee tested, which industrially is the most common squeegee employed. The harder squeegee results follow the qualitative trend predicted by the theory but are a factor of 10 larger. It was concluded from these results that no single theory governs the screen printing process, but that a combination of theories must be sought.

This thesis provides a successful representation of the screen printing process and can be used as a basis for development of a generic model to control the screen printing process. It is, however, concerned predominantly with the filling of mesh apertures, and thus recommends that further work explore the effect of increased squeegee speeds and changes in mesh tension. In addition, deposit characterisation techniques should be reviewed and developed to allow improved assessment of the print quality.

<u>Contents</u>	<u>Page</u>
Glossary	vi
Nomenclature	vii
Chapter 1 Introduction	1
1.1 Problem statement	
1.2 Overview of the screen printing process	
1.3 Process variation	
1.4 Definition of a good print	
Chapter 2 Literature Review	8
2.1 Quantifying the screen printing process	
2.1.1 Process models & their limitations	
2.1.2 Theoretical limitations	
2.1.3 Empirical methods	
2.2 Summary	
Chapter 3 Process Control Using Factorial Experiments	48
3.1 Introduction	
3.2 Selection of factors for experimentation	
3.3 Choice of experiment design	
3.4 Determining screen print process behaviour using full factorial experiments	
3.5 Experimental results	
3.6 Fractional factorial experiments	
3.7 Application of an alternative method of utilising FFE's	
3.8 Conclusions	
Chapter 4 The Process Fundamentals	63
4.1 Introduction	
4.2 Examination of a rigidly clamped cantilevered trailing blade squeegee	
4.3 Elastic forces	
4.4 Elastic forces versus fluid forces	
4.5 Pressure generated within the ink roll	
4.5.1 Experimentation to measure pressure generated within the ink roll	
4.6 Establishing the pressure required to ensure flow through a mesh	
4.7 Conclusions	
Chapter 5 Analysing screen printing using elastohydrodynamic lubrication theory	80
5.1 Introduction	
5.2 EHL Theory	
5.3 Adaptation of EHL theory for use with wedge geometries	

5.4	EHL theory for materials of low elastic moduli	
5.4.1	Elastic equations for soft EHL	
5.4.2	Pressure inside the contact region using Reynolds' Equation	
5.5	Derivation of equation to predict minimum squeegee speeds	
5.6	Screen printing parameter relationships	
5.7	Discussion and conclusions	
Chapter 6	Experimental evaluation of EHL screen printing model	100
6.1	Introduction	
6.2	Exit film thickness height, h_e	
6.3	Inlet film thickness height, h_i	
6.4	Determining the half contact width of the squeegee tip	
6.5	Predicting the minimum squeegee speed	
6.6	Experiment to determine minimum printing speeds	
6.7	Results and discussion	
Chapter 7	Discussion and conclusions	113
References		118
Appendices		123

Glossary

- Bleed out** seepage of ink around stencil resulting in a double thick edge being printed
- Bow wave** the ink roll in front of the squeegee
- Confounding** the inability to separate sources of variation in a particular experiment
- Darcy's Law** the law determining porosity of a medium expressed as a ratio
- Degrees of freedom** the number of fair comparisons that can be made from a data set
- Dot gain** increase in diameter of each individual dot of ink, where the dot size is defined by the mesh apertures
- Effective attack angle** the angle to which the squeegee deforms after it has been set at a specific angle, load and is travelling at a required speed
- Fabric roughness** the root mean square of the mesh surface asperities defined by the weave of the mesh
- Factor levels** the settings of a particular variable in a factorial experiment
- Fractional factorial experiment** a statistically designed experiment to evaluate several factors more efficiently than testing single factors one at a time
- Hertzian contact** the assumption that the pressure distribution in a contact region is the same whether or not a liquid film is present
- Hydroplaning** lifting of the squeegee, whilst in motion, due to the pressures generated within the fluid
- Mesh open area** the area of mesh apertures expressed as a percentage
- Mesh tension** the load applied to a mesh in both warp and weft directions, as it is stretched onto a frame
- Off-contact** screen is separated by the snap height from the substrate
- Orthogonal array** a matrix designed to ensure that a fair comparison may be made between factor levels, or their interactions, in independent columns
- Peel-off** action of screen lifting behind squeegee
- Pooling** combining the sum of squares and degrees of freedom of statistically insignificant factors
- Scavenging** resultant feature of deposit where the ink is effectively scooped out because the squeegee tip protruded through the stencil
- Scooping** a deformation in the print height caused by the squeegee tip protruding through the stencil aperture, and lifting a portion of ink from the deposit
- Screen** a mesh stretched across a frame
- Sharp squeegee** where the squeegee tip is ground to a point as opposed to a flat, or a squeegee with newly ground 90° corners
- Skipping** incomplete image is achieved when printing
- Slumping** a deposit which spreads out after printing due to incorrect print characteristics
- Smearing** seepage of ink to the underside of the stencil which is then subsequently printed
- Snap height** vertical distance between stencil and substrate
- Snap off** the action of the mesh returning under tension from the substrate surface
- Squeegee** a rubber blade used to apply vertical and translational forces
- Stencil** a film or emulsion applied to a mesh to provide a print pattern
- Thixotropy** the property of a fluid which shows a temporary reduction in viscosity with changes in shear rate

Nomenclature

%A	Percent open area
A	Area
A	Porosity of screen (Chapter 2 only)
A_{sw}	Distance between supporting aperture walls
a, b	Half width of line contact
A_o	Mesh open area
\hat{a}_z	Unit vector normal to the screen
B	Length of printed pattern
bV	Contribution to pressure on the squeegee from paste above the stencil
CFD	Computational fluid dynamics
d	Fibre diameter
D	Flexural rigidity of the squeegee
d_w	Wire diameter of mesh
E	Young's modulus
EHL	Elastohydrodynamic lubrication theory
F	Force
$f(Q)$	Factor increasing with ink quantity Q in front of squeegee roll
FFE	Fractional factorial experiment
F_M	Force pulling on each wire during screen separation
f_{mo}	Force acting on one mesh aperture
F_R	Fabric roughness
F_t	Fabric thickness
H	Printing mesh thickness
\bar{h}	Height at which $dp/dx = 0$
h_0	Minimum film thickness
H_0	Non-dimensional form of h_0
$H_{DP,S}$	Height of dry paste at start
H_E	Edge height
h_E	Thickness of emulsion build up
h_e, h_2	Exit height
H_F	Height at front
h_i, h_1	Inlet height
H_{PR}	Height of the paste residue left on the screen
h_s	Thickness of printing screen
H_{SC}	Equivalent flow passage height under the squeegee
$H_{SC,DP}$	Equivalent flow passage height under squeegee, dry paste
H_{st}	Stencil thickness
H_{WP}	Height of deposited wet paste
I_h	Estimated Ink Height
I_r	Ink wet to dry ratio
k	Constant
\underline{k}	Permeability tensor
k_x	Darcy's constant
ℓ	Distance along x-axis
L	Distance to the point where ink roll overcomes mesh wetting resistance
L'	Length of ink roll
L_{II}	Total load on squeegee
L_{sr}	Length of screen from frame to squeegee
m	Gradient
M	Mesh count per unit length

M_0	Mesh Opening
M_C	Mesh Count
m_e	Effective attack angle
n_K	Number of meshes
OA	Open area
P	Pressure
PLC	Programmable logic controller
pV	Pressure per unit width of paste below the squeegee
P_w	Pressure required to overcome the wetting resistance
Q	Volume flow rate
Q_0	Flow induced within the plane of the screen
Q_e	Volume flow rate at the exit
Q_i	Volume flow rate at the inlet
Q_{SCR}	Volume flow rate through screen
Q_{SQ}	Volume flow rate under squeegee tip
r	Distance from contact point between squeegee and screen
R	Radius
Re	Reynolds' number
RMS	Root mean square
r_Q	Extent of ink roll along surface of squeegee and screen
Rq	Roughness parameter
s	Integration variable for a fixed point of x
S	Screen size
S_{1F}	Twice the amplitude of the paste wavy surface at front
t	Non-dimensional form of s
$T(s\text{-dry})$	Stencil dried thickness
T_e	Emulsion thickness
T_m	Mesh weave thickness
U	Squeegee speed
$\underline{u}(x,y,z)$	Mean filter velocity of fluid
$V(x)$	Normal surface displacement outside of contact region
V_a	Screen snap off velocity
V_p	Average paste velocity
V_{scr}	Velocity through the screen
V_{SQ}	Squeegee translational speed
W	Load per unit length applied to the squeegee
x^*	Non-dimensional form of x
X_{CF}	Distance of circulatory flow
X_{US}	Distance of region under screen
y_0	Vertical height of the squeegee at the point where it is clamped
y_ℓ	Deflection at the squeegee tip
ϵ	Parameter accounting for the mesh hardness
α	Pressure viscosity coefficient
α_x	Slip coefficient
β	$(1-d/\ell)^2$
β_{SQ}	Function of the squeegee material (Young's modulus and Poisson's ratio)
χ	h_1/h_0
δ	Wet deposit thickness
Δ_{Edge}	Width of paste edge
Λ	Depth of squeegee deformation

ΔP	Pressure drop
$\Delta_{s,s}$	Twice the amplitude of the paste wavy surface at start
Δt	Time interval
Δ_{XSQ}	Width of flat portion of deformed squeegee
ε	Compressibility
ϕ	Angle of wedge
Φ, α	Squeegee angle
η, μ	Fluid viscosity
λ	Variable along the x-axis
ν	Poisson's ratio
θ_R	Angle from vertical at which the squeegee first rests on the screen
θ_W	Angle from vertical at which the squeegee contacts the screen under working load
ρ	Fluid density
σ_s	Screen tension
τ	Shear stresses between paste and mesh surface

SI units used unless otherwise stated

Chapter 1 Introduction

1.1 Problem Statement

If a manufacturing process is to be successfully employed it must be fully controllable. In the case of screen printing, where over 50 parameters [1] are involved it is hardly surprising that comprehensive control solutions are non-existent [2],[3]. The ideal situation for the manufacturer would be to be able to set all the process variables to give a known output, and to know exactly what drift can be expected. Prior to achieving this, substantial information about how the process works is required. Despite a recent increase in screen printing research, there are still very wide gaps in the process knowledge which prevent full control of the screen printing process. The aim of this work is to examine ways of improving the screen print process control from the viewpoint of the manufacturing engineer i.e. defining the inputs to the process which are required to give the desired process response. The objectives are to:

- determine parameter relationships using experimental techniques
- examine existing screen printing process models
- propose a theoretical model which governs the process
- experimentally evaluate the proposed model

This chapter explains how the process works and outlines the difficulties associated with the process components. In particular it shows that the output of the process is difficult to measure and the variation between samples at the same setting is large.

1.2 Overview of the screen printing process

Screen printing is essentially a straightforward technique, which has long been categorised as being something of a black art (Riemer [2], Atkinson [3] & Markstein [4]). The basic components of the process are depicted in Figure 1.1 overleaf.

A load is applied to the squeegee which in turn brings the mesh into contact with the substrate, overcoming a set gap, i.e. the snap height. The squeegee travels across the mesh at a speed and angle which provide a suitable shear rate and “hydrodynamic” pressure to allow the ink to fill the mesh apertures. The mesh, typically tensioned to 200N per linear metre, on a metal frame, peels back to its original snap height behind the squeegee and the ink is deposited onto the substrate underneath the mesh. The purpose of the mesh is to provide a permeable medium to carry a stencil, and the desired pattern to be printed is photo-exposed onto the stencil. The secondary function of the mesh is to provide a flexible membrane which gently peels off under

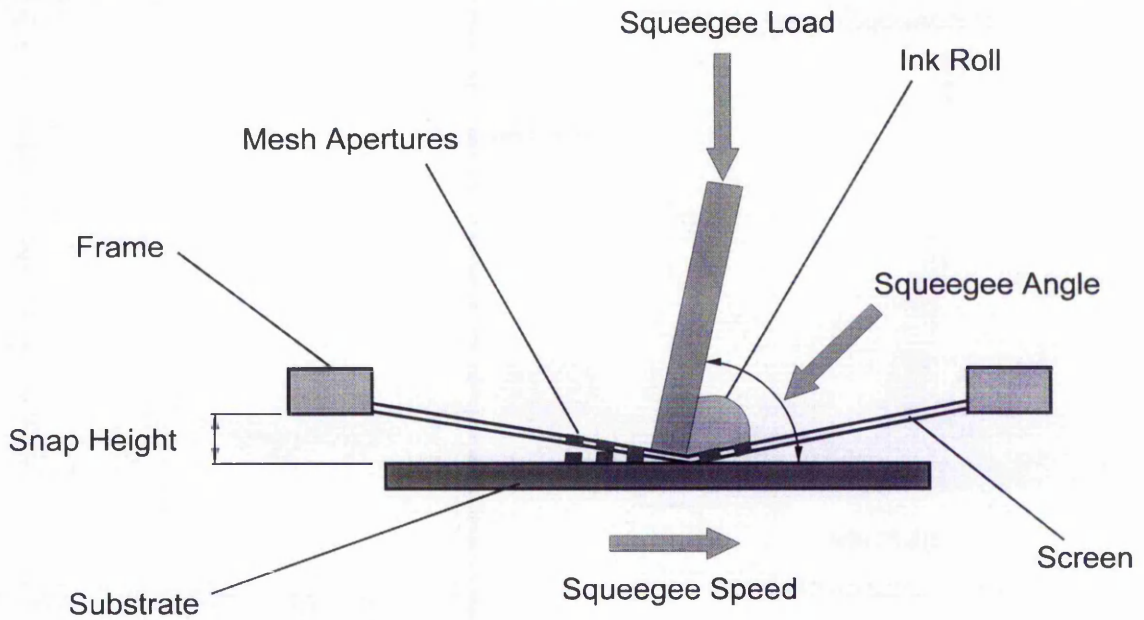


Figure 1.1 The basic components of the screen print process

tension to prevent image distortion. The mesh, stencil and frame are collectively labelled the screen. The resulting print deposit is influenced by many factors: Hughes and Lendle (see Cropper [5]) listed 47 variables and Kobs & Voigt [1] listed over 50 variables, but the main groups were summarised by Molamphy [6] as shown in Figure 1.2.

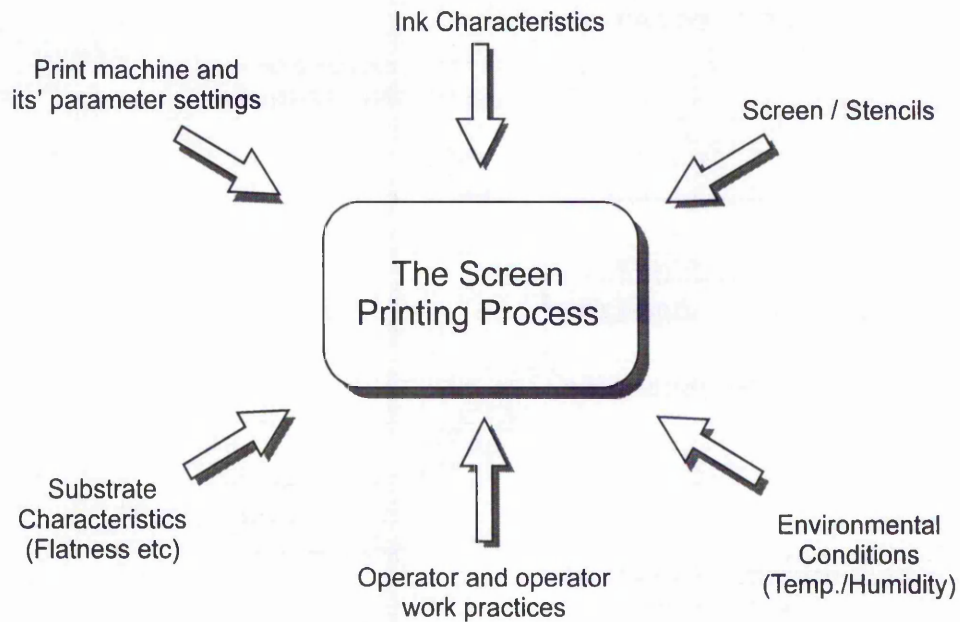


Figure 1.2 Screen printing variables

At the moment there is no theoretical or practical model on which to base the process set-up and many of the variables are interdependent, as reported by many workers, for example, Kobs & Voigt [1], Nickel [7], Anderson et al [8]. It is therefore difficult to set up and control the process in a manufacturing environment. The problem is exacerbated by the fact that there is a wide range of squeegee materials and geometries (see Appendix 1.1), a large selection of mesh types (see Appendix 1.2), inks, and substrates which can be as diverse as glass to corrugated cardboard. Studies [9] have shown that meshes of one manufacturer with exactly the same designation as those of another manufacturer may be physically and dimensionally very different and therefore print differently; this epitomises the lack of industrial standards. In addition to this, screen printing machines offer very different levels of parameter control [10]. To discuss the behaviour of the process in manageable terms it is possible to eliminate most of the parameters. For example the choice of the substrate and the nature of the end application are specified by the customer. These dictate the ink selection, which in turn limits the screen choice. The squeegee is then selected using the printer's or supplier's knowledge. It is outside the scope of this work to discuss these issues further. By eliminating the environmental conditions and selecting one type of machine, the variables are again reduced. The process can then be described, for a specific application, using just the main machine adjustable parameters which are squeegee speed, squeegee angle, squeegee load and snap height.

The squeegee load must be sufficient to overcome the tension in the mesh and bring the stencil into contact with the substrate. Insufficient load will result in poor prints as the ink will not be able to transfer to the substrate. Excessive load can result in scavenging or smearing due to the squeegee edge being forced through the stencil aperture and removing the top surface of the ink. Young [11] discusses print quality defects at length and Phippard [12] lists more than fifty possible conditions which could lead to print quality defects, along with their likely causes and possible corrective actions.

The squeegee speed is significant for two reasons. The first is that it determines the shear rate of the ink, which affects the flow characteristics, and secondly, it influences the print cycle time. The ink must be sufficiently thin to flow through the mesh but should regain its full viscosity on removal of the shear force to allow the ink to form a substantial deposit. It should also be thick enough to stay on the mesh surface without seeping through, as this leads to bleed out (i.e. seepage of ink around the stencil edge resulting in a double thick edge being printed) and smearing (i.e. seepage of ink under the stencil which is subsequently smeared across the underside of the stencil). Too slow a speed will prevent the mesh from lifting behind the squeegee at a rate to ensure good edge definition. Faster speeds may cause insufficient filling of the apertures and,

or, prevent the transfer of the ink to the substrate. This will cause an incomplete print, which is known as skipping. The speed must, therefore, be fast enough to thin the ink, but slow enough to allow the ink time to fill the aperture and transfer to the substrate. The ink's rheology must ensure that the time taken to regain original viscosity after shear thinning is not excessive as this may lead to poor print definition as the ink cannot support its own mass and effectively spreads out or slumps.

The angle of the squeegee determines the amount of contact area between the ink roll and the blade. This is generally taken to contribute greatly to the ink flow characteristics as it determines the shear rate and also the squeegee deformation which alters the resultant normal and tangential forces which are applied to the ink roll. The shear rate is effectively the squeegee speed divided by the height of the ink roll and is thus a variable. Figure 1.3 below shows how the squeegee angle will affect this. Too vertical a squeegee will fill the mesh very inefficiently, whilst too shallow an angle will not allow the correct shearing action to occur. A simple analogy is that of spreading butter on bread, if the knife is held almost at right angles to the bread the butter is scraped very thinly, but a shallow angle will allow good coverage of the bread. Squeegee deformation causes significant changes in the resulting angle of the squeegee blade to the substrate, i.e. the "effective attack angle" [7], and an allowance should be made for this. It is recommended that flat blades are set at an angle of between 45-75° [13].

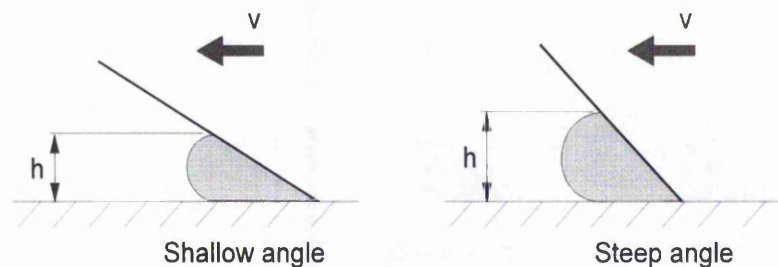


Figure 1.3 The shear rate is affected by the squeegee angle

A gap between the screen and the substrate is essential when using a mesh to provide the peeling action required in the ink transfer process. It is known as the snap height. The peeling action is required to ensure that the stencil is removed prior to the ink regaining its full viscosity. The snap height can cause x-y alignment problems. It also changes the angle of the peel off. An optimum snap height must be achieved whereby the peel-off is sufficient to transfer the ink and the misalignment is small enough to be regarded as negligible. As a rule of thumb, it is recommended that the snap height should not exceed ten times the stencil thickness [13]. Recent developments [14] have steered the industry toward the use of high tension meshes e.g. 350N/m as opposed to 200N/m, but it appears to have little if any influence on the final deposit characteristics. However,

higher tensions do allow a smaller snap height to be used because the tension in the mesh compensates for the reduced peel off.

Incorrect parameter settings will create poor printing conditions, but clear guidelines as to the correct set-up of the process do not exist because generally different printers use an entirely different combination of mesh, ink, stencil and squeegee. In addition to this, machines do not have any standard calibrations on their adjustment facilities. These variables, however, cannot be dealt with in isolation. Some of the possible interactions and their causes will be discussed here, but it is not possible to quantify the extent of the possible interactions without doing some more analysis.

The load required will increase with larger snap heights because there will be a need to overcome more resistance in the mesh. The squeegee load and speed are related because the pressure required to fill the apertures requires a sufficient amount of time to act. Also the resulting deformation under load changes the shear rate. The effective attack angle is by definition a function of the load as well as the elastic properties of the squeegee.

The squeegee speed and the angle might show an interaction where the resistance of the mesh must also be taken into consideration. An example of this is where the friction resistance between the mesh and the squeegee is greater than that of the force moving the squeegee. For an instant the deformation will become greater and the angle will therefore change. The speed and the snap height may also show an interaction simply because where the height is increased there will be more mesh resistance.

The angle and the snap height could possibly interact again due to the resistance forces caused by the steep angle of the mesh. The complexity of the process is quite often masked by the fact that the screen print process is in essence very simple; you take a screen, some ink, a rubber blade and you print. However, to provide quality and repeatability in a high volume manufacturing facility is a completely different matter.

1.3 Process variation

The first problem thus far outlined is that the exact method of setting up the process is not clear due to a lack of information on the effects of the large number of parameters involved. The second problem is that once the machine is set-up, several prints are required before an acceptable deposit is achieved. It is often then the case that subsequent prints will be unacceptable because of poor repeatability. This problem shows itself as a process variation

which is totally unacceptable. A study of this is outlined in Appendix 1.3 whereby 10 consecutive prints at the same settings were printed, with the process repeated at one week intervals and the maximum deposit height variation was found to be 35.65%. The reasons for this are probably:

- 1) the squeegee is a rubber material exhibiting hysteresis and creep, which means its' deformation properties would be different each time
- 2) screen print inks are thixotropic, i.e. show a temporary reduction in viscosity with changes in shear rate, and non-Newtonian. These properties in turn are sensitive to changes in ambient conditions.
- 3) different operators performed the tests, therefore small variations in set up may have occurred.

1.4 Definition of a good print

It is necessary to define a good print for this work, as an acceptable print varies from user to user. In the graphics and textile sectors a good print is determined by excellent reproduction of half-tones and critical parameters are colour and dot gain i.e. the thickness gain of each individual dot. In the electronics sector resistivity is critical which requires the correct volume of deposit. In all sectors the registration of the deposition on the substrate is critical. So at a more fundamental level it can be said that the printed deposit is good if it has good edge definition, uniform height and volume and is the right shape i.e. it has not slumped or had any ink scooped out of it by the squeegee. Figure 1.4 shows typical deposits which are achieved.

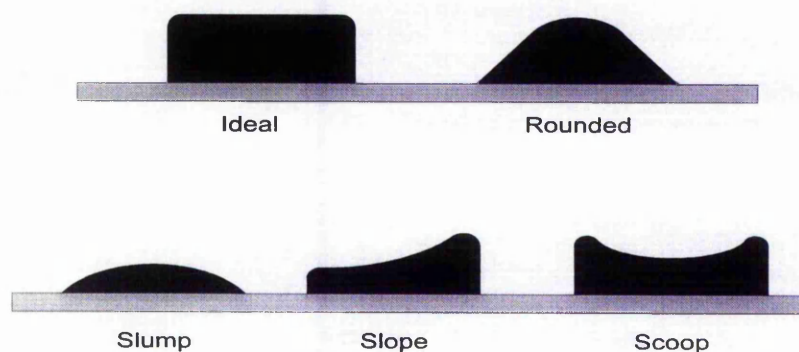


Figure 1.4 Typical deposit profiles

1.5 Summary

Screen printing originated as an art and, despite developments to provide automation for high volume low cost manufacture of a wide range of products, the process remains an art because it is poorly understood. The lack of standardisation of printing equipment, i.e. machines,

squeegees, screens and inks, as well as inadequate machine parameter adjustment, has only served to ensure that screen printing remains difficult to control.

It is clear that a large number of variables are involved but many are application specific and therefore the key parameters relating to process control are the squeegee variables of speed, angle and load and the screen snap height. These variables are thought to be interdependent and information regarding how these parameters should be set and subsequently adjusted in absolute and generic terms to produce an optimum print is not available.

There is no standard definition of an acceptable printed deposit and the process is known to have very poor repeatability. This work therefore aims to provide a generic and technical basis from which screen printing can be controlled in a manufacturing environment.

Chapter 2 Literature Review

2.1 Quantifying the screen printing process

This chapter provides the background to the existing research in screen printing, including process models, industrial guidelines and the application of experimentation. All of the work reviewed highlights the fact that the mechanism which governs the screen printing process is poorly understood. Danner [15] offers one explanation, describing the ink transfer as a vacuum process: "the vacuum develops when the fluid of the ink contacts the substrate and pulls the ink through the fabric during snap-off. The emulsion acts as a gasket permitting the ink to flow to its edge forming the definition of the pattern". Many authors do not even attempt to explain it but simply offer guidelines based on experience, for example: Phippard [12], Buttars [13], Hobby [16]-[19], and Ismail [20]. Others have used semi-analytical methods, e.g. Molamphy [6], Brown [21], or concentrated on very specific aspects of the process, for example, only the rheological aspects [7],[22]. Nevertheless, several efforts to model the process have been made by Riemer [2], Huner [23]-[29], Rangchi, Huner & Ajmera [30], Mannan [31], and Owczarek & Howland, [32] & [33] but to date none has offered satisfactory explanations or been completed to the point where it could be readily applied to the process.

Some of the earliest studies of screen printing involved investigating the pressure generated in the fluid. However, this was always carried out for a Newtonian fluid. Effects of attack angle, printing speed and squeegee load on the fluid bow wave constituted the basis for Cropper's [5] work, which resulted in an equation to predict the pressure profile in a bow wave. Cropper confirmed that the screen printing process is governed by Reynolds' lubrication equation. He also stated that the experimental work indicated a negative pressure being generated behind the squeegee blade as well as a deformed squeegee tip under dynamic conditions.

Cropper actually evaluated two theories for the screen mesh, firstly treating the screen as a porous medium obeying Darcy's law and then, as an alternative, regarding it as an assembly of woven strands which required drag theories to be considered. Additionally, the forces necessary to overcome mesh resistance were obtained empirically which laid the foundation for studying the possibilities of reducing hydrodynamic pressure to match screen resistance, thus reducing image distortion, which is one of the most difficult screen printing faults to overcome.

Cropper carried out an extensive literature survey which included references to the following researchers. Finch (1968, see Cropper [5]) described the mesh as a metering device and

evaluated a correction factor for the ink volume in the mesh. Salisbury (1970, see Cropper [5]) studied snap-height, screen substrate force, squeegee angle, squeegee speed and ink viscosity using percentage resistance change as the response variable. A range of ink viscosities was examined from 100 to 300 N s/m², establishing that there is a linear relationship between the percentage resistance change and the attack angle i.e. the deposit variation was linear with respect to changes in the angle of attack. The importance of the squeegee profile was emphasised by comparing the significant differences in deposits printed by a sharp* squeegee to that of a squeegee with a 0.025 mm flat portion at the tip. This work highlights the importance of the squeegee profile. Russell (1968, see Cropper [5]) examined filling of mesh apertures under static conditions, deriving an equation for the height of the ink in the mesh. Tak and Glastra (1970 see Cropper [5]) used Reynolds' theory to predict the influence of several screen printing variables on the pressure profile in the bow wave. It was assumed that the squeegee followed hydrodynamic lubrication theory and by integrating Reynolds' equation for flow between two stationary rollers an equation for the pressure was obtained, where h_1 and h_2 are as shown in Figure 2.1.

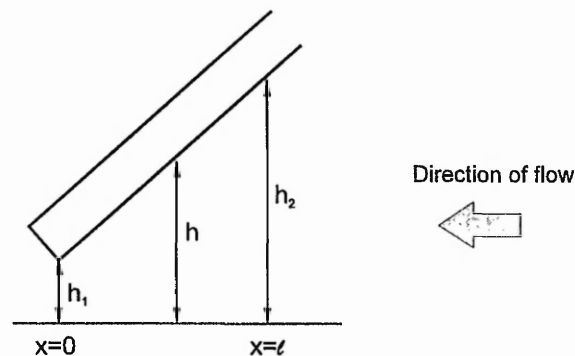


Figure 2.1 Definition of h_1 and h_2

$$P(h) = -\frac{6\mu U}{m} \left[-\frac{1}{h} + \frac{h_0}{2h^2} + c \right]$$

where

$$h_0 = \frac{2h_1h_2}{h_1 + h_2}, \quad c = \frac{1}{h_1 + h_2} \text{ and } m \text{ is the gradient of the slope from } h_1 \text{ to } h_2$$

* A sharp squeegee is defined as having the tip ground to a point as opposed to a flat, when dealing with wedge geometry squeegees, but the definition is equally applicable to blades with 90° corners which have become 'blunt' with wear.

which rewritten gives

$$P = -\frac{6\mu U\ell}{h_1^2 - h_2} \left[\frac{(h_1 - h)(h - h_2)}{h^2} \right] \quad (2.1)$$

where ℓ is the value of x where the distance of separation is h_2 .

The issue is that hydrodynamic lubrication, as defined by Reynolds', was considered for a relatively large attack angle for which it is unsuitable and Cropper notes that hydrodynamic forces will either be present in front of the squeegee blade or under the line of contact. If the squeegee is incompletely lubricated Cropper suggests applying Hertzian theory. Cropper states that from calculations it is shown that the bow wave passes over a screen element in 0.02s and during this time Cropper derives that pressures in the order of 10^4 N/m^2 must be generated. The fluid may also experience additional pressures from the squeegee line of contact. Cropper's discovery of negative pressures forming behind the squeegee blade may be explained by Riemer's piston action [2]. Cropper was looking for hydrodynamic lubrication, and Hertzian contact pressures, and the pressures he found to be generated in the bow wave were in excess of those he claimed were required to force ink through the screen. This claim is disputed in this work (see Chapter 4). He described the Hertzian pressures along the line of contact at the squeegee tip as being there to seal the stencil to the substrate thus preventing lateral ink flow. The hydrodynamic pressure was found to be greatly influenced by the distance of minimum separation (h_1) and the effective attack angle (m_e). Cropper noted that the squeegee tip deformed due to the hydrodynamic pressure which caused hydroplaning[†] and a subsequent decrease in the effective attack angle. In addition, it was shown that Darcy's law was obeyed, and Reynolds' equation was found to be relevant.

Boyacigiller [34] showed that the flow through the screen is laminar and constructed an apparatus to measure the flow rates and pressures generated in the ink beneath the screen. However, he only recorded static not dynamic pressures as recorded by Cropper [5]. Boyacigiller also showed that speed and viscosity influenced the hydrodynamic pressure which was measured at a maximum of 10^5 N/m^2 . Using Darcy's equation, apparent viscosities and rates of shear were calculated. Other parameters were also examined using the model apparatus. These included squeegee speed, angle and thickness in relation to hydrodynamic pressures

[†] A definition of hydroplaning is given by Huner [24], who describes it as being a colloquial term for the Hertz problem in lubrication theory.

generated between the screen and the squeegee. Boyacigiller's work includes chapters on viscosity, rheological studies and mechanism of flow through a porous medium.

From the experimentation Boyacigiller noted that the pressure distribution under the squeegee was similar to that of a linear wedge section of a lubricated bearing. The maximum pressure was found to be almost at the nip region, i.e. 0.5 mm away from the nip. The effects of squeegee speed, ink viscosity and the angle of attack were tested. From the theory it was expected that an increase in speed would result in an increase in hydrodynamic pressure, but due to the non-Newtonian inks the change in shear rates complicated this. As the angle between the squeegee and the screen decreased, the hydrodynamic pressures increased. A general relationship between the hydrodynamic pressure build up and viscosity, speed, force, density and squeegee angle, is given below in Equation (2.2) but it could not be applied in practice without deriving an equation to determine all the constants. Boyacigiller suggested the use of the "least mean squares method" but it required computation of a large number of results and he did not attempt it. In conclusion he stated that the purpose of the squeegee is to restrain the hydrodynamic pressure build up and therefore to prevent the squeegee from hydroplaning.

$$P \propto \frac{\eta^a u^b F^c \rho^d}{\Phi^e} \quad (2.2)$$

where η = viscosity

u = squeegee speed

F = squeegee force

ρ = fluid density

Φ = squeegee angle

and a, b, c, d, and e are constants

There was a large gap in screen printing studies from 1973 to 1987. Presumably, the late 1960's and early 1970's work stemmed from the focus on tribology at that time, and the interest in the late 1980's was influenced by advances in the electronics sector: hybrid circuits were becoming more dense, with thick film circuit manufacture on the increase, [3], [35], and with the advent of surface mount technology, stencilling[†] was the best method of solder paste application. This was accompanied by significant advances in machine control during the late

[†] Solder paste is applied by stencil printing. This is closely associated to screen printing but instead of a mesh a solid metal stencil is used. The process fundamentals are essentially the same, but the absence of a mesh peeling action requires the stencil to remain in contact until the end of the squeegee stroke, when the stencil snaps off uniformly. The squeegee parameters are the same as those for screen printing.

1980's. Serious attempts to model the process fundamentals have only recently been made by Riemer [2], [36]-[41], Huner [23]-[30] and Owczarek et al [32] & [33].

2.1.1 Process models & their limitations

Rice and McAlister (see Huner [26]) tried to model the screen print process first in 1966 using a modified Taylor solution but they could not overcome the singularity in the pressure at the point of contact with the screen. Jones and Walters (see Huner [26]) progressed Rice and McAlister's work in 1971 by making the screen flow proportional to the local pressure drop across the screen instead of a uniformly distributed flow into the screen. Riemer [2] was the next researcher to examine the Taylor solution in the screen printing context, along with Rangchi et al [30], who examined the process using the lubrication theory approximation of the Navier-Stokes equation. Further process models will be discussed in detail in this section and they include:

- work by Riemer which is based on mesh geometry and screen elasticity, screen behaviour analogous to a hydrodynamic pump and ink flow governed by the Hagen-Poiseuille Law.
- Huner's models which include adaptation of blade coater theory, overcoming the wetting resistance of cloth for forced wetting applications, treatment of the screen as an in-plane permeable bearing, screen print process behaviour discussed in the context of fluid versus elastic stresses, where the squeegee is described as a trailing blade cantilevered system.
- Owczarek and Howland's separation of the ink roll into three pressurisation regions.
- Mannan's model to predict skipping and scooping.

Lubrication theory approximation of the Navier-Stokes Equation

The model for deposition of ink by Rangchi et al [30] deals with Newtonian ink using the lubrication theory approximation of the Navier-Stokes Equation. The mesh apertures are filled by the ink because the motion of the squeegee across the screen generates a hydrodynamic pressure. The difficulty of there being an infinite pressure at the tip is overcome by the fact that there must be a gap, h_0 , underneath the squeegee. This is because the print screen is not smooth and so a perfect seal between the squeegee blade and the screen cannot be made. The fluid flow between the screen and the squeegee is modelled using the Navier-Stokes equation to derive the wet deposit thickness, δ . The thickness is independent of the squeegee speed and the fluid viscosity and is only dependent upon the geometry of the machine parameter settings and the screen characteristics. Really, it only emphasises the importance of the mesh geometry because it is known that changing the speed alters the deposit [2], [42] & [47].

Riemer's models

The basis for Riemer's [36] model is the geometrical relationships which govern the filling and emptying of a cavity. He describes the mesh as being a lattice of cavities, or capillaries. However he acknowledges that the geometry alone is insufficient to model the deposition of ink which occurs in the screen print process and explains that other factors are important. These include: hydrodynamic pressure being generated in the ink roll; a pressure reduction in the ink at the point of snap-off; and the effect of fabric sticking behind the squeegee.

In his later work, Riemer [40] starts with the assumption that the ink roll is analogous to a hydrodynamic pump, injecting ink into the mesh openings, for which he obtains the Navier-Stokes Equation. By modifying Taylor's stream function, as shown in Figure 2.2, Riemer demonstrates that the ink pressure under the squeegee is highest at the squeegee tip to screen interface. This is useful as that is where a high pressure is required to fill the mesh cavities. The stream function equation, the Stokes equation, which quantifies the velocity and pressure relationship, and the boundary conditions at the squeegee and screen surfaces are used to produce equations for the theoretical surface pressures. From the Stokes relationship it is known that the ink pressure is the highest where the velocity is minimum, thus it can be seen that the maximum pressure is directed toward the squeegee and screen nip region. This also shows that the minimum ink velocity is at one third of the squeegee angle, $\alpha/3$, on the stream line chart using Stokes' relationship of viscous movement and pressure. The extent of the ink roll along the squeegee surface is denoted by r_Q .

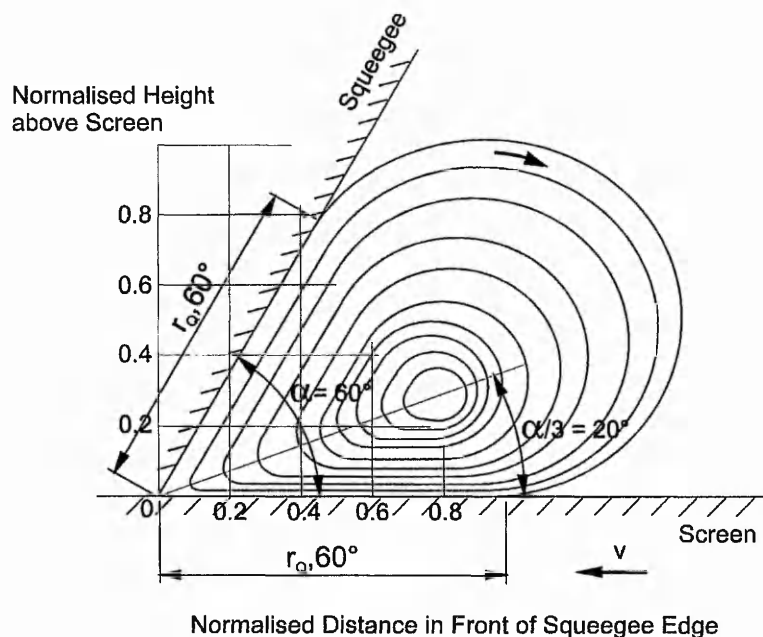


Figure 2.2 Streamline pattern in a limited ink quantity rolling in front of the squeegee

The squeegee and screen pressures are calculated using equations (2.3) and (2.4) respectively.

$$P_{\text{squeegee}} = \int_0^r dP_{\text{squeegee}} = [2\alpha \sin \alpha / (\alpha^2 - \sin^2 \alpha)] \eta V (1/r) \quad (2.3)$$

$$P_{\text{screen}} = \int_0^r dP_{\text{screen}} = [2 \sin \alpha / (\alpha^2 - \sin^2 \alpha)] \eta V (1/r) \quad (2.4)$$

where r = distance from contact point between squeegee and screen

α = squeegee angle

V = squeegee speed

η = ink viscosity

Riemer points out that the reciprocal term, $1/r$ in the above equations causes very high values of pressure at the squeegee tip. In practice though he says that the ink strength and the seal between the squeegee and the screen are important. Riemer explains that the total pressure acting on the squeegee surface can be described as a lifting force, F_{Lift} , which causes the squeegee to hydroplane. This is significant because it means that any parameter causing an increase in hydrostatic pressure will produce an increase in deposit thickness. Presumably, his argument is derived from the fact that as the squeegee lifts, the mesh will also lift from the surface which has the same effect as increasing the mesh thickness.

$$F_{\text{Lift}} = \int_0^{r_Q} P_{\text{squeegee}} dr = f(\alpha) f(Q) \eta V$$

where r_Q = Extent of ink quantity along squeegee surface

$f(Q)$ = Factor, increasing with ink quantity Q in front of squeegee

$f(\alpha) = [2\alpha \sin \alpha / (\alpha^2 - \sin^2 \alpha)]$

Riemer [2] quotes work which he has undertaken showing that increasing the speed resulted in thicker deposits and reducing the angle from 60° to 30° increased the wet deposit thickness by a factor comparable to that of a three fold increase in speed. Riemer [41] relates the maximum permissible shear rate to the ink's capability to build hydrostatic pressure. Insufficient hydrostatic pressure would prevent mesh openings from being filled and Riemer states that high shear rates up to $10,000\text{s}^{-1}$ are generated at the squeegee tip. By arguing that surface

tension alone cannot be responsible for the ink transfer, he explains that an additional force is created during snap off which causes a pressure differential between the ink below the mesh and the ink on the screen, which is at atmospheric pressure. Thus the ink is effectively pushed out. This low pressure is formed due to the piston action of the mesh strands whilst separating from the substrate. Poor transfer results when this low pressure cannot form, e.g. at pattern edges, where atmospheric pressure is acting. This theory restricts the maximum pressure to that of atmospheric pressure. The pressure required to push the ink out is calculated using the Hagen-Poiseuille law.

$$Q = \frac{\pi D^4}{128\eta} \cdot \frac{\Delta p}{L} \quad (2.5)$$

Q = Fluid volume flow rate ($V_a D^2 \pi/4$)

V_a = Average fluid velocity in pipe

Δp = Pressure drop

η = Fluid viscosity

D = Diameter of pipe

L = length of pipe

Pipe and mesh dimensions, according to Riemer, are related as follows:

$$D = \frac{1}{M} - d_w$$

D = diameter of mesh openings

M = mesh count per unit length

d_w = wire diameter of mesh

The pressure generated by the squeegee only contributes to the lifting force exerted on the surface of the squeegee. This determines the resulting height of the ink in the mesh pores after the scraping action of the squeegee blade. According to Riemer the pressure has no other influence on the ink transfer. The actual ink transfer process is then attributed to the low pressure formed due to the snap off action.

The ink flow rate from the mesh to the substrate is considered equal to the screen snap off speed, and this is related to the squeegee speed thus allowing the maximum ink velocity for a

given mesh size to be determined. Riemer found that low values of mesh flow resistance (d_w/D^2) exhibited better print deposit characteristics, as did a smaller snap height.

$$V\alpha = \frac{V_a}{\left[\left(\frac{S}{2}\right) - \left(\frac{B}{2}\right)\right]} \quad (22.6)$$

where

S = screen size

B = length of printed pattern (assumed to be centred on screen)

Riemer approximates this ink velocity to the snap-off speed and produces a speed and viscosity relationship. Using the principle that a sufficient pressure drop is required to transfer the paste at the rate set by the snap-off velocity, and by combining the adapted Hagen-Poiseuille equation with the equation for the snap off velocity, an equation is derived which gives the maximum product of ink viscosity and squeegee speed. Equation (2.7) relates the paste velocity, squeegee speed, snap height, angle of attack and pressure, stating that a small snap height gives better ink release. It also shows that there is an increase in film thickness with a rising squeegee speed and a decreasing angle. Brown [47] also confirms this idea.

$$\eta V \leq \frac{1}{128} \frac{D^2}{d_w} \frac{S - B}{a} p_a \quad (2.7)$$

where a = snap off distance screen/substrate

Riemer mentions that it is more often the case that ink fails to transfer than that the mesh cavities are incompletely filled. Riemer stresses the need for peel-off to occur immediately behind the squeegee, otherwise the time delay might allow the ink viscosity to increase prior to transfer, or the fabric might spring back suddenly at the end of the print stroke. To ensure that this immediate peel off occurs, the tension force in the mesh must be greater than the drag forces of the mesh. Ink transfer is poorest at the back of the print which contradicts the fact that better ink transfer occurs when the mesh movement is slower, i.e. at low snap off velocity and Riemer also attributes this to the fact that fabric sticks behind the squeegee.

Fabric sticks to the substrate when the mesh lifting forces are less than the ink drag forces acting on the mesh , as illustrated in Figure 2.3 below.

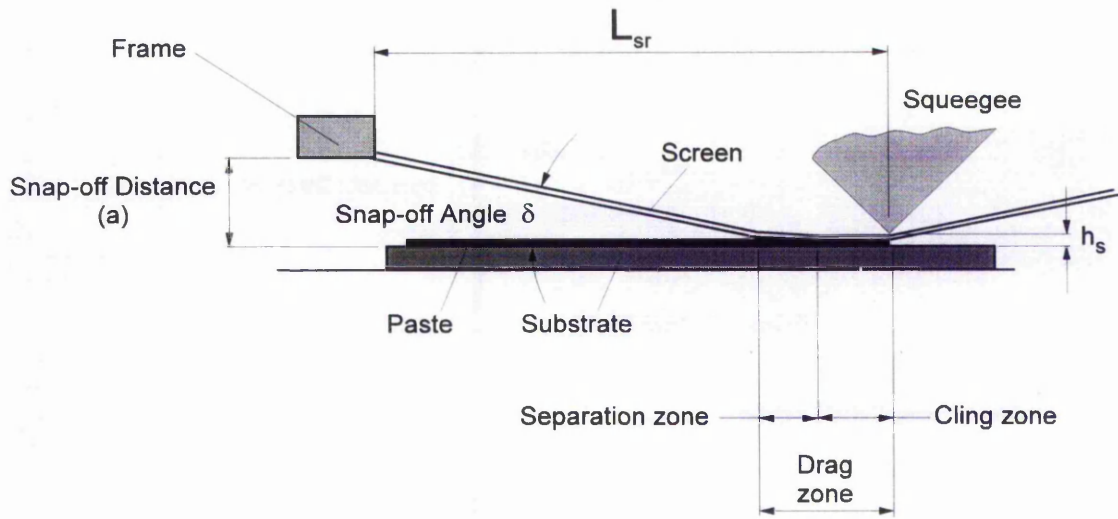


Figure 2.3 Sticking of fabric behind the squeegee

This means that there is a very high separation speed when the squeegee is lifted from the mesh at the end of the print stroke, where the whole frame is usually then lifted clear of the table and the resulting excessive snap velocity causes:

- a rippled print deposit;
- ink to remain in the mesh;
- poor edge resolution due to the ink cavitation.

The force in the mesh strands pulling the fabric up is given by the screen tension, σ_s . To prevent fabric sticking behind the squeegee the screen tension forces must be greater than the drag forces between the ink and the mesh. The upward forces increase as the angle between the fabric and the substrate increases and therefore as the snap height is increased, so at the end of the print the forces in the mesh behind the squeegee are at their smallest. The expression for the angle between the fabric and the substrate as the fabric separates immediately behind the squeegee can be given in geometrical terms as $\delta = \tan^{-1} a/L_{sr}$ and thus:

$$\sigma_s \left(d_r^2 \frac{\pi}{4} \right) \sin \delta \approx \sigma_s \left(d_r^2 \frac{\pi}{4} \right) \tan \delta = \sigma_s \left(d_r^2 \frac{\pi}{4} \right) \frac{a}{L_{sr}} > F_M \quad (2.8)$$

$$\sigma_s > \left[4F_M / (d_r^2 \pi) \right] L_{sr} / a$$

the forces acting on one mesh aperture can be described as:

$$f_{mo} = \tau 4d_r 2d_w + d_w (m + d_r) P_a \quad (2.9)$$

where

τ = Shear stresses between paste and mesh surface

$$\tau = \eta \frac{\partial V_m}{\partial r}$$

d_w = Wire diameter

m = Wire pitch

d_r = Effective mesh diameter ($m - d_w$)

P_a = Atmospheric pressure

$V_m = f(r)$ = Paste velocity in mesh during screen snap off given by

$$V_m = \frac{32}{\pi} \frac{Q}{d_r^4} \left(\frac{d_r^2}{4} - r^2 \right)$$

and r = Distance from mesh centre

Q = Flow volume = $(d_r^2 \pi / 4) V_a$

V_a = Screen snap-off velocity

Therefore Equation (2.9) can be expressed as:

$$f_{mo} = d_r \left[\frac{64\eta V_a}{L_{sr}} + (m + d_r) p_a \right]$$

and thus the force pulling on all the mesh strands in contact with the substrate during screen separation is derived by Riemer as follows:

The force pulling on each wire F_M during screen separation when a number of meshes, n_K , are in contact with the paste on the screen, can be calculated as:

$$\begin{aligned} F_M &= (\frac{1}{2}) n_K f_{mo} \\ &= (\frac{1}{2}) L_K f_{mo} / m \\ &= d_f (L_{sr} / a) f_{mo} / m \end{aligned}$$

which gives:

$$F_M = \frac{d_f^2}{m} \left[64\eta V + \frac{L_{sr}}{a} (m + d_r) p_a \right] \quad (2.10)$$

By substituting equation (2.10) into equation (2.8), Riemer derives an expression for the minimum tension required for immediate fabric separation

$$\sigma_s > \frac{L_{sr}}{a} \cdot \frac{1}{m} \cdot \frac{4}{\pi} \left[64\eta V + \frac{L_{sr}}{a} (m + d_r) p_a \right] \quad (2.11)$$

which can be re-written to define the maximum viscosity and speed product at a particular tension to ensure good fabric separation

$$\eta V < \left(\frac{\pi}{256} \right) \left(\frac{a}{L_{sr}} \right) m \sigma_s - \left(\frac{L_{sr}}{a} \right) (m + d_r) p_a \quad (2.12)$$

where L_{sr} = Distance from squeegee edge to screen frame

m = wire pitch

d_r = effective mesh diameter [$m-d_w$]

Figure 2.4 is a plot of equation (2.7) and equation (2.12) showing the optimum operating conditions i.e. when the speed is set to ensure that ηV is below both curves. The optimum condition is at the intersection point.

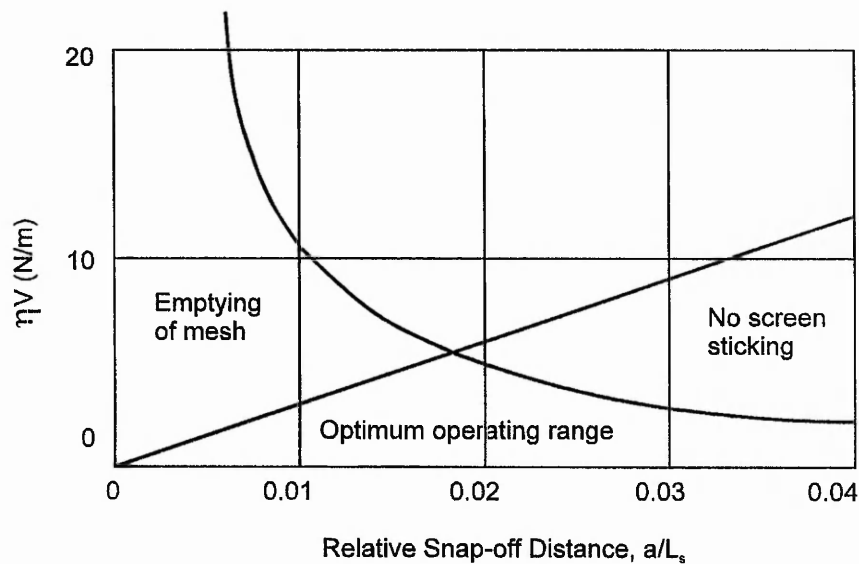


Figure 2.4 Optimum operating conditions

Riemer [38] explains that the mesh elasticity plays a significant role in the fabric and paste separation and thus advises that low printing speeds and small snap-off angles be used with high tension meshes. Riemer regards the snap-height as the most critical parameter during print set-up and has tabulated snap-heights for a wide range of screen sizes and tensions to show the optimum settings, but this is based on geometries alone.

Huner's criticism of Riemer's model

Huner [23] disputes many of the theoretical relationships which Riemer [2] puts forward. This is because Riemer assumes that the ink flow obeys the Hagen-Poiseuille law which requires:

1. the mesh capillary to be longer than it is wide;
2. an infinite amount of fluid at both ends of the capillary;
3. circular capillaries,

all of which hardly hold true for screen printing. The explanation for a poor print at the trailing edge is completely overturned by the argument that it is an inherent characteristic of a liquid film departing from nearly parallel surfaces rather than a result of the ink thixotropy as cited by Riemer [38]. In addition, Huner [37] rules out the ink rheology as a cause for patchiness occurring in printed deposits, claiming that it is due to air entrainment, despite only having anecdotal information to support this idea. Huner [24] disagrees with Riemer's use of Taylor's flow solution because continuity of flow between the ink in the ink roll, and that within, and passing through, the screen is not maintained. Huner proposes that hydroplaning accounts for the pressure singularity which occurs at the squeegee tip which allows the screen printing process to be associated with the Stokes type flows but, on the other hand, if this were the case then the theory would break down again because the gap at the squeegee tip invalidates the boundary conditions. Thus, it cannot explain the flow anywhere ahead of the squeegee tip. The Taylor solution cannot cope with the infinite stress at the squeegee tip nor the inertial effects at the outer edge of the ink roll. To apply it, the ink roll would need to be divided into three regions:

1. near the squeegee tip
2. intermediate region where Taylor's solution is valid
3. a far region in the vicinity of, and including, the free surface of the ink roll.

To accommodate regions (1) and (3) the Navier-Stokes equations could be used to match the Taylor solution of region (2). However, Huner finally decides that the Taylor solution is completely invalid, because after considering the velocity components of the fluid, no relationship to the radial distance from the squeegee origin is found. Thus, it can only be used in a small viscous length $\mu/\rho U$ in front of the wedge apex. This prohibits its use as a bridge from region (1) to (3). Although, some of the assumptions are not necessarily the case in screen printing, as rightly pointed out by Huner, Riemer's work does provide a thorough and practical basis for modelling the process.

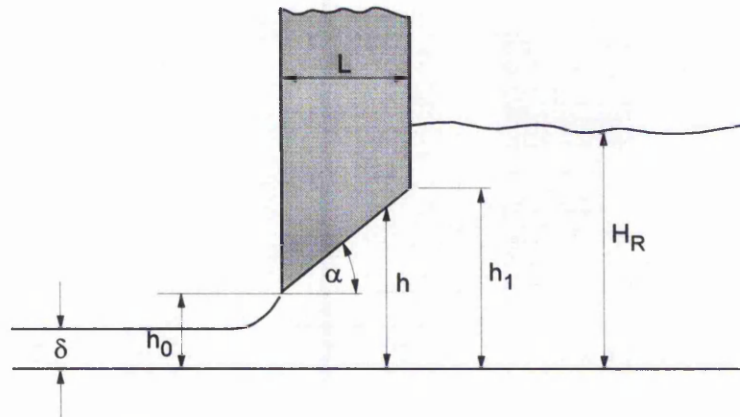
Adaptation of blade coater theory

Figure 2.5 Definition of variables from blade coating theory

An alternative model basis is then sought by Huner [24] in 1989 whereby an estimate of wet deposit thickness, δ , is provided by adapting blade coating theory to the screen printing process. Figure 2.5 defines the variables which are used in equation (2.13)

$$\delta = \frac{h_1 h_0}{h_1 + h_0} \quad (2.13)$$

The parameter h_0 is nominally the thickness of the screen because it is the upper boundary of the wet film thickness. However, h_1 , L and α are more difficult to obtain. He proposes that these must be associated purely with the squeegee tip and that they are products of the squeegee tip deformation resulting from the screen and the ink hydrodynamics which are identified as being related by the Hertz problem and elastohydrodynamic lubrication theory (EHL). Difficulties emerge with a singularity in the pressure distribution because the equation which calculates the maximum pressure, P_M , as shown in equation (2.14) predicts that infinite pressure will exist at the squeegee tip on the stencil areas.

$$P_M = \frac{3\mu UL}{2h_0^2} \frac{\chi - 1}{\chi(\chi + 1)} \quad (2.14)$$

where $\chi = h_1/h_0$ and the maximum pressure occurs at a point along the x axis, X_M , defined as:

$$X_M = \frac{h_0 L}{(h_1 + h_0)} \quad (2.15)$$

To compensate for this the squeegee blade must deform to produce a finite value for h_0 and, or, the squeegee must lift creating a gap at the tip. The first scenario is governed by EHL but Huner does not discuss it further. The second case is governed by the hydrodynamic forces

based on the argument that for a given squeegee loading there must be a hydrodynamic lift to balance it. The integral of the lifting force, F , is written as

$$F = \int_0^L p(x) dx$$

which results in

$$F = \frac{6\mu U}{\tan^2 \alpha} \left(\ln(\chi) + 2 \frac{1-\chi}{1+\chi} \right) \quad (2.16)$$

which allows this lifting force to be calculated and shows that as h_0 increases the lift decreases. This allows an equilibrium equation to be derived by setting the load per unit length applied to the squeegee, W , equal to F , which can only be solved using numerical methods. An estimation can be made analytically at large values of χ because in this case h_0 is given by:

$$h_0 = h_1 \exp \left\{ - \frac{W \tan^2 \alpha}{6\mu U} + 2 \right\}$$

which shows that high loads or attack angles will cause thicker deposits. Also as the speed increases the deposit will increase. An important point is that as the parameter $W \tan^2 \alpha / 6\mu$ becomes larger, higher squeegee speeds must be reached before the squeegee load has any effect on the squeegee displacement. Thus, at a fixed speed and attack angle, increased load effects thinner print deposits, whereas increasing the viscosity does the opposite. Reducing the attack angle also causes a thicker deposit.

Wetting resistance of cloth analogy

In 1989 Huner [25] changed tack again, this time postulating that the screen print problems are the same as those encountered by the forced wetting of cloth. Huner points out that studies on forced wetting of cloth were published in the textile industry and were thus overlooked by workers in the screen printing field. The screen is presented as an anisotropic porous medium, rather than matrices of short non communicating capillaries, thus allowing solutions to many areas of the screen printing process not explained by the former representation. He summarises a series of works which have studied systems of monofilament monoporous structures which operate at low Reynolds numbers in the context of anisotropic porous media. By examining the wetting resistance of cloth, the pressure drop across the plane of the model can be found in terms of drag theories and the Reynolds number. The Clarks & Miller model (see Huner [25]) of wetting and dewetting is used to explain ink transfer, which states that the primary force which controls wetting or dewetting is the capillary attraction of the liquid to the fibres of the mesh. Basically, the liquid meniscus has a pressure drop governed by the liquid surface tension and the radius of curvature of the meniscus. This is related geometrically to the liquid shape between two mesh strands which then allows the maximum and the minimum pressure drop across the screen to be derived. These pressure differentials are governed by the size of the

initial pressure drop required to overcome the fabric's natural wetting repellancy. The pressure required for this in screen printing only occurs near the squeegee tip, and if the squeegee speed is too slow for a given screen, ink and attack angle then no deposit will be produced as the peak pressure required will not be achieved. Conversely, if the speed is too fast the pressure required will occur well ahead of the squeegee tip and this may be before the point where the stencil gaskets with the substrate, which would lead to smearing or bleed out. This is contrary to results discussed from practical work [11]&[12], which shows that too fast a print speed leads to skipping. This would indicate that the optimum print settings would be those which delivered a peak pressure equal to the maximum wetting pressure, as close to the squeegee tip as possible. The transfer of ink is likened to that of a flexible porous bearing, but instead of creating positive pressures it must develop negative pressures to pull the ink out of the screen. Quoting the speed and the angle of attack as being the simplest parameters to adjust, he describes the resultant behaviour of altering these parameters with respect to porous bearings i.e. increasing the angle increases the pressure whilst moving it toward the squeegee tip, but at high angles, a further increase in the angle results in a decrease in the maximum pressure. Huner suggests that this is compensated for by adjusting the speed. He omits to mention that the actual attack angle of the squeegee is invariably unknown, as it is a function of the angle set by the squeegee holder, the flexural rigidity of the squeegee material and the effects of hydroplaning. These points are discussed in greater depth in Huner [29] and will be dealt with later in this section.

A further problem with the model based on cloth wetting resistance is that the snap-off action must create a pressure which is equivalent to the dewetting resistance of the mesh. For fine mesh the pressure required would probably distort the screen, because high mesh counts require very large negative pressures to pull the ink out. This could be alleviated by increasing the percentage open area. In practice this would not be achievable where fine features are required, therefore according to Huner's explanation very fine features could not be printed without screen damage, or defective print quality. Presently, the finest printable detail is unknown as efforts are continuously underway to produce more densely packed circuitry in electronic circuit production. An alternative solution offered by Huner would be to use a very low surface tension mesh. A non-wetting ink is unsuitable as the ink transfer consists of small dots which must flow together once on the substrate.

Once the print run is in progress a few prints are usually required before an acceptable print is achieved. This is only for very high viscosities as low viscosities print immediately. Huner's explanation of this is that for dry cloth the peak wetting pressure, and thus the wetting

resistance, is a variable, but once the mesh strands become completely immersed in the ink the wetting resistance is reduced and stabilised. This would account for the settling down period required prior to printing.

Huner [25] claims that flow occurs within the porous medium which is beneficial. This flow is dependent on fluid viscosity and the permeability tensor of the fabric which Huner describes as being related to the weave and mesh diameter of the screen. To achieve an isotropic fluid flow, Huner suggests that the principle axis and the diagonal elements of the permeability tensor must be equal. In practice this would mean that the print orientation would have to match the cloth orientation. To overcome air bubbles printing at 45° is recommended [11]. According to Huner this could only be done if the cloth was mounted at 45° to the frame. Provided that there is sufficient ink along the length of the squeegee, flow along the face of the squeegee is unnecessary and it is difficult to accept that it occurs at all.

The possibility of having a complete screen printing model which can include stencils is dismissed by Huner as each screen and stencil system must be treated individually. This is because the stencil apertures are inherently irregular and this upsets the permeability tensor. Huner [25] argues the point that the screen printing is actually 3-D and as such a 3-D model should be developed. He derives an equation which does not include surface tension effects and is therefore restricted to the squeegee tip only.

$$\underline{u}(x, y, z) = -\frac{1}{\mu} \underline{k} \cdot \nabla_2 P(x, y, z) - \frac{1}{\mu} k_z \frac{\delta P}{\delta z} \hat{a}_z$$

where

$\underline{u}(x, y, z)$ is the mean filter velocity of the fluid

μ is the fluid viscosity

\underline{k} is the permeability tensor

$\nabla_2 P(x, y, z)$ is the three dimensional space gradient of the fluid pressure $P(x, y, z)$

$$k_z = \frac{2d(2d + \epsilon) \beta}{k_0 (1 - \beta^2)}$$

d is the fibre diameter

ϵ is a small value accounting for the hardness of the mesh

$\beta = (1 - d / \ell)^2$ where ℓ is the wire spacing

k_0 is a constant

\hat{a}_z is a unit vector normal to the screen

This calculates the fluid velocity in the x,y,z direction, but it is arguable as to whether or not this is necessary as the flow in front of the squeegee and down through the mesh are actually

the only points of interest. This 3D model fails to provide sufficient information for all of the constants and then in his next paper [26], a year later, he reverts back to the use of a 2D model without progressing the 3D model any further. The 2-D model is difficult enough and remains incomplete despite several attempts to pursue it [2],[5],[32] & [33].

The screen modelled as in-plane permeable bearings

The next approach taken by Huner [26] describes the screen printing process as being akin to lubrication of in-plane permeable bearings, suggesting that the screen is a two-dimensional porous medium which satisfies Darcy's law. This provides more accurate information regarding the drag forces on the capillaries, because, as pointed out by Cropper [5], the drag force in a porous medium is higher than the sum of the drag forces of individual capillaries in an equivalent area. Huner assumes that screen printing operates at low Reynolds numbers, which was initially verified by Cropper. In-plane permeability also presents an alternative solution which provides a finite pressure at the squeegee tip and allows the substrate to be accounted for. The screen is treated as a 2D permeable layer. Flow is divided into two regions, (I) is the ink roll and (II) is the volume of screen underneath region (I). The total flow passing the squeegee tip, Q , is obtained by applying the Morgan-Cameron approximation. The assumptions which Huner applies are that:

1. the pressure is continuous across the ink screen boundary to get equation (2.17)

$$v(x, y = 0) \approx \frac{k_x H d^2 P}{\mu dx^2} \quad (2.17)$$

where

- $v(x,y)$ = normal component of ink velocity
- k_x = Darcy's constant
- H = printing screen thickness
- P = $P(x)$ is the pressure in the ink
- η = viscosity of printing ink (assumed to be Newtonian)
- x = point along the x-axis

2. there is 100% transfer of ink , even though Riemer [2] quotes work by Martin et al (1974) which proves that 25-30% of ink remains in the mesh after a print stroke, thus 100% ink transfer does not occur.
3. the wet deposit thickness must be given by

$$\delta = \frac{Q}{U} \quad (2.18)$$

because in a certain time interval, Δt , the squeegee advances a distance, $U\Delta t$, therefore, the wet deposit thickness is derived in terms of porosity, print screen thickness and the stencil emulsion thickness build up.

Flow past the squeegee tip is found by determining the pressure beneath the squeegee as given in equation (2.19)

$$P(x) = \int \frac{\frac{sh^2U}{2(1+sh)} - Q_0}{\frac{K_x H}{\mu} + \frac{h^3}{12\mu(1+sh)}} dx + P_w \quad (2.19)$$

and Q_0 is found by assuming that the pressure at the squeegee tip is 0. Therefore

$$Q_0 = \frac{P_w + \frac{U}{2} \int_0^L \frac{\frac{sh^2}{(1+sh)}}{\frac{K_x H}{\mu} + \frac{h^3}{12\mu(1+sh)}} dx}{\int_0^L \frac{1}{\frac{K_x H}{\mu} + \frac{h^3}{12\mu(1+sh)}} dx} \quad (2.20)$$

where

P_w = pressure required to overcome the wetting resistance

U = squeegee velocity

$$s = \alpha_x / \sqrt{k_x}$$

(α_x is dimensionless constant, the slip coefficient)

$h = h(x)$ is the squeegee shape as measured from the surface of the screen to face of squeegee $h(x)$ for a wedge shaped squeegee = $(L-x) \tan \alpha$ (α = angle of attack)

L = distance to the point where ink roll overcomes the wetting resistance

By manipulating his equations, Huner derives the flow past the squeegee tip as being

$$Q = AHU + Q_0$$

where A = porosity of the print screen

H = screen thickness (not including stencil)

U = squeegee velocity

Q_0 , given in (2.20) above is the sum of any flow leaking under the squeegee tip and the filter component escaping through the screen, which is the element which allows the pressure to remain finite. This model from Huner still leaves the fact that when the in-plane permeability

of the screen is zero, i.e. wherever there is stencil mask, the squeegee pressure is infinite. He states that with these formulae, it should now be possible to quantitatively evaluate the operational characteristics of any proposed screen printing system, but he does not continue to do this.

He then argues that the peak pressure generated in the ink greatly exceeds the wetting resistance of the screen and P_w becomes negligible, leading to (2.21).

$$Q = AHU + \frac{\frac{U}{2} \int_0^L \frac{sh^2}{12k_x H + h^3} \frac{(4+sh)}{(1+sh)} dx}{\int_0^L \frac{1}{12k_x H + h^3} \frac{(4+sh)}{(1+sh)} dx} \quad (2.21)$$

For a smooth surface $sh \rightarrow \infty$, and in this special case a non-dimensional form of Q , Q^* can be obtained

$$Q^* = \frac{\frac{1}{2} \int_0^{L^*} \frac{h^*}{\Phi^3 + h^{*3}} dh^*}{\int_0^{L^*} \frac{1}{\Phi^3 + h^{*3}} dh^*}$$

and as $L^* \rightarrow \infty$, $Q^* \rightarrow \Phi/2$. The final wet deposit thickness is derived as

$$\delta = (A + \Phi / 2)H$$

where A = screen porosity

H = mesh thickness

$$\Phi^3 = 12k_x H / H^3$$

From the implications of this type of flow, an equation for the wet film thickness is found but this model really only deals with the flow through the porous medium and under the squeegee tip whilst ignoring the ink transfer.

Another estimation of the wet deposit thickness is made by Huner [27] in 1990. A correction to the Navier Stokes Equation accommodates the screen thickness and the emulsion build up and allows the flow under the squeegee tip to be given:

$$Q = U \frac{(h_s + h_e)h_1}{(h_s + h_e) + h_1} - (1 - A)h_s U$$

where h_s = thickness of the printing screen

h_e = thickness of the emulsion build up.

In screen printing $h_1 \gg (h_s + h_e)$, and a reasonable value for $(h_s + h_e)$ is 0.0254mm with a 1cm ink roll, therefore by approximation, $h_1 \approx 39(h_s + h_e)$. Thus using the assumption that $\delta = Q/U$, the wet film thickness can be rewritten as

$$\delta = Ah_s + h_e$$

Squeegee analysis based on a cantilevered trailing blade system

In a further contribution to the screen print process model, Huner treats the squeegee as a rigidly clamped, cantilevered plate loaded at its tip [29]. The work assumes small deflections and that the squeegee is within the lubrication limit. If the fluid forces and load at the substrate on the squeegee cause the squeegee to deform then the final deposit thickness may be affected. This work is significant as it eliminates the need for the pressure generated within the ink roll to be known. However, it is only the basis for further work as it considers only the two extreme situations whereby either the fluid forces in the ink roll dominate, or, the elastic forces of the squeegee blade dominate, which, in practice, do not occur. It is also not independent of his earlier work and thus must be linked back through several stages to be applied in a practical situation.

Using the Bernoulli-Euler law, along with an approximated squeegee and screen contact position, ℓ , and previous work which allowed the pressure ahead of the squeegee to be found, he obtains a mathematical model (2.22) which consists of two parts. The first part of the relationship is based on fluid viscosity and squeegee speed, i.e. viscous stresses ($\mu U/\ell$) and the second part regards the contact force at the squeegee tip as being based on elastic stresses (D/ℓ^3).

$$\frac{d^2 y}{dx^2} = \frac{6\mu U}{D \sin^3 \theta_R} \int_x^\ell (\lambda - x) \left[\int_x^\lambda \frac{y - \frac{2Q_0}{U}}{12k_x H + y^3} d\chi \right] d\lambda + \frac{F}{D \sin^3 \theta_R} (\ell - x) \tag{ 2.22}$$

where

μ = fluid viscosity

U = squeegee velocity

D = flexural rigidity of the squeegee

λ = a variable along the x-axis

Q_0 = flow induced within the plane of the screen

k_x = Darcy's constant

H = thickness of the mesh

F = contact force at the squeegee tip

θ_R = the angle from vertical at which the squeegee first rests on the screen

ℓ = the squeegee screen contact point

x and y are co-ordinate references

This relationship $\mu U \ell^2 / D$ is of importance because he says that when it is $\ll 1$ elastic stresses are dominant and when it is $\gg 1$ fluid stresses are dominant.

The assumption is that if the flow of fluid is steady then the final print deposit will be predictable. The two extremes are dealt with separately. Firstly, if the elastic stresses are dominant then, providing that there is a sufficient length of ink roll in front of the squeegee, and the squeegee exhibits minimal deflection (quantified by Huner as $u \leq 2.5$, where u is a parameter related to squeegee load and angle defined by $u = \tan \theta_R \cot \theta_W$ and θ_W is the working angle of the squeegee) the screen print process will operate at 'self-metering' conditions, i.e. that there will be a steady flow state. Under these conditions there is minimal variation in the normalised ink flow, and the flow is not very sensitive to flexing of the squeegee. These assumptions are based on numerical evaluations using an adaptive Simpson's rule. Huner summarises that in practical terms a minimal down force with adequate ink volume produces least variation in flow due to changes in the attack angle. Secondly, at the other extreme, the case is considered where the fluid stresses are dominant. Other work reported by Misele (see Huner [29]) shows that increasing the squeegee pressure causes the deposit height to decrease, and then increase, which is contradictory to Huner's plot of normalised flow against ink roll length. This normalised flow does not allow for the relationship of film thickness to squeegee speed and ink viscosity. Huner [29] explains that when the $\mu U \ell^2 / D$ ratio is not small then the fluid stresses are also influencing the actual squeegee deformation, which in turn influences the final deposit. When $\mu U \ell^2 / D \gg 1$ hydroplaning is occurring and another equation can be produced from (2.22).

$$\frac{d^2y}{dx^2} = \frac{6\mu U}{D \sin^3 \theta_R} \int_x^{\lambda'} (\lambda - x) \left[\int_{\lambda'}^{\lambda} \frac{y - \frac{2Q_0}{U}}{12k_x H + y^3} d\chi \right] d\lambda \quad (2.23)$$

This cannot be solved analytically, so the squeegee shape is approximated to that of a linear function as suggested by Saita (see Huner [29]). Contrary to earlier work, Huner now dispenses with the fact that the screen is permeable and states that the total flow to the breakaway region is the sum of ink in the screen plus the amount flowing under the squeegee. Assuming total immersion of the mesh in front of the squeegee he derives an equation to calculate the size of the gap at the squeegee tip, thus estimating the flow under the squeegee tip, Q_0 , as

$$Q_0 = \frac{uy_0y_t}{(y_0 + y_t)}$$

where

y_0 = the height of the squeegee at the point where it is clamped

y_t = the deflection at the squeegee tip

From this analysis he states that a quantitative model can now be derived, but again he does not do it.

Finally, in 1994, Huner [38] represents the ink flow ahead of the squeegee tip as being that of a fluid flowing ahead of a wedge, with an ideal fluid sink at the apex. The infinite pressure at the tip is deemed not to be physical but simply a fault in the model due to the assumption of no slip boundary conditions. Elastic deformation and flow through the screen could remove these problems but to get quantifiable solutions numerical methods are required.

Pressurisation wedges in the ink roll

Recently, Owczarek and Howland [32] & [33] have used different assumptions which discuss the process in terms of wedges which are split into pressurisation regions for analytical purposes.

There are three important regions which they consider:

1. pressurisation
2. downward screen cross flow
3. paste collecting

which are illustrated in Figure 2.6 overleaf.

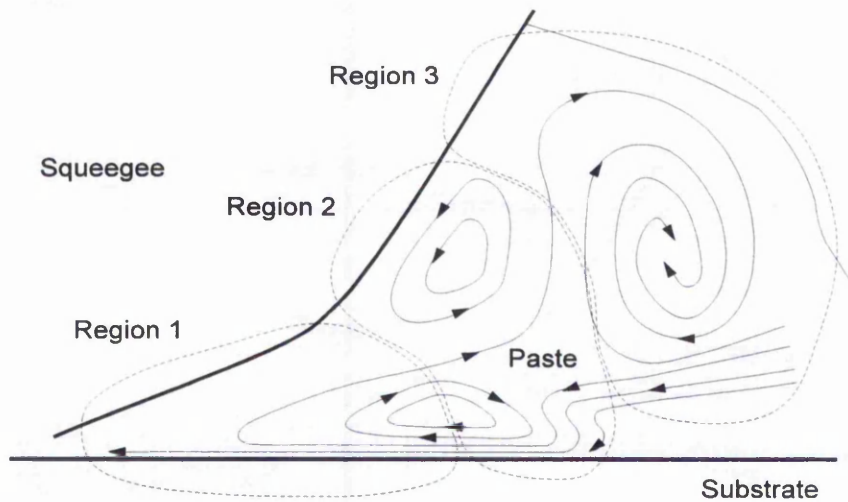


Figure 2.6 Three pressurisation regions

Owczarek et al allow the effects of squeegee deformation to be considered in their analysis which is a very important issue, particularly when using softer squeegees (e.g. < 80 shores). The analysis provides an equation which gives the flow passage height under the squeegee from which the wet thickness can be derived. Equation (2.24) demonstrates the relationship of the wet paste thickness to that of the paste flow height underneath the squeegee and this is illustrated in Figure 2.7 below.

$$H_{WP} = H_{SC} \left(1 + \frac{V_P}{V_{SQ}} \right) - H_{PR} \quad (2.24)$$

where

H_{WP} = height of the deposited wet paste

H_{SC} = equivalent flow passage height under the squeegee

V_P = paste flow speed under the squeegee

V_{SQ} = squeegee translational speed

H_{PR} = height of the paste residue left on the screen

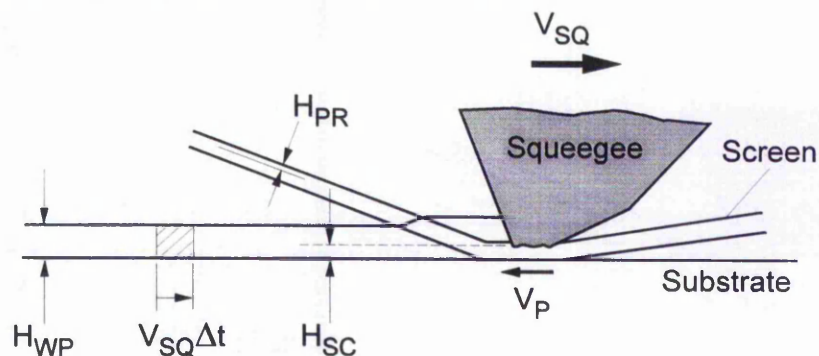


Figure 2.7 Paste flow height beneath the squeegee

The paste flow height underneath the squeegee cannot be determined without the knowledge of either the squeegee penetration depth into the screen or, alternatively, by conducting an interrupted print using a quick setting paste from which the flow height beneath the squeegee tip must subsequently be measured using a profilometer. Owczarek & Howland undertook a series of interrupted tests using a screen printable epoxy. A typical paste profile is depicted in Figure 2.8.

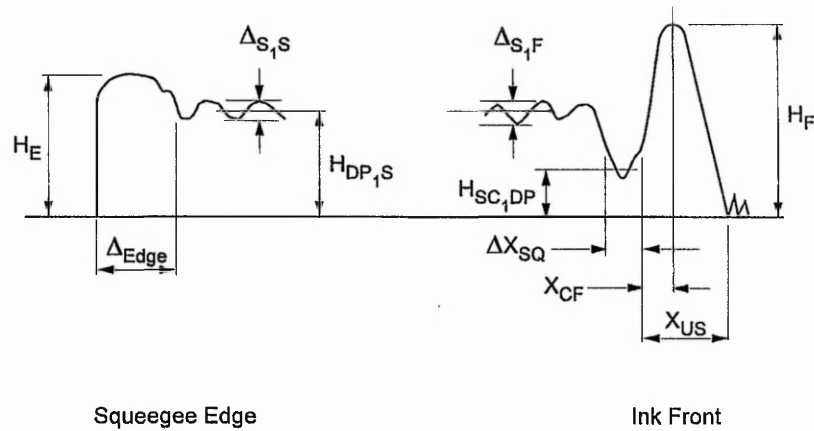


Figure 2.8 A typical paste profile from the interrupted test

The definition of the symbols used in Figure 2.8 are as follows:

H_E	Edge height
Δ_{Edge}	Width of paste edge
$\Delta_{S,S}$	Twice the amplitude of the paste wavy surface at start
$H_{DP,S}$	Height of dry paste at start
$\Delta_{S,F}$	Twice the amplitude of the paste wavy surface at front
$H_{SC,DP}$	Equivalent flow passage height under squeegee, dry paste
$\Delta_{X_{SQ}}$	Width of flat portion of deformed squeegee
X_{CF}	Distance of circulatory flow
X_{US}	Distance of region under screen
H_F	Height at front

The 'edge' is assumed to refer to the ink behind the squeegee, and appears to be synonymous with the term 'start', as opposed to the 'front', which is in front of the ink roll.

The interpretation of the paste profile, showing the small tip deformations and the associated fluid heights, is questionable as the squeegee does not freeze solid at the moment of interruption of the print stroke, i.e. the tip deformation changes as the squeegee slowly sinks to touch the substrate.

Additionally, the mesh effects have to be accounted for separately. Like Huner, they assume that the process is governed by hydrodynamic lubrication theory. An important part of this work is that the effects of the screen tension are accounted for. A disadvantage is that the squeegee is treated as if it has no gross curvature, they merely represent it using two angles, as depicted in Figure 2.6 above. A second part to the analysis allows conversion of the wet thickness to dry thickness, which takes the analysis one step further than Huner's, which only provides an equation for the wet thickness expected.

Mannan's model to predict skipping and scooping

Using the work of Owczarek & Howland as a reference point, Mannan et al [45] present a model to predict scooping and skipping of solder paste. The model is not directly applicable to screen printing but the fundamentals relating to the geometrical deformation of the squeegee and the resulting fluid flow of paste are relevant and thus have been included here. Firstly, the squeegee static tip deformation was measured and found to be approximately 100-200 μm . Then the depth of squeegee penetration into the stencil aperture was recorded, but it must be borne in mind that these are usually at least five times thicker than screen stencil aperture depths. The assumption was made that the squeegee velocity did not affect the penetration depth as there was no difference between the depths recorded in parallel apertures when compared with results from perpendicular apertures. The parallel and perpendicular pads use the squeegee contact line as the datum. It was also argued that the paste flow underneath the squeegee tip would not contribute to the printed deposit height, H , based on the equation from Owczarek et al:

$$H = (H_{st} - \Lambda) \left(1 + \frac{V_p}{V} \right)$$

where

V_p = average paste velocity

H_{st} = stencil thickness

Λ = depth of the squeegee deformation

V = squeegee velocity

This was based on the fact that no difference was seen on perpendicular pads when compared to parallel pads, but a metal squeegee was used to conduct this test which would not be expected to deform greatly into a small aperture and thus casts doubt on this argument. Disregarding the paste flow height under the squeegee it is then assumed that the paste heights are only affected by the pressure which the paste exerts on the squeegee, the squeegee load, the geometry of the aperture and the squeegee material properties. Models are created to predict the scooping depths, Λ_{perp} and Λ_{par} for the perpendicular and parallel apertures respectively; this, surely, would not be necessary if the tests had showed there to be no orientation related difference.

$$\Lambda_{\text{perp}} = \varepsilon \left(\frac{F - bV}{B} - pV - d \right)$$

$$\Lambda_{\text{par}} = \varepsilon \left(\frac{F - bV}{B} - qV - d \right) \left(1 - \frac{1}{\cosh(\beta_{\text{SQ}} A_{\text{sw}})} \right)$$

where

- ε = compressibility
- F = loading force on the squeegee
- bV = contribution to pressure on the squeegee from paste above the stencil
- B = horizontal squeegee length
- pV = pressure per unit width of paste below the squeegee
- d = pressure due to paste trapped between the squeegee and the aperture wall
- A_{sw} = distance between supporting aperture walls
- β_{SQ} = function of the squeegee material (Young's modulus and Poisson's ratio)
- b, p & q = coefficients used in quantifying loads from above, below and in between respectively.

For one particular squeegee and paste with a 150 μm stencil the values were found to be:

$$\varepsilon = 4.2 \times 10^{-7} \text{ Pa}^{-1}$$

$$\beta_{\text{SQ}} = 1.3 \times 10^4 \text{ m}^{-1}$$

$$d = 90 \text{ N / m}$$

$$\frac{b}{B} + p = 1.8 \times 10^3 \text{ Pa.s}$$

$$\frac{b}{B} + q = 4.2 \times 10^3 \text{ Pa.s}$$

The model predicts that the heights of the parallel deposits increase as, A , the geometrical factor decreases and this is shown to be true up to a point, after which it reduces again. This reduction is not accounted for. It is also expected that harder squeegees will reduce the scooping and the variation between prints because both are proportional to ε , which becomes smaller as the squeegee gets harder. They say "this effect would be difficult to explain if the height was caused by a layer of paste being swept along with the trailing edge of the squeegee in the parallel aperture".

The model also predicts that the loading force on the squeegee, F , and the squeegee velocity, V , should not be interactive, but in practice this is shown not to be the case. This is explained because under high loads the attack angle decreases thus increasing b , which is a coefficient of V .

Table 2.1 Results of squeegee comparisons by Mannan et al [45]

Blade Shore A	Height (μm)	Scooping (μm)
Metal	157.6	-5.2
90-94	122.0	30.4
60-85	116.7	35.7
70-75	88.0	64.4
Backing/Tip 94-98/75-80	107.6	44.8

Six squeegees were tested (see Table 2.1) for deposit height variation. The softer squeegees gave thinner deposit heights because of the scooping. This result was comparable to screen print testing carried out by the author at TNTU where the softer squeegee gave thinner deposits in 69% of the cases as shown in Appendix 2.2, although it is difficult to say whether this was because of scooping as opposed to the squeegee not hydroplaning. The methods used to calculate the scooping were not described by Mannan et al. The final conclusion by Mannan et al was that harder squeegees prevented scooping but softer squeegees were better to prevent skipping. Brown [21] confirmed these results in an independent test, but found that the softer squeegee produced more erratic results and that metal squeegees gave very poor results, whilst damaging the solder mask.

2.1.2 Theoretical limitations

Inconsistencies in the approximations, difficulties in applying the models in practice and the limitations in the scope of the models clearly indicate that further work is essential. An interesting point to note is that Huner [23] criticises Riemer (see Mannan [31]), but later on Owczarek and Howland [32], mention the particular value of Riemer's work. A computational fluid dynamics study [46] of the ink roll confirms that Riemer's approximations are broadly justified and Mannan concludes that Riemer's work is of initial benefit. Unfortunately, Mannan points out an assumption made by Owczarek & Howland, regarding the calculation of the volume flow rate, which is in error. Despite these conflicts in the studies, equations are derived from the models which allow wet film thickness to be calculated as a function of the stencil thickness, but some of the variables are difficult to quantify for normal production use. Huner and Owczarek et al agree on the fact that the wet thickness of the deposit is directly related to the effective paste height under the squeegee tip, as defined by Owczarek et al, or flow of ink past the squeegee tip which

was defined by Huner. This has important implications because if this height or flow could be quantified then it would be possible to predict the final wet thickness.

The link between the theory and the practice is somewhat non-existent. It is not possible to use the derived equations to start up a production run as too many variables are unknown in each equation. The models rely on certain variables being known, or at least quantifiable. In practice they may be difficult, if not impossible to obtain. Viscosity, for example, is an influential factor in many of the equations but as the inks are highly non-Newtonian and sensitive to relative humidity and temperature, it is difficult to predict their behaviour. Another example is hydrostatic pressure in the ink. The equation provided for this assumes that the quantity of paste in front of the squeegee is known, which in reality would be quite difficult, if not impossible, to monitor accurately. Assumptions are made that in practice would not be determinable and thus verification would not be possible. Consideration to particle sizes and many other variables is not always given and it is wrong to assume that these have no influence.

2.1.3 Empirical methods

Semi-analytical methods have also been used to evaluate the screen printing process. Brown [47] uses operational characteristic curves (OC curves) to determine correct choice of mesh and emulsion thickness. An example of the OC Curves generated by Brown is given in Figure 2.9. It is split into three regions and Brown describes his interpretation for each region corresponding to the print deposit obtained. The process sensitivity to snap-off, squeegee speed, squeegee length and squeegee pressure is also considered. From the OC curves a clear interaction between speed and snap height was observed. Firstly, Brown set up a mesh for the desired film thickness using the geometrical equation:

$$T(\text{s-dry}) = ((T_m \times A_o) + T_e) \times I_r \times 25.4$$

where $T(\text{s-dry})$ = stencil dried thickness

T_m = mesh weave thickness

A_o = mesh open area

T_e = emulsion thickness

I_r = ink wet to dry ratio

From this a table of mesh and emulsion values for a range of deposits was generated. Then operational characteristic curves were generated for three samples at ten different pressure

levels. These values were plotted and linear regression analysis transformations were carried out to obtain squeegee pressure settings.

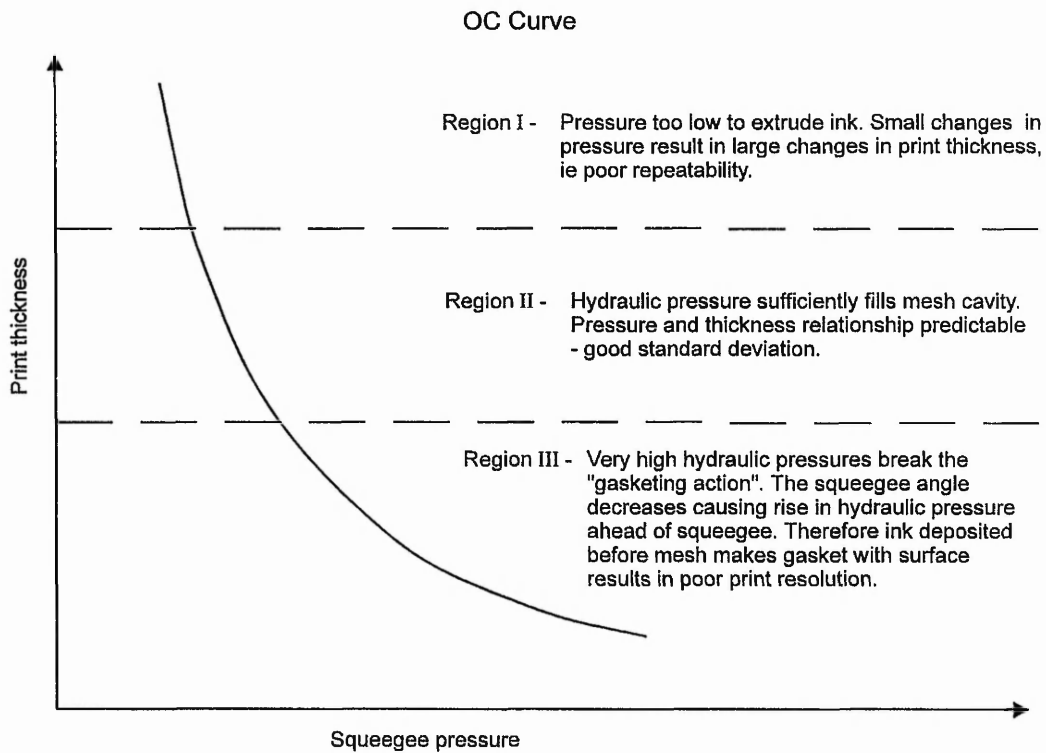


Figure 2.9 Operational Characteristic curve defined by Brown

Brown performed 8 sets of testing to give relationships between 2 different machines, 2 mesh types and 2 different inks, thus providing 240 points to obtain a statistical average. Only pressure changes, not squeegee angle, speed or material types, were examined. From these tests, model equations were derived whereby the print thickness was found to have an inverse relationship to squeegee pressure. The equation was found by performing transformations on the print thicknesses, finding the best fit from linear regression analysis. The reliability was determined to be within $2\mu\text{m}$ of the required deposit thickness. Process sensitivities were then examined by comparing three different speeds at three different snap heights for different pressure settings. The squeegee speed and pressure were found to interact at different snap heights, but it was possible to determine that the print thickness increased with higher speeds, until the speed reached a limit beyond which there was no deposit. Brown states that at increased speed there is an increased speed differential and that at increased pressure, the thickness differential is maintained indicating that the squeegee is hydroplaning. These statements are all true, but it was finally concluded that the best response was obtained from a

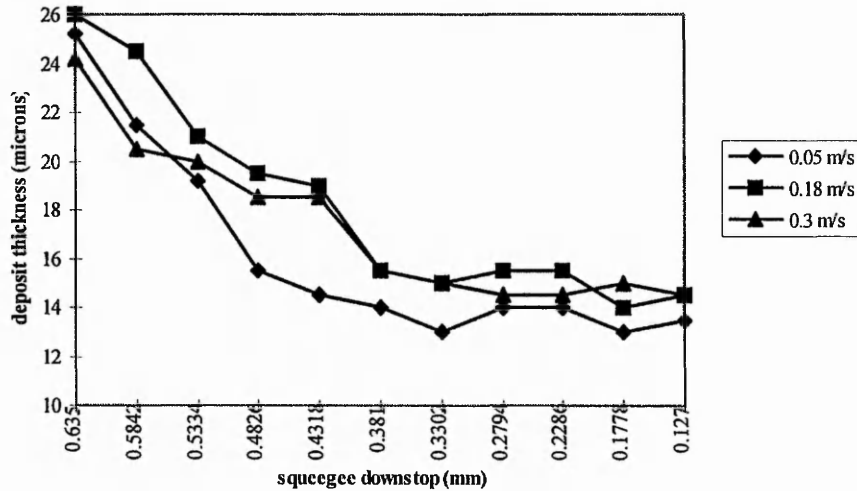


Figure 2.10 The OC Curve for varying squeegee speeds

setting with a 0.762 mm (30 mil) snap off at a squeegee speed of 0.05-0.178 m/s (2-7"/s), as shown in Figure 2.10. However, according to the graph to get the target of 25 μ m thickness 0.58-0.63 mm (23-25 mils) of squeegee down-stop[§] would be applied not the 0.49 mm (18.5 mils) predicted. In addition, the curve appears to be very steep and is, therefore, highly sensitive to change. The better operating ranges appeared to give deposit thicknesses of 13-15 μ m, giving a conflict of interests regarding the first part of the work which has not been dealt with at all. Geometrical relationships were made and then the significance of changing one variable at a time was checked. These curves were then used to predict interpolated outcomes and finally process sensitivity was examined as a separate case, showing that a different set of optimum parameter settings was required for the best manufacturing situation, i.e., least process sensitivity.

This work simply underlines the fact that the process is complex, outlining a useful approach for moving forward whilst highlighting the need for further work to be continued in this area. Stencil selection is made simpler and for each machine and mesh etc. a predictable set-up can be determined if the additional parameters of speed and snap height are left out, otherwise conflicts occur which are difficult to resolve. The work would allow a knowledge base to be formulated and the interactions to be observed but it is not generic because of the way in which the machine parameters were set up. It should be noted that guidelines based on geometrical

[§] Down-stop is equivalent to a linear load

relationships are given by the mesh suppliers and have also been referred to in other papers, for example [48],[49].

A full factorial experiment was carried out on the solder paste printing process by Molamphy [6]. The experiment examined three factors at two levels: squeegee hardness, squeegee speed and pressure. The results showed the percentage contribution to variation for each parameter was as follows: hardness, 52.47%; pressure, 7.52%; and all the other variables were less than 5%, with an error of 40.02%. A signal to noise ratio analysis was also carried out which showed a much higher contribution from the squeegee hardness at 95.14% but the error was only 4.86%. Accepting this at face value the 90-95°A SH squeegee was much better for solder paste printing than the 80-85°A SH squeegee.

A second experiment, again a full factorial, examined squeegee speed, pressure and the snap height, each at two levels. This time measling diagrams** instead of wet deposit thickness were used as a measure of print quality. The pressure accounted for 38.12% of the variation, squeegee speed and pressure interaction for 16.08%, speed 13.94% and error 31.85%. The best setting was with the lower pressure and higher speed. Error values were high and these were associated with adding more solder paste, the stencil clogging between some prints necessitating cleaning, and the paste being too tacky, i.e. the squeegee moved upward before the paste had time to leave it. The authors highlighted that the main benefits of the experiment included familiarisation with the machine and providing a tool for adopting a structured approach to investigating the printing process, but they conceded that knowledge of the process at the experimental design stage was necessary to obtain good quality information. This perhaps explains why only a small experiment was undertaken, from which a result was selected in isolation, and then another experiment, looking at different settings, was carried out. No information was drawn from the first experiment, i.e. it was not known if the squeegee selected from the first experiment would have performed better with the parameter settings from the second experiment.

Small tests have been carried out concerning squeegee pressure and angle by one or two other workers. Bernauer [50], who mostly deals with colour work, plotted squeegee pressure in relation to free height adjustment and showed an optimal printing region at 1N/cm. A second plot indicated that the colour thickness is independent of squeegee pressure. Further printing tests show the smaller the angle, the greater the achievable colour thickness. This is particularly

** Measling diagrams are made by marking a photocopy of the stencil artwork where defects occurred on the print deposit.

noticeable as the grey scale increases. These effects of the angle were studied in greater depth by Nickel [7], who created a model for the ink stream examining flow of ink through the mesh and establishing a relationship between the paste stream, effective attack angle and the printed deposit thickness. It was noted that during printing the ink chemically attacks the squeegee and can therefore change its mechanical properties. There is a defined effective attack angle in the German Standards DIN 16 1611. Nickel used a Seri-Ragon paste, which stiffens within approximately 10 minutes, to model the bow wave and the effective attack angle. This determined that the first 1000 μm from the edge of the squeegee was the most important region. Hard and soft squeegees were found to bow differently, which was to be expected, but the author did not report the finds of this work further.

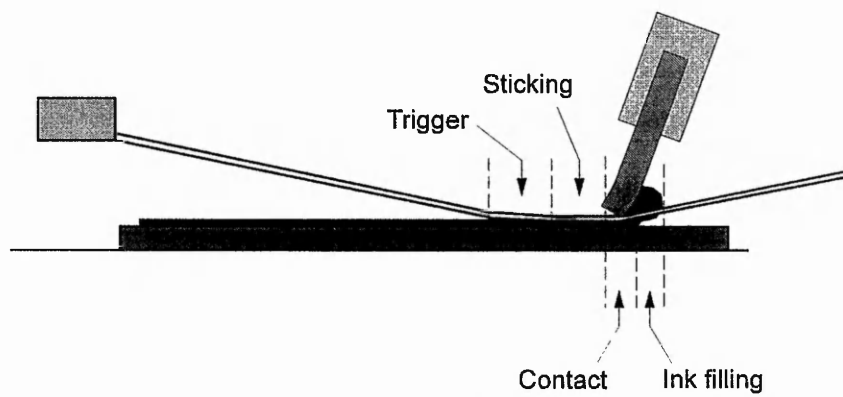


Figure 2.11 Effective attack angles and their relationship to contact areas

Nickel cut out the bow wave including the enclosed mesh strands and viewed this using a shadowgraph. From this side view it was concluded that the ink flow stages can be separated into 4 separate regions; two in front of, and two behind the squeegee as shown in Figure 2.11. In the region beneath the bow wave the ink sinks into the screen i.e. filling area. The second area is where the pressure in the ink stream squeezes the ink down onto the printing substrate. This contact area is described as being a very small but important area and was measured at 470 μm using a squeegee which was set at 75°, travelling at 0.14m/s. In the third section it can be seen that the mesh sticks to the printing substrate before the final “trigger” section forces the mesh strands away from the substrate.

Examining the ink stream shows that at the squeegee surface a high pressure area arises where the fluid velocity stagnates. The stagnation area divides the ink flow into different directions. The ink mostly leaves this area by flowing upwards vertically until it meets the squeegee surface where it flows down again, thus increasing the contact area of downward flowing ink which is then transferred to the substrate. The effective attack angle determines the distance

from the printing edge of the squeegee and the stagnation point. A large contact area will result from a more acute angle and this will then result in a thicker printed deposit. An illustration of this is shown in Figure 2.12.

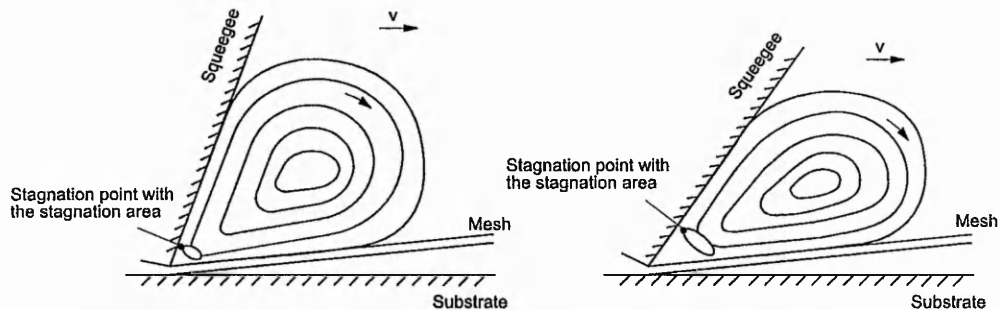


Figure 2.12 Stagnation point comparison

The aim of the solder paste printing process is always given in qualitative form e.g., Buttars [13] describes the process objective as being to “supply the solder to form the interconnections between the components and the printed circuit board. The solder should be supplied in an amount sufficient to provide both electrical and mechanical connections without producing bridging. Solder paste should only be deposited in specific areas”. This is analogous to screen printing in that the right quantity of ink should be put in the right place with the required definition of the print at the edges. The solder paste stencil design determines the volume of paste which is transferred and stencils are preferred over mesh screens as large paste particles and higher paste viscosities can be accommodated, however it is thought that screens somewhat dissipate the problem of scooping. The action of the squeegee is described as forcing the paste into the apertures and then shearing it off in line with the stencil surface. The squeegee speed must provide the correct shearing action, ensuring a good rolling action without causing a drop in the viscosity, or skipping because of insufficient time to fill the aperture.

Buttars recommends that experimentation is used to achieve optimum squeegee speeds, stating that it should be somewhere in the region of 0.02-0.15 m/s, more commonly around 0.05-0.07 m/s. As a rule of thumb, the maximum snap off should be set not exceeding ten times the stencil thickness. The required squeegee pressure is dependent on the squeegee speed; an increase in speed will require a corresponding increase in pressure to ensure that paste completely fills the apertures. Excessive pressure causes scooping and it may also cause the stencil to move slightly resulting in smearing. Again a rule of thumb for setting the pressure is applied: first set the desired snap off, then lower the blade until the stencil comes into contact

with the substrate and keep applying load until the squeegee passes over the print pattern leaving no residue. It is known that varying the pressure can cause a variation of $\pm 50 \mu\text{m}$ of the stencil thickness. The optimum pressure range will be somewhere between 0.1 and 1 kg per linear centimetre of squeegee. The angle is generally set between 45 and 75° from the stencil. Harder squeegee material is recommended for higher paste viscosities, but these are less accommodating of surface irregularities which can occur naturally on printed circuit boards (PCB's) and may be present on other types of substrate. Softer squeegee materials will cause scooping. High viscosity pastes produce sharper prints, but require more of a shearing action to print. Low viscosity pastes are easier to print but have more of a tendency to slump. Viscosities below $650\text{Pa}\cdot\text{s}$ are considered low and those above $1000\text{Pa}\cdot\text{s}$ are considered high in solder paste printing. Tackiness should be high enough so that the paste prefers to adhere to itself rather than the walls of the stencil.

A later paper by Buttars [51] repeats the discussion in his first paper, adding that the stencil aperture aspect ratio should be 1.4 or greater. The recommended squeegee hardness is greater than 90° A Shore Hardness, and the paste viscosity for fine pitch applications is quoted to be best between 850 - $1100\text{Pa}\cdot\text{s}$, but this is not substantiated by any test work. He has also changed the recommended pressure to between 0.1 and 0.3 kg per linear centimetre of squeegee.

The practical function of the squeegee is described in an anonymous paper [52], where definitions are given regarding: squeegee holder, blade, dimensions (thickness or width, height, free height, length), edge, profile, sharpness, durometer, set squeegee angle, effective squeegee angle. Criteria for selecting a squeegee are proposed as: durometer, profile and edge profile i.e. sharpness. These categories are split further, based on their shape and when sharp or not sharp. Hard squeegees are thought to transmit more force, whilst adapting less to the surface than soft ones. Bevelled profiles give maximum adaptability and a greater change is seen in the relationship of the set angle in comparison with the effective attack angle. Sharper edges are known to give thinner deposits. The selection criteria are outlined but it is noted that it is only a rough guide and that the other process parameters must then be considered once the right type of squeegee is selected for the application.

The Screen Printing Technical Foundation (SPTF) have produced some very useful and interesting work over the last 10 years. Their work is based on extensive trials of industrial products and experimental techniques. One of the studies [53] estimates ink heights. Four of the formulae currently used by industry are as follows:

1. The higher the mesh count the lower the deposit

2. Theoretical Ink Volume $V_{th} = \frac{M_0^2 \times F_t}{(M_0 + D)^2}$

3. $I_h = F_t \times (\%A \div 100)$

4. Frescka $I_h = (1.82 \times D) \times (1 - M_C D)^2$

where

I_h = Estimated Ink Height

F_t = Fabric Thickness

$\%A$ = Percent Open Area

(calculation $(1 - M_C D)^2 \times 100$)

D = Thread Diameter

M_C = Mesh Count

M_0 = Mesh Opening

The main assumption in industry is that a higher mesh count will give a thinner deposit, but this is shown to only hold true for mesh counts up to 100T, after which there is no link between mesh count and ink deposit. Stencil effects have been ignored. The remaining three formulae produced comparable results but varied from actual deposit thicknesses by up to 10µm in places.

SPTF have evaluated dimensional changes which become apparent once the mesh is tensioned and used them to develop a mathematical model by calculating the total volume of a mesh cell and then extracting the volume that the threads took up in that space. This method provided a factor for estimating the ink height which varied by a maximum of 5µm on only two mesh counts whilst all the other mesh counts were within 2µm. This factor was split into three different categories: plain weave meshes with mesh counts between 43 and 130T; plain weave meshes with counts higher than 140T; and twill weave meshes. SPTF have defined the variables which affect the printed deposit as primary (e.g. mesh, ink, substrate and stencil) and secondary (e.g. squeegee pressure, angle, speed, durometer, free height and snap height) parameters. These estimates only involve the primary group and thus make no reference to the actual machine settings used. However, there is a warning that the secondary group will affect the deposit and that the estimates should serve only as information to be borne in mind when setting up the process. The SPTF Ink height estimation formulae are laid out in Table 2.2

Table 2.2 SPTF Ink height estimation formulae

Mesh weave	Mesh count	Estimated Ink Height Formula
Plain	43-130T	$0.285 \times Ft^*(\mu\text{m})$
Plain	$\geq 140\text{T}$	$0.35 \times Ft^*(\mu\text{m})$
Twill	All	$0.31 \times Ft^*(\mu\text{m})$

* The fabric thickness should be measured at tension

SPTF also carried out an experiment, a half fractional factorial whereby five factors were examined: squeegee durometer, ink viscosity, squeegee pressure, stencil thickness and squeegee brace. The experiment was evaluated using different areas of the print as the response criteria. In the first part the wet deposit in open areas was measured. The significant factors came out as being viscosity and brace interaction which contributes 40.35% of the variation. The other factors were found to contribute much less to the variation: pressure (12.53%), durometer and stencil thickness (12.53%), durometer and viscosity (11.20%), and pressure and brace (7.11%). Increasing the pressure decreased the deposit thicknesses which was attributed to the squeegee penetrating deeper into the mesh removing a portion of ink. This result is in agreement with that of Brown [47], who also showed that an increase in pressure gave a decrease in deposit thickness.

The squeegee durometer and stencil thickness showed a process interaction which could not be explained. The 15 μm capillary film with hard squeegee gave smaller deposits than those produced with the soft squeegee, but the 25 μm film produced thicker deposits with the hard squeegee. There was only a 1 μm difference in the deposit produced with both capillary films. This could have been due to natural variation and was not explained, but depending on the size of the stencil aperture the soft squeegee may have had room and time to get inside and scoop some ink out, or the soft squeegee hydroplaned, or the aspect ratio was much greater.

An interaction was also present between the squeegee durometer and viscosity. A low viscosity and hard squeegee produced higher deposits, and the argument put forward to explain this was that the hard squeegee glides over the mesh, creating more shear stress. This allows more ink to pour through the mesh whereas, the soft squeegee dips in to the mesh apertures and removes some ink. A thicker deposit was produced using a high viscosity ink with a soft squeegee. SPTF proposed that the thicker viscosity exerts greater force on the soft blade causing it to ride up, resulting in less deposit, but hard squeegees overcome this resistance producing thicker

deposits. The overall analysis showed that in mesh open areas the change in the five parameters resulted only in a deposit variation of $2\mu\text{m}$ thus the mesh was the most influencing factor, disregarding the stencil.

Re-analysing the results for wet ink analysis in small image areas, the contributory factors to variation changed considerably. Stencil thickness was most important, 56.45%, then viscosity and pressure, 15.56%, viscosity and brace, 6.19%, pressure and brace, 4.27%. The viscosity and pressure interaction was interesting; low pressure and low viscosity gave a low deposit ($23.1\mu\text{m}$) and low pressure and high viscosity gave a higher deposit ($25.3\mu\text{m}$). High pressure and low viscosity gave a higher deposit ($24.1\mu\text{m}$) whereas high pressure and high viscosity gave a lower deposit ($22.2\mu\text{m}$). This does, however, show that increased pressure gave an increased deposit height for thicker inks, denoting that thicker inks are more sensitive to pressure changes. The ink deposit this time was found to increase with pressure, the converse to what has been discussed above.

Further analysis is abandoned as, to quote the author, "more questions were raised than answered by the experimentation". A final note was given as a general guideline for the printer:-

- | <u>To increase deposit</u> | <u>To decrease deposit</u> |
|------------------------------|------------------------------|
| • Increase stencil thickness | • Decrease stencil thickness |
| • Use higher viscosity ink | • Use lower viscosity ink |
| • Use low pressure settings | • Use low pressure settings |
| • Do not use a brace | • Use a brace |

Other experimentation undertaken examined 0.05mm (2 mil) image resolution. Better resolution was obtained using lower viscosity and pressure. Larger stencil thicknesses required greater pressures. The effects of high tension on the ink deposit [14] were established by undertaking a full factorial analysis of three snap heights, three pressure settings and four mesh tension values. The tension itself did not significantly affect the deposit. The biggest contribution was from the squeegee pressure and snap height interaction followed by pressure and mesh tension interaction then snap height and finally mesh tension. The maximum variation at 10N/cm was $2.28\mu\text{m}$, at 20N/cm it was $1.12\mu\text{m}$, at 30N/cm it was $1.56\mu\text{m}$ and at 40N/cm it was $1.16\mu\text{m}$. Another interesting point shown in this study is that the deposit thickness did not continue to decrease with higher mesh counts above 100T mesh, at which the curve flattened out considerably and all the deposit heights were between $15\text{-}17\mu\text{m}$. Deposit

variation also occurred when using different manufacturers' meshes [9], e.g. Saati Hitech 305/40LE performs very differently to a 305/40LE from International Fabric Corp-PES.

Due to its importance, a complete paper on controlling the off-contact [54] was also published by the SPTF. The off-contact distance is defined as being the "necessary small space to keep the screen from adhering to the substrate". Peel-off is separate to the mesh peeling away behind the squeegee and is defined as the frame gradually moving upward during the print stroke. 1-3mm are cited as being common distances but some are as high as 12mm. The drawbacks of high off-contacts are poor print quality and registration. The lower the off-contact the better, as increased pressure will be required to overcome greater off-contact distances. The screen tension should be set at the maximum level which can be achieved comfortably: rule of thumb is 18-25N/cm. Methods of controlling snap height are crude to say the least, shimming the frame at the corners being typical. Some machines provide adjustments but many without any calibration, and others are simply so far out in terms of accuracy they might as well not be there at all. SPTF has developed an electronic gauge for this purpose, but it is not widely used in industry.

2.2 Summary

Some fundamental early work has been carried out using fluid mechanics relating hydrodynamic pressure to image distortion, speed and viscosity; examining mesh and squeegee parameter effects on the printed deposit; and determining laminar flow. The early work was useful examining hydrodynamic pressure and explaining the role of the squeegee as a control device with respect to hydrodynamics. Initial efforts are disjointed, examining potential avenues of exploration but suffering from the complexity and wide range of variables.

Later work again examined a large range of related topics, especially Riemer who covered geometrical models, hydrodynamics, mesh peel off and sticking behind the squeegee, but the work was split into distinct groups:

- Hagen-Poiseuille flow
- In-plane permeable bearing treatment
- Cantilevered trailing blade system
- Pressurisation regions

Unfortunately, none of the authors had seen the work of the earlier studies and furthermore were not aware of each others work in every case. Important points are drawn out, though, and these include suggestions regarding mesh wetting resistance in relation to optimum print parameter settings, conceptualising squeegee behaviour in terms of fluid versus elastic forces, minimum boundary conditions relating to the ink roll and other model constraints associated with the ink flow and areas of maximum pressure. The main area of investigations can be narrowed down as being hydrodynamic properties and all the areas point back to squeegee and mesh effects as being key areas.

The semi-analytical methods provide useful information regarding the trends of squeegee parameters with respect to the final printed deposit, but the relationships have never been used to provide clear guidelines as to how the process reacts under certain conditions. The next chapter will concentrate on determining the extent of usefulness of these methods.

Models to date are controversial and insufficient information is available to allow any of them to be applied in practice. This indicates that further work is required to substantiate them. In this work Huner is examined in further detail, where the squeegee is treated as a cantilevered beam operating in hydrodynamically lubricated conditions. This was selected in preference to the theory whereby the process is governed by Hagen-Poiseuille flow as this was thoroughly cross examined by Huner, disputing the Taylor flow solutions and the basic assumption that the mesh apertures are longer than they are wide. The work of Owczarek & Howland could also have been examined in more depth but their work assumes knowledge of the squeegee penetration height into the screen or the equivalent paste flow height beneath the squeegee. The authors describe a method to obtain both of these, but the techniques are questionable and could not successfully be reproduced for the purposes of this work.

Chapter 3 Process Control Using Factorial Experiments

3.1 Introduction

The literature review highlights the lack of information related to controlling the screen printing process. Furthermore, the initial set up of the process is not easy: the engineer is completely reliant on his experience and information from mesh, squeegee and ink suppliers. The supplier information is reasonably useful but does not explain how the product will relate to the other components of the process. The logical approach, based on the fact that there is no complete working model at a fundamental level, is to analyse the process using experimentation. The objectives of this experimentation are to:

- gain an understanding of the process
- determine how changes in the parameter settings will affect the printed deposit
- establish the optimum settings

The overall aim should be to map the process so that it operates as illustrated in Figure 3.1.

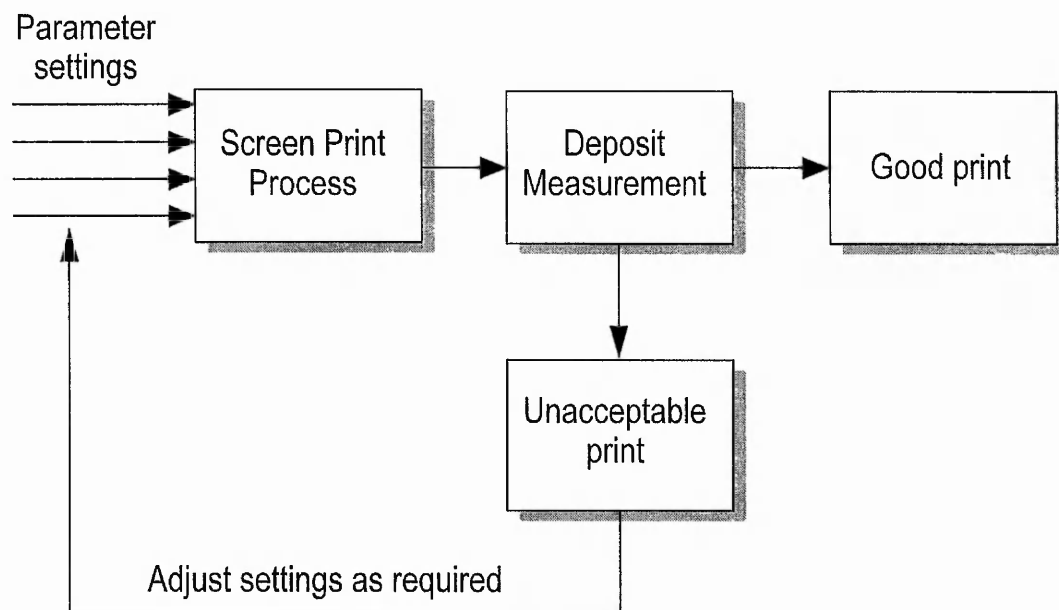


Figure 3.1 Mapping the screen printing process

To operate in the format as described above it is of course necessary to know exactly how any adjustments which are made to the process will affect the performance. This information, however, is not available and thus the experimental approach is adopted to establish these relationships. The framework for an experimental approach is outlined in Figure 3.2.

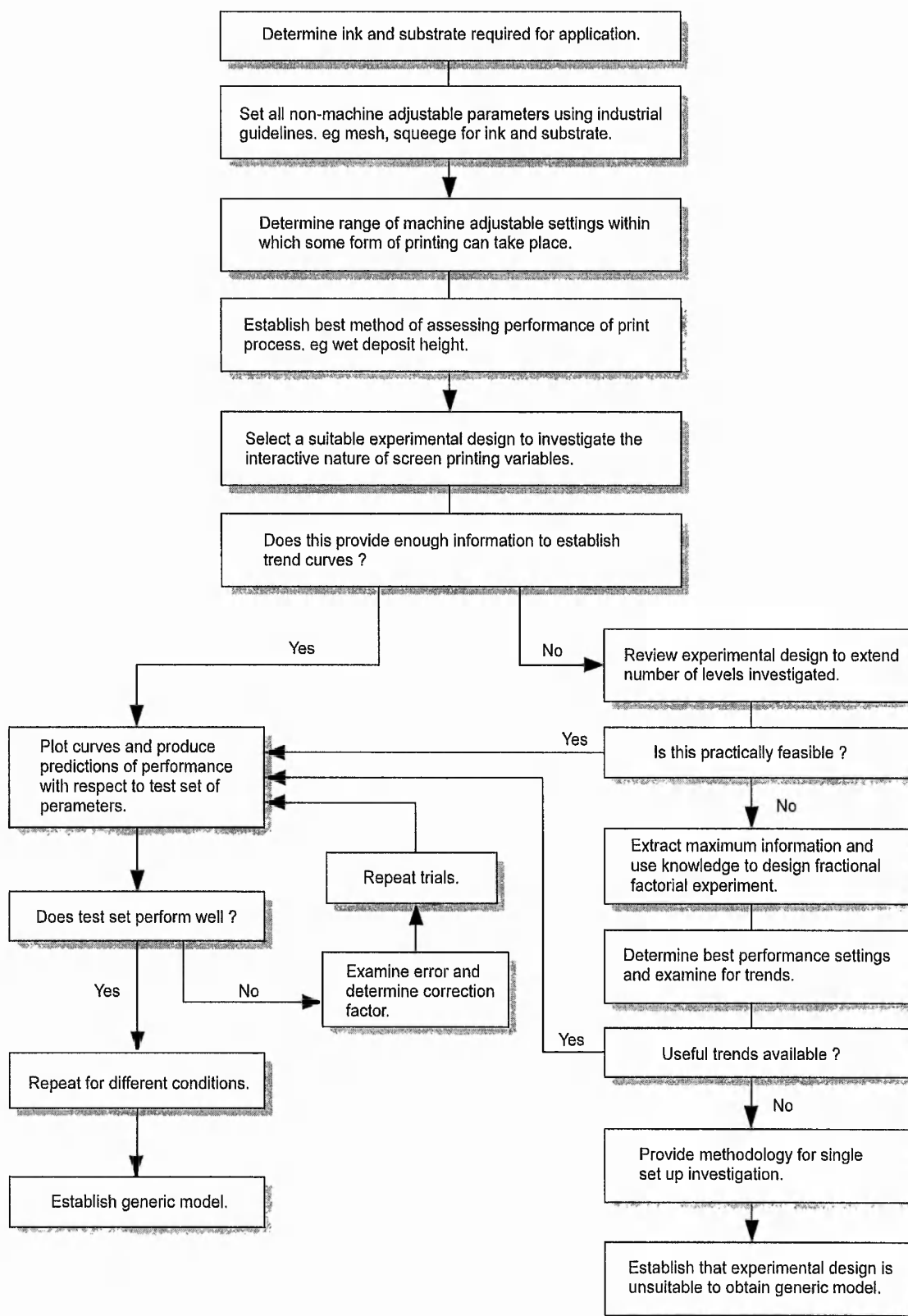


Figure 3.2 Framework for an experimental approach

The response variable is dependent upon the type of screen printing which is being carried out, but for the purposes of this work only the deposit height will be considered. This is also subject to controversy as deposit heights and their related measuring techniques are known to vary considerably [55], [56] and the methods adopted here are outlined in Appendix 3.1.

3.2 Selection of factors for experimentation

As detailed in Chapter 1, section 1.1 the supplier's details can be used to select the mesh to match the ink and generally a squeegee and stencil system which is suitable for a particular mesh type and print definition will be recommended. Many of the other variables will be determined by default, e.g. customer-specified substrate, and most can be accounted for by the fact that they are constant parameters. Thus, by process of elimination, the essential parameters which need to be investigated initially are the main machine- adjustable parameters: squeegee speed, squeegee load, squeegee angle and snap height. It could be argued that the flood parameters should also be accounted for, but as it is possible to print without using a flood blade these will be ignored.

3.3 Choice of experiment design

Over the last ten years the benefits of fractional factorial experiments (see Box [57]) have been popularised by Taguchi [58] and others [59]-[61]. There is much controversy surrounding the use of these techniques and they have been heavily debated [62],[63]. It must be made clear that although fractional factorial experiments (FFE) can be very useful for eliminating lengthy and impractical testing, their use is limited to process optimisation once the process has been well set up in the first place. The bottom line for this type of experiment is that the process must be very well understood before FFE's can be applied. The main reason for this is that a compromise is made in the form of loss of degrees of freedom, which in full factorial experiments would have given information about any interactions between process parameters. This information can be extremely useful, and in the case of screen printing is probably vital due to the interdependent nature of the process variables.

Table 3.1 Full factorial experiment: 3 factors at 2 levels

Column no.						
1	2	3	4	5	6	7
A	B	AxB	C	AxC	BxC	AxBxC

Table 3.2 Fractional factorial : 4 parameters at 2 levels

Column no.						
1	2	3	4	5	6	7
A	B	AxB	C	AxC	BxC	AxBxC
BxCxD	AxCxD	CxD	AxBxD	BxD	AxD	D

The real danger with FFE's for screen printing is that when the interactions are traded off for smaller size experiments, they are not lost but could be compounding the main effect in another column. An example of this is illustrated in the tables above. Table 3.1 is an L8 array at resolution 4 (source: table 3-14 p.81 Ross [64]). It is a full factorial with 3 parameters at 2 levels, and each factor, i.e., parameter, and interaction have been assigned to an individual column. However, in Table 3.2, 4 factors at 2 levels have been assigned and immediately it can be seen that the columns are now confounded. For example, column 1 could be the main effect of parameter A, or it might show an interaction of parameters B,C and D. For most processes a 3 level interaction, or higher, would not occur, but in screen printing, the angle and the pressure are normally found to be inter-related and the speed of the squeegee will affect the ink's shear rate, therefore it is possible that higher levels of interaction may be present. Thus, the results from fractional factorials could be very misleading. It should also be borne in mind that fractional factorials are best for well established processes which only require fine tuning [63].

The conclusion is that if the process variables are as interactive as described by Hohl [65], Molamphy [6], Brown [47], then the only feasible experiment is a full factorial. To confirm the interactive nature of the process a full factorial experiment was carried out.

3.4 Determining screen print process behaviour using full factorial experiments

Full factorials are extremely large experiments, even when assessing processes, such as screen printing with only four parameters. The number of trials in the experiment is determined by the number of levels which are to be tested, L , as a power of the number of parameters or factors, F , to be investigated. In this case there are four variables to be considered: snap height and the squeegee variables: pressure, speed and angle, and these will each be tested at three levels. Therefore $F=4$ and $L=3$ so the number of trials is given by $L^F = 3^4$ i.e. 81. However, to gain a reasonable confidence level it is necessary to repeat each trial at least twice, preferably four times, but as it takes an hour to carry out twenty trials and an hour to measure fifteen individual deposits, repetitions greater than two would be impractical within a reasonable time scale. The size of the experiment is denoted by an array L81. Three levels were chosen to give high, medium and low values, but it should be noted that these were not set at the extremes of the machine parameters. The settings are given in Table 3.3.

Table 3.3 Parameter settings for full factorial, 4 parameters at 3 levels

Parameters	A Snap height (mm)	B Angle (°)	C Speed (m/s)	D Load (N/m)
Level 1	1	60	25	48
Level 2	3	65	40	56
Level 3	5	70	55	63

The mesh used was 120T yellow dyed low extension mesh tensioned at 140N per linear metre. The squeegee was 70-75°A shore hardness and the ink was blue dielectric 40-516. The stencil was 30µm capillary film. During the experiment the temperature was between 21 and 22°C at a relative humidity of 53%. The experimentation was carried out on a modified Svecia printing machine. The machine has been developed to run using a programmable logic controller (PLC). A proximity encoder controls the squeegee speed and position. A closed loop electro-pneumatic controller regulates the pressure via the PLC to provide the advantage of automatic pressure compensation, thus ensuring a constant pressure is always maintained. Calibrations of the speed and squeegee load (or pressure) applied are given in Appendix 3.2. Squeegee angles were set at graduations using the horizontal plane as the reference. The snap height was set at fixed points on the frame edge using slip gauges.

3.5 Experimental Results

The order of experimentation and the results are in Appendix 3.3. Appendix 3.4 shows the analysis of variance and the resulting percentage contributions are shown below in Figure 3.3.

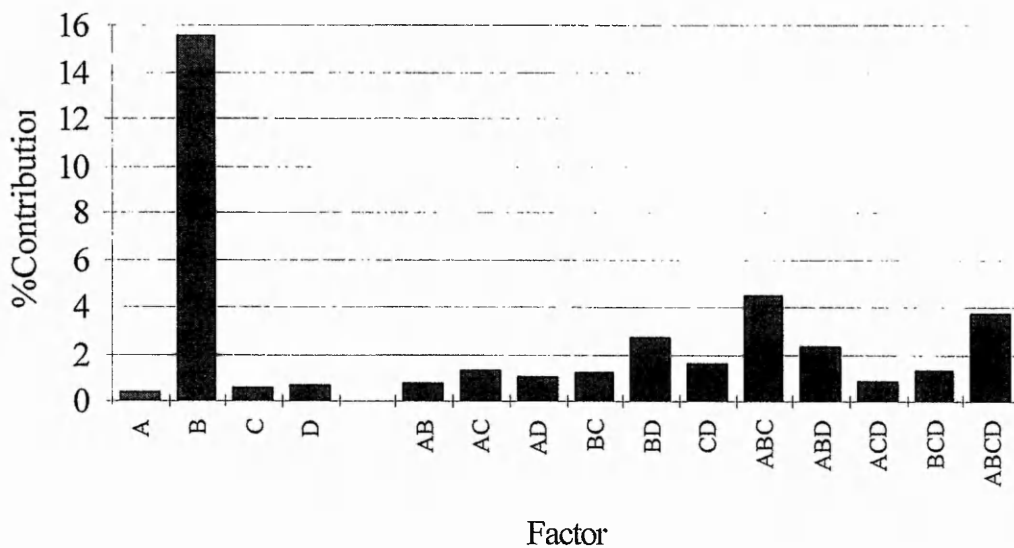


Figure 3.3 Percentage contribution of screen print parameters

These results demonstrate that apart from the angle, B, the individual main effects have little contribution to the process in comparison with the interactions. The three factor interaction of snap, angle and speed is the second highest contributory factor to variation at 4.48% and the

interaction of all four factors comes a close third with 3.72%. All of the two and three factor interactions have higher contribution than the three remaining individual factors.

The F-ratio determines the level of confidence of the testing, by taking the mean sum of squares (MS) for the individual factor and dividing it by the sum of squares of the error. Unfortunately only the main interaction of B gives a confidence level of greater than 95%. This highlights another source of error with this type of experimentation. This result means that the error within samples is large with respect to that between samples. On closer inspection of the variation within and between samples from the results shown in Appendix 3.3, it can be seen that the maximum variation between samples was 41.21% and the variation within samples was 25.59%. This is the main reason why confidence levels are at less than 95%. However, from Figure 3.4, it can be seen that for 66 out of the 81 samples (81.5%) the repeatability is better than 10%, and 75 out of 81 (92.5%) are under 15%, with just 6 (7.5%) giving unacceptable levels of variation.

This variation can be attributed to the method of deposit measurement used which is susceptible to errors of up to 19%, as illustrated in Appendix 3.5. Due to the quantity of trials necessary to perform such a large experiment it was not possible to scan complete areas and thus single profile scans were used to measure the response variable i.e. deposit height.

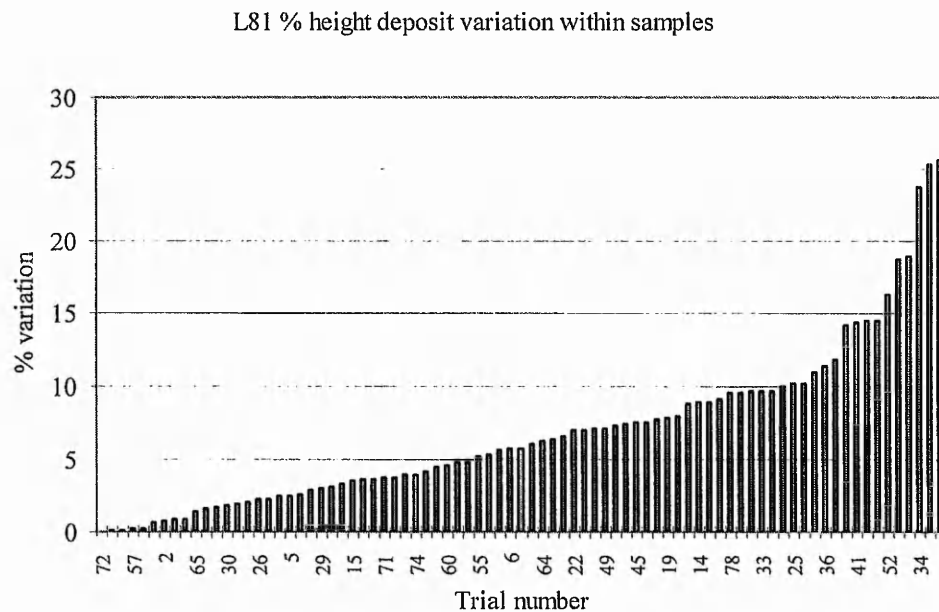


Figure 3.4 Percentage height deposit variation within samples

Further analysis of the experimentation is limited. It is possible to sort the data into individual groups and plot angle against snap, angle against pressure and angle against speed. This can then be repeated for each of the other combinations. But considering the high order interactions present this only provides information regarding any two variables at once, and also from the design of the experiment there are only three points available for each graph, an example of which is shown below in Figure 3.5.

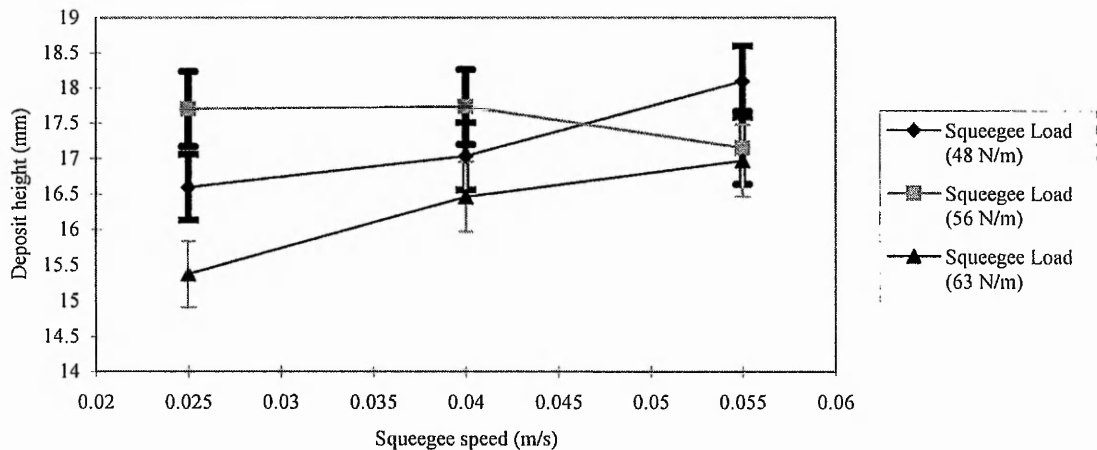


Figure 3.5 Interaction graph of speed and pressure at an angle of 70° and a 1mm snap height setting

A great deal of work is required for very little information. From the full factorial experiment it is possible to show that the angle alone is the most significant parameter followed by three, four and two level interactions. These results can be compared in the broadest sense to findings by Brown [47], who states that as the squeegee speed is increased so is the deposit thickness. However, Brown showed that an increase in pressure resulted in a decrease in deposit height, whereas this experiment showed that, depending on the speed, higher pressure caused an increase in height followed by a decrease in height as the pressure was increased further. At a different angle setting, as illustrated in Figure 3.6, the inverse pressure and thickness relationship is more closely followed again, up to the point where the pressure and speed are highest at which the lowest deposit height is found to occur. Brown's work ignores the effect of the angle entirely.

The Screen Printing Technical Foundation (SPTF) also undertook some experimental work which showed that increases in pressure resulted in decreased ink deposit, but the experiment again did not examine changes in angle or, in this case, speed. The evidence points to the fact that the squeegee is effectively scooping the ink out of the stencil aperture as the pressure is increased, but if the angle is shallower, or the speed is increased, then the hydrodynamic effects take over, allowing the squeegee to clear the top of the mesh asperities until the point is reached where the pressure overcomes the hydroplaning and the squeegee lift due to this is prevented. Above this pressure limit the squeegee then scoops the ink out of the apertures resulting in lower deposits.

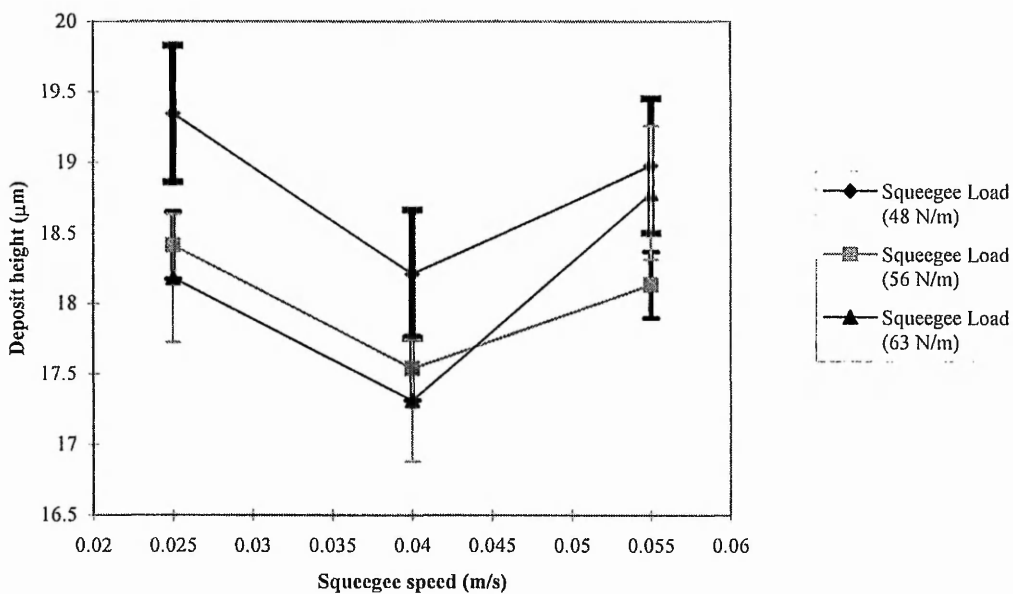


Figure 3.6 Interaction graph at snap height 1mm and angle 60°

In conclusion, it may be said that full factorial experiments are too time consuming to allow sufficient gathering of information regarding the response variable or enough replicates of each trial to ensure high confidence levels. An L81 experiment is relatively speaking very large and it has only provided a small amount of information. More importantly, it is apparent that high order interactions are present in the screen print process and therefore it is not possible to make general statements about the process, as each setting will give different responses depending on where the other parameters are set. This is also confirmed by Mitchell et al [42]. Using full factorials thus has limited use, and for setting up the process using experimental techniques the only possibility is to use fractional factorials in a strategic approach, whilst compromising process understanding and being aware that compound effects will be present.

3.6 Fractional factorial experiments

Fractional factorial experiments can be used to determine the approximate settings which can be used to obtain a satisfactory print deposit. This approach is outlined as follows. Firstly, a fractional factorial is selected which allows the required number of parameters to be investigated using several levels set at as wide a range as possible. In this case the same four parameters as mentioned in the last section were selected. An L25 was selected as it allows 6 factors at 5 levels to be tested. The first and second factors have been set at dummy levels, i.e., they were kept constant throughout the experiment. The settings for this experiment are given in Table 3.4. This experiment was carried out using the same mesh and squeegee as in the previous experiment. This time three replicates were taken; the first was measured immediately after printing, whilst the second two replicates were measured 24 hours later. The order of experimentation and the results for the replicates are given in Appendix 3.6. Each trial was identified by the slide number (slide #) and the repetition of each trial was labelled a, b and c respectively.

Table 3.4 Fractional factorial experiment: 4 parameters at 5 levels

Parameters	Snap (mm) D	Angle (°) C	Load (N/m) E	Speed (m/s) F
Level 1	2	50	44	0.025
Level 2	6	65	53	0.065
Level 3	5	74	63	0.090
Level 4	4	60	73	0.130
Level 5	3	70	85	0.170

An analysis of variance of these results is given in Appendix 3.7, but it must be remembered that the main effects will be confounded with their interactions and thus it is not possible to determine whether factor F, the squeegee speed, is really of such significance or whether it is one of the many possible combinations of interactions which also occur in this column. Therefore, it cannot be stated that speed, which is assigned to column F, has more significance than snap height in column D. The only reason for carrying out an analysis of variance is to obtain an F-ratio so as to obtain a confidence level.

By pooling the least significant factor, it is possible to obtain a set of F ratios for the data as shown in Appendix 3.7. These results show that the confidence level is greater than 99.9%, which means that the error within samples is very small compared to that between samples, indicating very good repeatability.

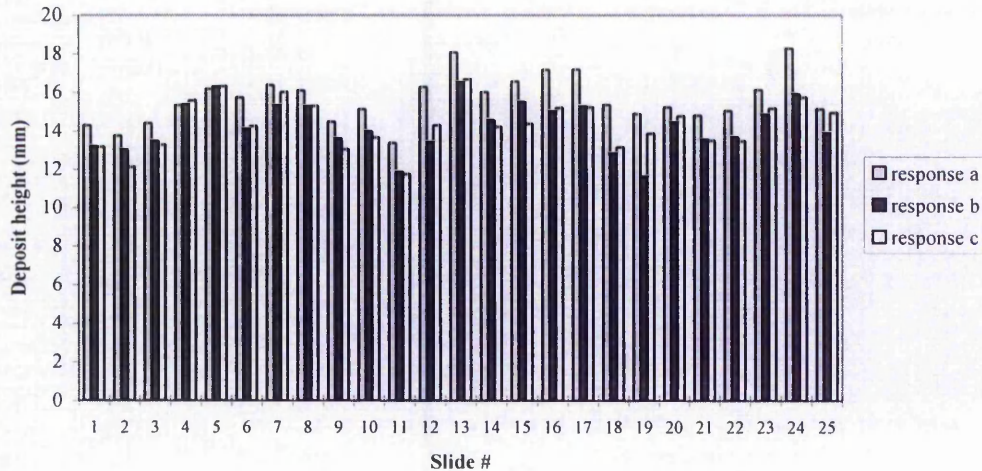


Figure 3.7 L25 results (actual deposit heights)

Plotting the actual deposit heights, as shown in Figure 3.7, demonstrates the settings which give deposit heights closest to the nominal values expected for the particular mesh used. The values of deposit height and the variation in their repeatability are given in Table 3.5.

Table 3.5 Deposit heights closest to nominal value 17.22

Slide #	response a	response b	response c	% variation
10	17.05	16.52	16.37	4.94
12	17.26	16.61	16.29	5.40
4	17.27	15.66	12.7	26.25
18	17.5	14.98	15.62	13.01
14	17.57	15.27	16.08	11.32

On evaluating the print deposits for each trial, slides 4, 14 and 18 were eliminated because the repeatability was so poor. Thus, only the settings of trials 10 and 12 remain as being appropriate. This, however, does not help to explain the process because the parameter settings for these two trials, apart from the angle, are not very closely related, as shown in Table 3.6. Perhaps it is possible that there is more than one combination of settings which will provide an optimum result. This is possible due to the interactive nature of the variables demonstrated in the first experiment (L81).

Table 3.6 Experimental setting for trials 10 and 12

Slide #	Snap (mm)	angle (°)	load (N/m)	Speed (m/s)
10	6	70	73	0.025
12	3	70	85	0.170

If this is the case, then the deposit profiles should be of a good shape for the print deposits obtained on both slides 10 and 12. These are depicted in Figure 3.8.

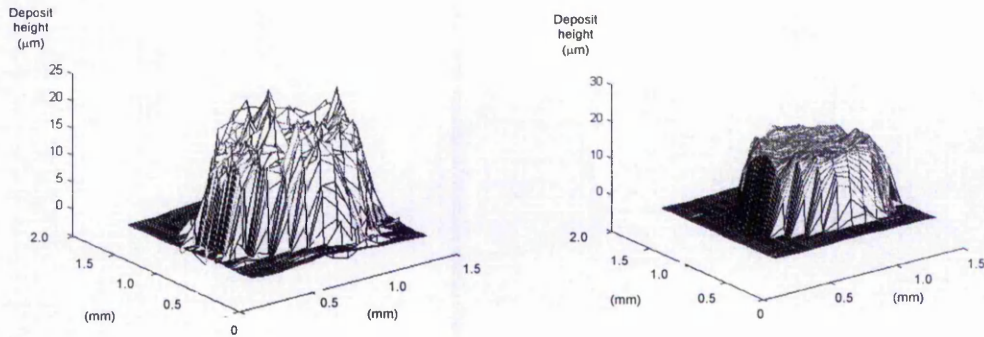


Figure 3.8 Deposit profiles of slides 10 (left) and 12 (right)

As can be seen the deposit for slide 12 is much more uniform than the deposit for slide 10. Thus it can be concluded that out of the parameter levels selected for this experiment, those for slide 12 were the best. This is not to say that these are the optimum for the process as it is impossible to predict the outcome had the settings been set in the middle of the levels selected as these variables are discrete. A separate test would be required to investigate deviations around the settings chosen. This experiment was confirmed in a repeat experiment. The Anova table and results are given in Appendix 3.8. Using the same criteria as above, i.e. $17.22\mu\text{m}$ is the nominal best height, the best heights are found to be those of profiles 16 and 17 in the repeated experiment (see below). The repeatability cannot be used to eliminate any of the results as the overall repeatability was poor.

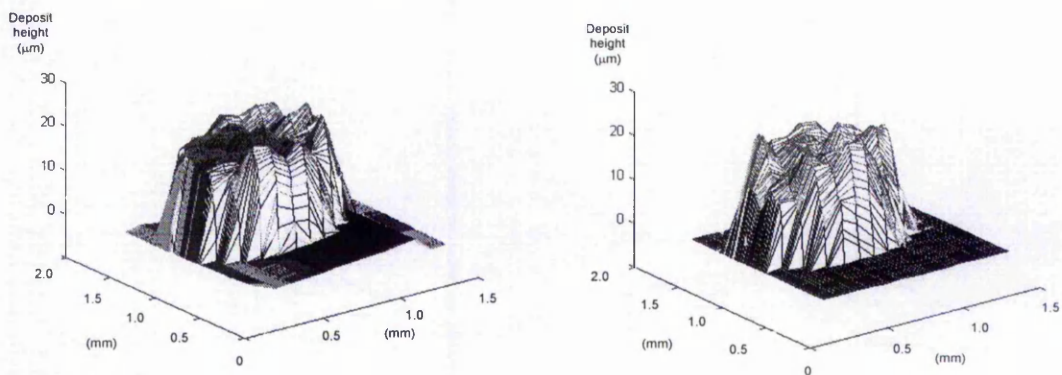


Figure 3.9 Deposit profiles of slides 16 and 17

Table 3.7 shows the prints from the repeated experiment which are closest to the nominal value. They are completely different to those of the first experiment.

Table 3.7 Deposit heights from L25t2 closest to nominal value

Slide #	response a	response b	response c	% variation
15	16.57	15.50	14.38	16.49
16	17.17	15.01	15.20	12.83
17	17.19	15.27	15.23	11.56
13	18.07	16.53	16.68	4.94

The experimental settings for slides 16 and 17 are shown in Table 3.8 below.

Table 3.8 Experimental settings for L25t216 & 17

Slide #	Snap (mm)	Angle (°)	Load (N/m)	Speed (m/s)
16	2	60	63	0.17
17	3	50	73	0.90

Thus to return to the original idea of mapping the experiment, as discussed earlier in section 3.1, this repeat experiment completely upsets the routine as not only is there no useful trend but there are actually conflicting sets of results. The settings which produced good profiles in the first experiment are completely different to those of the second experiment. Many experiments of this nature would need to be repeated for each element of the map and the initial response does not bode well for a high degree of confidence that the work would provide the desired information. In addition, further analysis, as with the full factorial in plotting individual two factor interactions, is not at all possible when using this type of experimentation because no two settings have the same values due to the fractional nature of the array.

3.7 Application of an alternative method of utilising FFEs.

Using the standard process of elimination, the above analysis cannot be used to gain any further insights into the process. However, application of a fuzzy rule based system [66] allows the deposit profiles to be sorted into 'classes' which can then be used to narrow down the possible combination of parameter settings. Once a class has been selected as providing a good deposit, smaller experiments can be set up to determine a smaller range of parameter levels which will still achieve a good print. The output from the fuzzy system showed that the best settings were 3-5 mm for snap height, 65-70° for the angle, loads at 60-68 N/m and speeds of 0.055-0.085 m/s. [This is interesting because the best samples from the L25 were at snap heights of 4-6 mm, angles of 60-74°, pressures of 52-85 N/m and speeds of 0.025 m/s and 0.17 m/s.] These settings were then used as a basis for an L9 experiment, which allows 4 factors to be examined at 3

levels each, but again no information is available on the interactions. The parameter settings are outlined in Table 3.9.

Table 3.9 L9 parameter levels

Parameter	Snap (mm)	Angle (°)	Load (N/m)	Speed (m/s)
	A	B	C	D
Level 1	3	65	60	0.055
Level 2	4	67	63	0.073
Level 3	5	70	67	0.085

This experiment used the same equipment as in the previous experiments, and the room temperature and humidity were at 25°C and 45% respectively. The results are shown in Appendix 3.9 and were all found to be within class 3. The best settings were found to be those for trials 7 & 8. To verify that these settings really were the best, both trial settings were repeated 10 times to check for variation, the results are tabulated in Appendix 3.10. The variation within the samples, at 12.81 and 10.14%, is greater than between the samples, maximum 10%, so both settings are poor for repeatability, with settings for trial 8 being slightly better. The profiles have been plotted in Figure 3.10 and Figure 3.11 in 2-D representation to give a basis of comparison between each replicate and then in 3-D format for the first replicate from each trial in Figures 3.12 and 3.13.

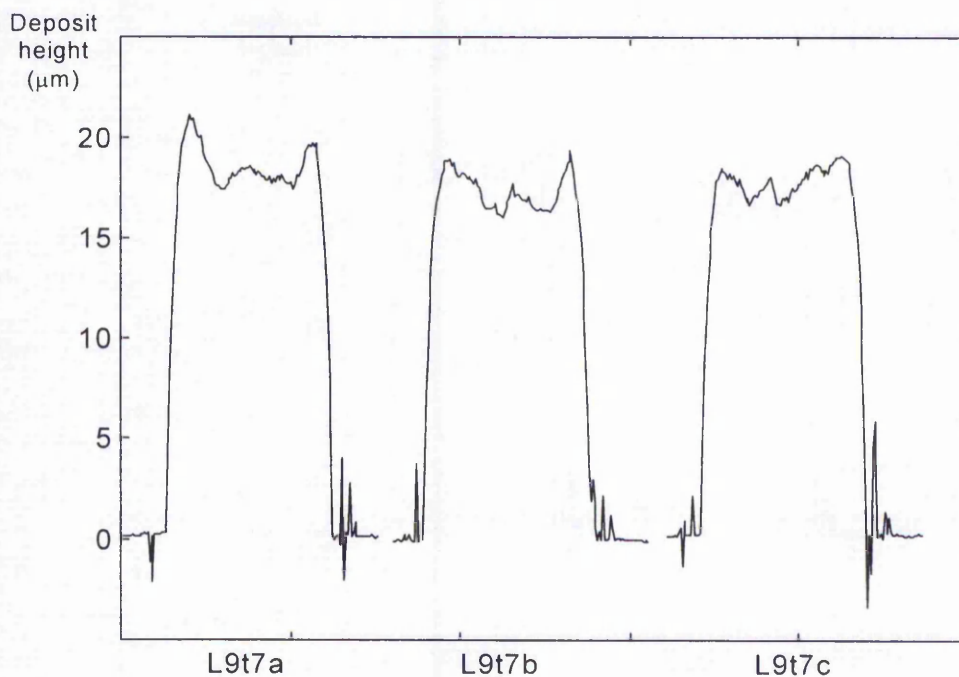


Figure 3.10 Profiles of L9t7a,b,c

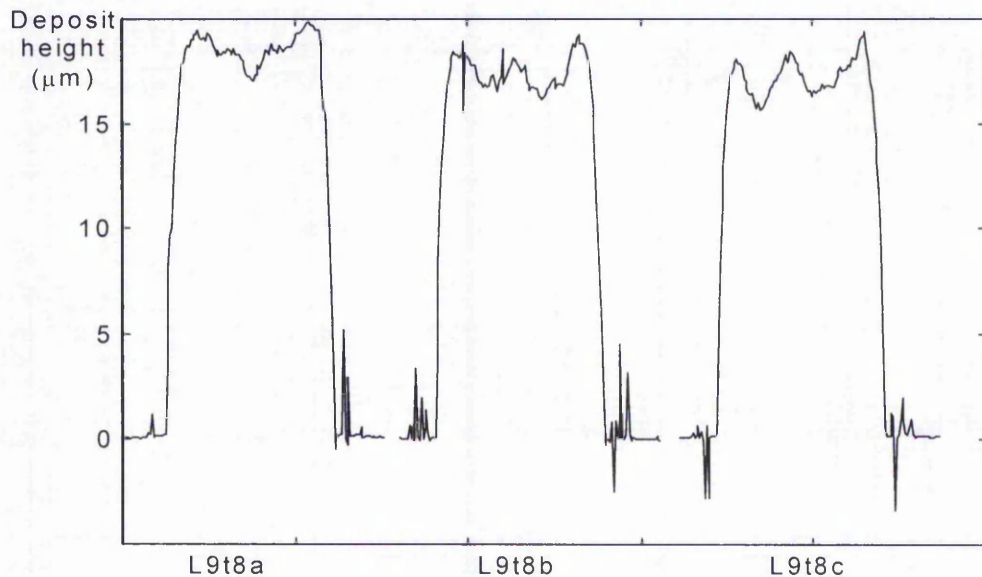


Figure 3.11 Profiles of L9t8a, b, c

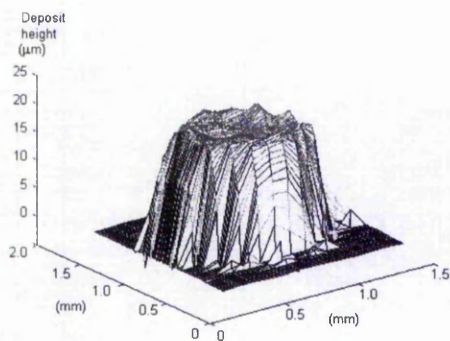


Figure 3.12 L9t7a

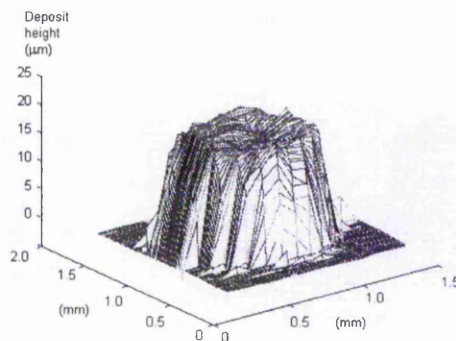


Figure 3.13 L9t8a

3.8 Conclusions

Experimentation is useful when applied in a strategic way e.g. select wide settings with a reasonably large fractional factorial and then zoom in using smaller fractional factorial experiments, but the information is limited as it is not possible to predict how a slight adjustment to any parameter will affect the process.

To gain a thorough understanding of the process, full factorial experiments are required. This would then allow the process to be set up correctly and improved upon. However, these are far too lengthy to set up and carry out, and prone to errors of nearly 20% which compromises any real benefit to a better understanding of the process. Plotting graphs to cope with the interaction is also difficult and results in confusion when trying to illustrate trends. Measurement techniques hinder the process and repeatability cannot be guaranteed due to the inherent instability of the rubber squeegee and non-Newtonian behaviour of the inks.

Fuzzy rule based systems currently being developed provide an alternative route of investigation and thus merit further work but these also do not provide an understanding of the process. Thus it must be concluded that the process fundamentals should be further investigated. This should give additional useful information on which to base a better strategy for further experimentation e.g., it may be possible to determine a narrow window of operation for one or more of the variables thus reducing the levels for a full factorial experiment. Alternatively it might explain why only full factorials can be used.

The longwinded nature and limited usefulness of this kind of experimentation has highlighted the need for a better understanding of the process fundamentals before experimental techniques could be meaningfully applied.

Chapter 4 The Process Fundamentals

4.1 Introduction

The screen printing process has thus far been described as being inadequately defined and, as discussed in the literature review section, Huner's model [29] is the nearest approximation derived to date. His work leads research in screen printing, due to the volume of publications and because of the number of ways in which he has conceptualised the process: for example, as a blade coater, a porous bearing, and now as a cantilevered plate. Unfortunately, his work is rarely commented on and none of the initial assumptions has yet been verified. This section examines Huner's latest analysis, which depicts the squeegee as a rigidly clamped cantilevered trailing blade, which forms a hydrodynamic wedge to generate a printing pressure, and relates it to practical aspects of screen printing.

To date definitive values for pressures in the ink roll have not been obtained. An attempt to establish the pressures was made by Cropper [5] in 1974. However, the ambiguity of the report prevents useful interpretation of the data, or of the experimental procedure, thus Cropper's own conclusions must be relied upon. This chapter reports on some fundamental experimentation, undertaken by the author, to measure this pressure and to obtain a rigidity value for a squeegee. A comparison is made between the actual pressures generated in the bow wave ahead of the squeegee and those predicted by Huner's theory. The results are also compared to the value of pressure found by Cropper. This section then continues by examining if these pressures are sufficient to ensure flow through the screen within the limited time dictated by the squeegee velocity, a consideration which has been ignored in the literature to date.

4.2 Examination of a rigidly clamped cantilevered trailing blade squeegee

Huner treats the squeegee blade as a wide, rigidly clamped cantilevered blade and a schematic of his representation is illustrated in Figure 4.1.

The squeegee force and angle are set by rotating the blade from the initial angle, θ_R , at which it rests on the screen, to a smaller working angle, θ_W , as shown in the inset of Figure 4.1. Huner then combines the equations for the loads required to bend an elastic plate (see [29]) with the expression he developed for finding the pressure ahead of the squeegee tip [26] to give a relationship of squeegee shape with respect to the fluid and elastic stresses within, and acting on, the ink. The fluid stresses are determined by the expression $\mu U/\ell$ and the elastic stresses are given by D/ℓ^3 , where μ is the fluid viscosity, U is the squeegee speed, and ℓ is the horizontal

distance to the point at which the squeegee tip first makes contact on the screen ($\ell \cong L \sin \theta_R$, $L =$ length of trailing blade). D is the flexural rigidity of the squeegee given by $D = \frac{Eh^3}{12(1-\nu^2)}$, where E is Young's modulus, h is the squeegee thickness and ν is Poisson's ratio for the squeegee.

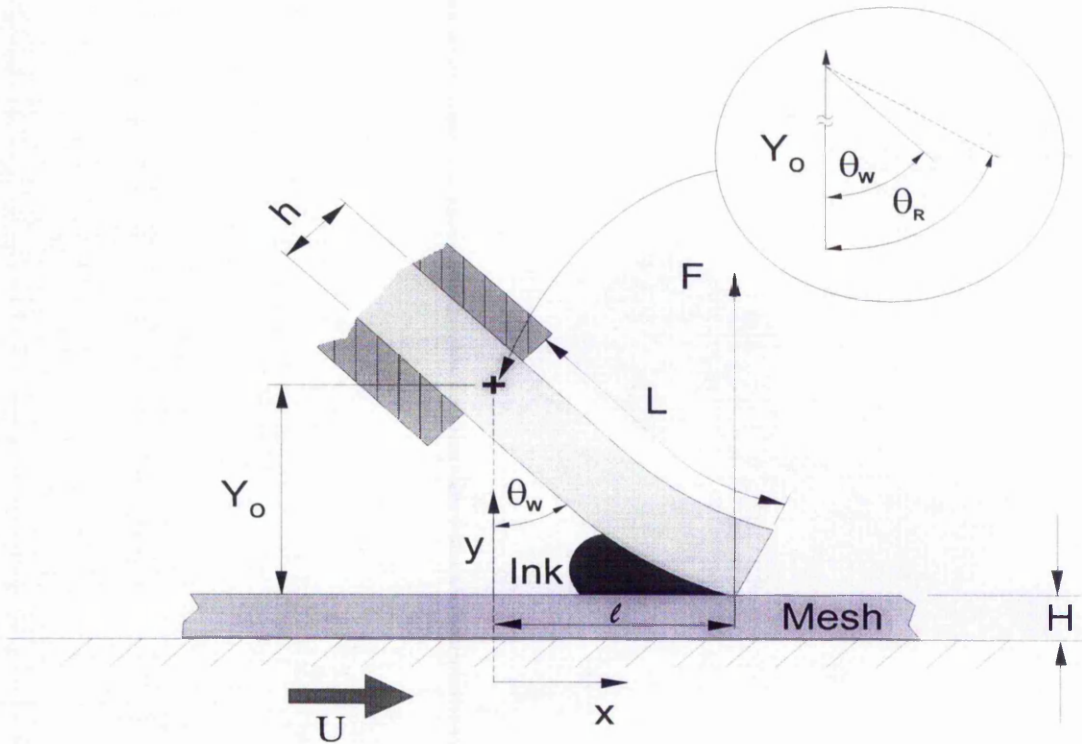


Figure 4.1 Huner's trailing blade squeegee system

Huner then argues that the ratio of $(\mu U \ell^2)/D$ will determine whether elastic forces or fluid forces are dominant. If the ratio is very much greater than 1, then fluid forces dominate, if they are very much less than 1 then the elastic forces dominate.

4.3 Elastic forces

Huner provides an equation to allow the net flow of fluid past the squeegee tip to be calculated. The unstated assumption here is that if the system allows the flow to be consistent, then the ink deposition must also be consistent. Huner derives an equation to determine the squeegee shape when neglecting any influence of the fluid as outlined in Equation (4.1), and the solution to this equation is given in (4.2).

$$\frac{d^2uy}{dx^2} = \frac{F}{D \sin^3 \theta_R} (\ell - x) \quad (4.1)$$

the co-ordinates for any point (x,y) on the centreline of the deformed squeegee blade are related by:

$$\frac{y}{y_0} = \frac{FL^3}{2Dy_0} \left[\left(\frac{x}{\ell} \right)^3 - \left(\frac{x}{\ell} \right) / 3 \right] - u \left(\frac{x}{\ell} \right) + 1 \quad (4.2)$$

and the contact force at the squeegee tip is given by

$$\frac{FL^3}{3} Dy_0 = (u-1)$$

where $u \equiv \tan \theta_R \cot \theta_w$, which is effectively a non-dimensional measure of load with $u = 1$ representing zero loading and $u = 6$ representing a load which heavily deforms the blade.

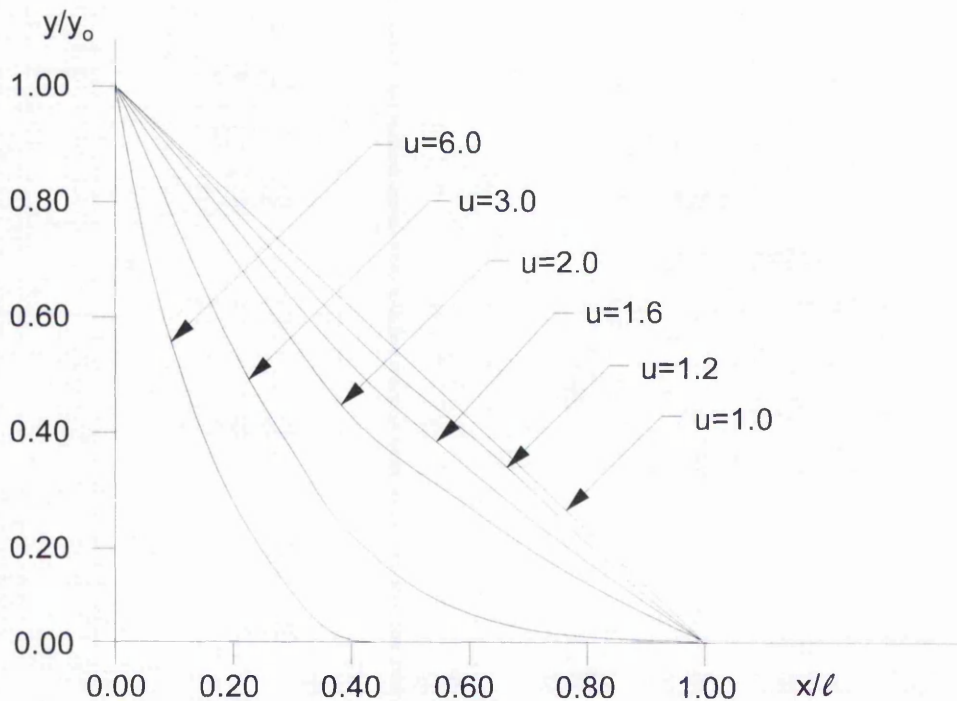


Figure 4.2 Huner's predicted squeegee shape

To verify that the calculated squeegee shape from Equation (4.2) as illustrated in Figure 4.2 was correct, a comparison with experimental data for squeegee bending was made. It was necessary to do this experimentally because calculating a value for the flexural rigidity of rubber proves difficult as Young's modulus is hard to define.

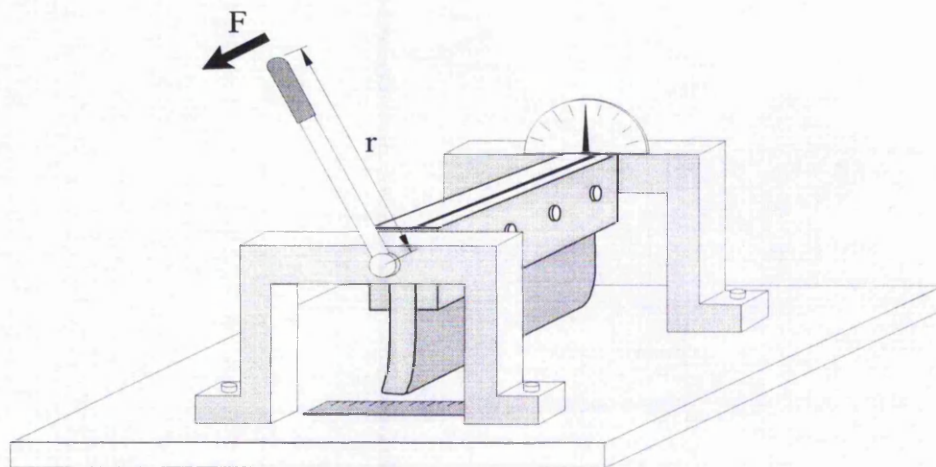


Figure 4.3 Test rig to determine squeegee bending characteristics

A test rig was set up as shown in Figure 4.3. The squeegee was clamped in a specially designed holder, which allowed free rotation to any angle and adjustment of height to accommodate different trailing lengths of squeegee. The squeegees tested had a trailing length of 53 mm and the rig was adjusted so that it came to rest at an angle of 45° . To provide close comparison with the work of Huner, the set angles which corresponded to Huner's parameter u were used for (θ_w). Values for u were obtained using Huner's approximation $u = \tan \theta_R \cot \theta_w$.

Using a Cannon 50E 35mm SLR camera with zoom facility, a photograph of the squeegee curvature was then taken whereby the angles and lengths were recorded, of which an example is illustrated in Figure 4.4. A complete set of photographs showing all of the curvatures tested is shown in Appendix 4.1. Two squeegee material types were used : Shore Hardness $65^\circ A$, defined 'soft'; and Shore hardness $85^\circ A$, defined 'hard', both were 140 x 10mm with trailing lengths of 53 mm.

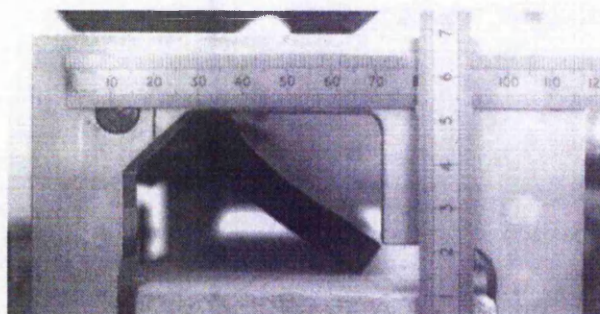


Figure 4.4 An example of a squeegee profile

From the squeegee curvature photographs, the height of the squeegee was read, y , at various points along the x -axis. The squeegee height was then divided by the height of the squeegee pivot point, y_0 , and the value of x was divided by the length of the squeegee along the x -axis when the tip first rested on the surface. These terms and reference points are as depicted in Figure 4.1. By plotting y/y_0 against x/l , the actual squeegee shape from the experimental data is plotted in Figure 4.5.

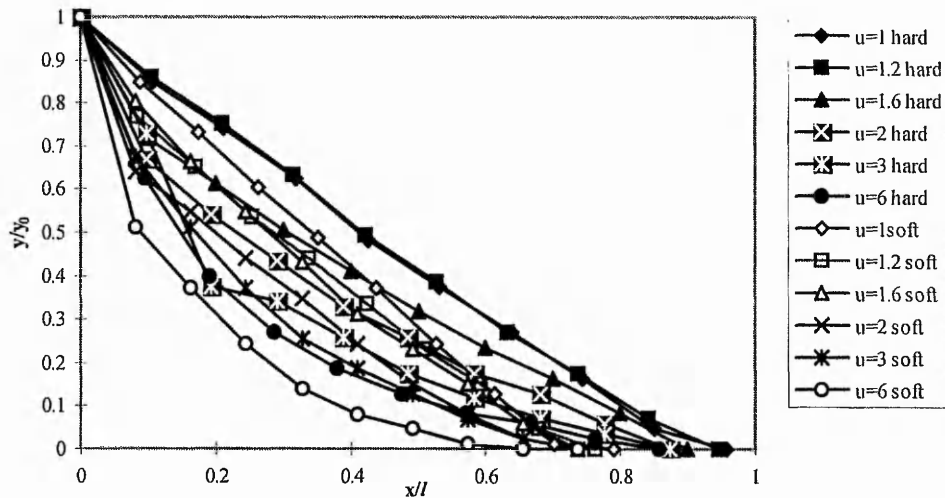


Figure 4.5 Plot of shapes obtained from experimental data for soft and hard squeegees

This can be compared to Huner's calculated shape which was shown in Figure 4.2, and an example showing a direct comparison of squeegee shapes where $u = 1.6$ and $u = 3$ for both hard and soft squeegees plotted against Huner's predicted values is given in Figure 4.6. It can be seen that Huner's calculated shape is a reasonable approximation.

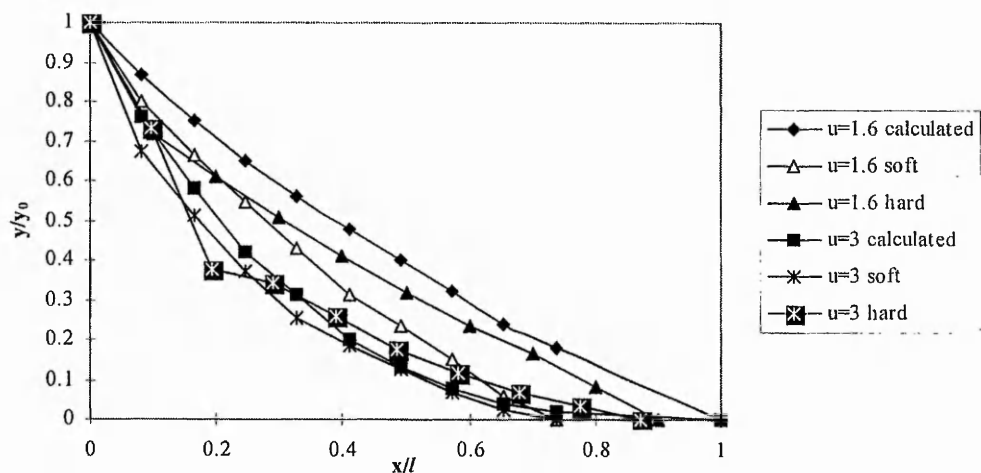


Figure 4.6 Comparison of calculated and experimentally obtained squeegee shapes

This plot does show that the squeegee becomes more concave and that the angle of attack decreases as the force applied to the squeegee is increased, but Equation (4.2) does not compensate for different squeegee hardnesses or thicknesses. The variation between the different squeegee hardnesses appears to be very small. However when conducting some basic experiments using different squeegee hardness values, whilst keeping all other parameters constant, this small variation in practice was found to be significant [68]. There is a difference in printed deposit thickness when using a hard as compared to a soft squeegee of up to 50% less.

An important note made by Huner is that the assumption of a single point contact at the squeegee tip breaks down once sufficient load is applied and he alters his boundary conditions to compensate for this. However, in the case of the soft squeegee the length of contact is found experimentally to be appreciable ($\approx 0\text{-}2$ mm, depending on load), and this situation is completely ignored by Huner.

The next statement made by Huner is that there is a minimum ink roll diameter beyond which the process becomes insensitive to the squeegee behaviour when $u < 2.5$. This would indicate that an optimum printing condition could be obtained with sufficient ink and applied squeegee load, but as Huner rightly points out there is no room in this part of the model for changes in squeegee speed, or ink viscosity, because the elastic deformation only is considered and so he continues by assessing the impact of fluid stresses on the ink deposition.

Huner bases all his further work, regarding flow past the squeegee tip, on the calculated shape of the squeegee predicted by Equation (4.2). This experiment showed that his prediction is close to the actual shape, but that different squeegee hardnesses are not considered. Thus it must be concluded that this model requires further work before it can be adapted for practical purposes.

4.4 Elastic forces versus fluid forces

To determine whether the screen print process is predominantly governed by elastic or fluid forces, it would be useful to simply calculate the value for the ratio $(\mu U \ell^2)/D$. To do this a value must be obtained for the flexural rigidity, which is a function of the elasticity modulus. This is difficult when dealing with rubber because there is no single value for Young's modulus, due to the fact that it is a highly compressible solid, with the dimensions changing markedly under load. Approximations have been made [69], [70], by assuming that rubber is an incompressible solid. Young's modulus is then simply derived as being 3 or 4 times the

shear modulus. However, other workers, for example, Martin [70] and Brown [71], state that because rubber has a non-linear stress-strain curve a single modulus cannot be obtained. Other factors, including previous stress cycles, time, exposure to temperature and humidity, immersion in ink and solvent also affect the flexural rigidity. An alternative approach is outlined by Lindley [69] which uses experimental data to correlate the hardness of the rubber to a value of Young's Modulus, but it is based on load-deflection data from specimens which have only been subjected to very small deflections (just a few percent) in tension and compression modes. This does not look at flexural rigidity nor at larger deformations as experienced by the squeegee. Thus an alternative method for evaluating the flexural rigidity was employed as outlined in Appendix 4.2. This provided average flexural rigidity values of 1.7 Nm and 3.3 Nm for soft and hard squeegee materials respectively.

The average flexural rigidity values from Appendix 4.2 were then used to determine the value of the ratio of fluid to elastic stresses $(\mu U \ell^2)/D$. For a hard squeegee material the ratio was 1.136×10^{-4} whilst for a soft squeegee the value was 2.206×10^{-4} (see Appendix 4.3). These results show that, as expected, the elastic forces are higher for the harder squeegee material, but in both cases the ratio is very much less than 1, thus the elastic stresses far exceed the fluid stresses. According to Huner this indicates that the process is insensitive to parameter changes. Early work conducted by the author [42], which is described in Chapter 3, showed that this is not the case.

4.5 Pressure generated within the ink roll

Huner provides an equation which gives the pressure within the ink just ahead of the squeegee tip:

$$P(x) = 6\mu U \int_{x'}^x \frac{h - \frac{2Q_0}{U}}{12k_x H + h^3} dx + P_w \quad (4.3)$$

and Q_0 is defined by Huner [2] as being the flow induced within the plane of the screen as a result of leaking under the squeegee tip for which the equation is:

$$Q_0 = \frac{P_w + \frac{U}{2} \int_0^L \frac{\frac{sh^2}{(1+sh)}}{\frac{k_x H}{\mu} + \frac{h}{12\mu} \frac{(4+sh)}{(1+sh)}} dx}{\int_0^L \frac{1}{\frac{k_x H}{\mu} + \frac{h}{12\mu} \frac{(4+sh)}{(1+sh)}} dx} \quad (4.4)$$

where μ = Ink viscosity

U = Squeegee speed

k_x = In - plane Darcy constant

l' = Point in ink roll where screen wetting resistance first exceeded

P_w = Screen wetting resistance

H = Screen thickness

h = $h(x)$, i.e. the squeegee shape as measured from the surface of the screen

L' = length of ink roll

$$\text{where } s = \frac{\alpha_x}{\sqrt{k_x}}$$

and α_x = the slip coefficient, a dimensionless constant.

The no slip boundary condition is used on the squeegee side because it is impermeable, but as the screen boundary is permeable the ink and screen interface condition is used from Beavers and Joseph as modified by Saffman (see Huner [2]):

$$\frac{\partial v}{\partial y} \Big|_{y=0} = \frac{\alpha_x}{\sqrt{k_x}} (v - U) \Big|_{y=0}$$

where α_x = slip coefficient

U = squeegee speed

$v = v(x,y)$, tangential ink shear stress expressed in terms of the x component of ink velocity

Huner describes the squeegee action governing the flow of ink into the screen as being analogous to that of the blade of a blade coater, where the screen is a rough web. This allows the product of sh to be interpreted as a surface smoothness parameter. In the case of screen printing, this is very smooth and thus tends to infinity.

For zero slip $s \rightarrow \infty$, so $\frac{sh^2}{1+sh} \rightarrow h$ and $\frac{4+sh}{1+sh} \rightarrow 1$

4.5.1 Experiment to measure pressures generated within the ink roll

To examine whether or not Equation (4.3) holds true, it was adapted for an experimental rig which was modified to allow the pressure generated within the ink roll to be measured. To date the assumption has always been made that the pressures generated in screen printing are purely hydrodynamic and efforts to determine the pressures were only attempted using very crude pressure transducers in the 1970's. These experiments described here therefore represent the first successful direct measurement of fluid pressures in the ink roll during simulated screen printing. The experimental rig is a modified tilting pad lubrication demonstration apparatus, with a squeegee holder fitted over the belt and is shown in Figure 4.7. Height and angle

adjustment facilities were added for experimentation purposes. The squeegee blade was modified to allow manometer tubes to be fitted to measure the pressure generated within the ink roll.

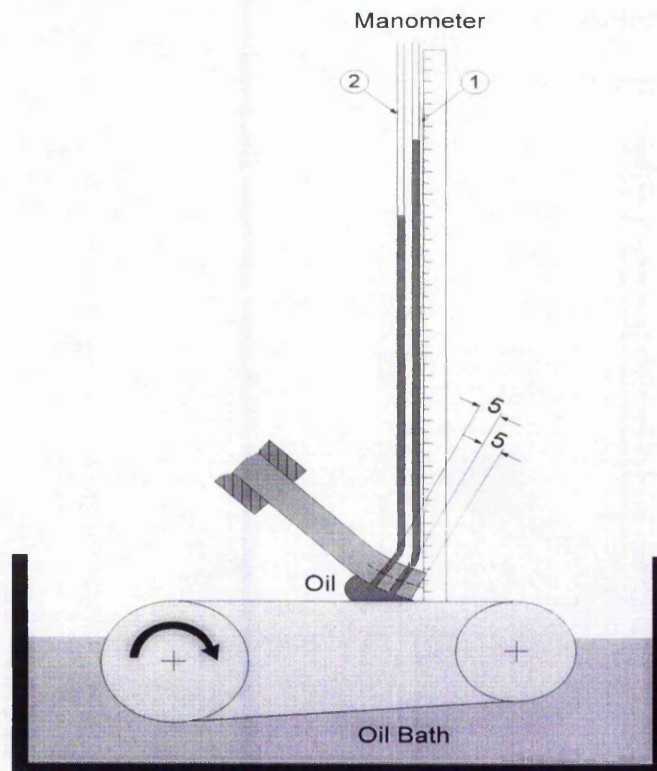


Figure 4.7 Modified Michell Tilting Pad Apparatus

For the converted lubrication apparatus the squeegee directly contacts a solid rotating belt and there is no screen. Thus, the wetting resistance, screen thickness and Darcy's constant are no longer applicable and, therefore, $P_w=0$, $H=0$ and $k_x=0$. Applying these conditions to Equation (4.3) results in the Equation (4.5):

$$P(x) = 6\mu U \int_0^x h - \frac{2Q_0}{U} \frac{1}{h^3} dx \quad (4.5)$$

Applying those same conditions, along with the conditions for zero slip as described above, the equation for Q_0 reduces to:

$$Q_0 = \frac{U}{2} \frac{\int_0^{L'} \frac{1}{h^2} dx}{\int_0^{L'} \frac{1}{h^3} dx} \quad (4.6)$$

To obtain an approximate value for the height of the ink roll, h , and the length of the ink roll L , it is assumed that they are equivalent to the ink roll diameter. An example of a large ink roll diameter is 1.5cm which equates to a value of 1.5×10^{-4} m for Q_0 . Thus, Q_0 can be assumed to be very small and Equation (4.3) can now be written:

$$P(x) = 6\mu U \int_0^x \frac{1}{h^2} dx$$

To analyse this relationship for a range of squeegee curvatures resulting from different loads, the height of the ink roll, h , needs to be expressed in terms of the radius of curvature at varying points along the x -axis.

If the squeegee is considered as an arc with a radius, R , as shown in Figure 4.8, it can be seen that

$$R^2 = (R-h)^2 + x^2$$

and $\therefore h = x^2/2R$

Thus

$$\begin{aligned} P(x) &= 6\mu U \int_0^x \frac{4R^2}{x^4} dx \\ &= 24\mu UR^2 \left[-\frac{1}{3x^3} \right]_x^\infty \end{aligned}$$

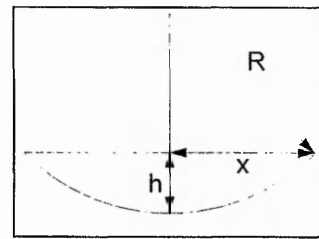


Figure 4.8

The final adapted equation is:

$$P(x) = \frac{8\mu UR^2}{x^3} \quad (4.7)$$

Using this modified equation the pressure values were calculated for a range of angles and speeds, using values of R which were obtained from the photographs in Appendix 4.1, using the approximation of the radius of curvature as explained in Appendix 4.2. The results of the calculated pressure values are tabulated in Appendix 4.4. Then for the same parameter settings pressure head readings in mm were recorded from the experimental rig, as shown in Appendix 4.5. A comparison of the calculated and experimental results is shown in Figure 4.9.

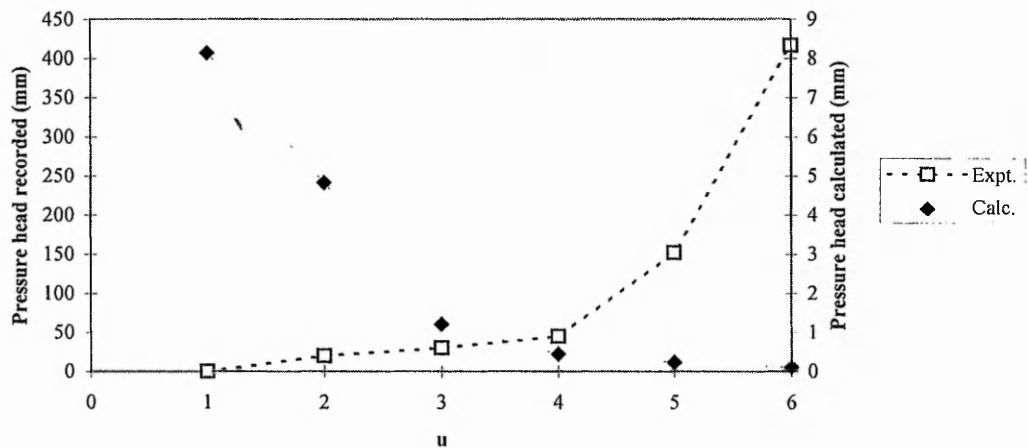


Figure 4.9 Comparison of calculated and measured pressure heads ($U = 0.095\text{m/s}$, $x = 5\text{mm}$)

As expected, in the experiment there is an increase in pressure with a corresponding increase in speed, as shown in Figure 4.10 below. The maximum pressure head recorded experimentally was 417 mm when u was set at 6 and U was set at 0.095m/s , which was the highest load and speed investigated. At zero squeegee load, i.e. when u was 1, zero pressure was recorded. However, for the calculations the converse is true. The highest pressure head, 8.152 mm, was found to occur when u was set at 1, whilst at $u = 6$ the pressure was only 0.105 mm for the same speed. This is because the radius of curvature of the squeegee, R , gets smaller as the force is increased. Overall the calculated values are not in agreement with the experimental values. This suggests that Huner's argument is fundamentally flawed.

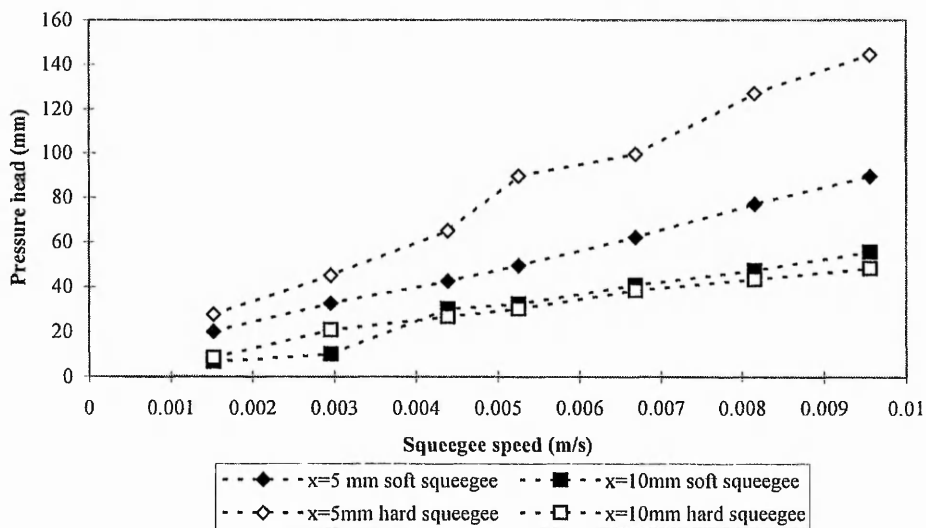


Figure 4.10 Experimentally recorded pressures at a value of $u=5$ for different squeegee types at 5 and 10mm along the x -axis

The second manometer, number (2) in Figure 4.7, showed no pressure head at all. This is an important point because it shows that the pressure build up must be happening in a very short space.

These results also show that the experimental pressure heads generated using the tilting pad apparatus were fairly low, even though they were many times greater than theory, giving a maximum of 417 mm. It can be argued that the physical positioning of the manometer tubes at 5 and 10mm along the central axis of the squeegee will affect the maximum pressure obtained, but nevertheless these pressures are still quite small and the question must then be raised as to how much pressure is actually needed to ensure flow through a mesh. To date this value is unknown and therefore the next section will investigate this experimentally.

4.6 Establishing the pressure required to ensure flow through a mesh

To obtain the pressure required for flow through a screen a simple experiment was devised to measure the flow rate through a mesh under a static head. The actual pressure required for a given squeegee speed was then estimated using the recorded flow rate. To do this it was first necessary to derive a theoretical squeegee speed based on the time taken to fill a mesh pore in relation to the squeegee velocity.

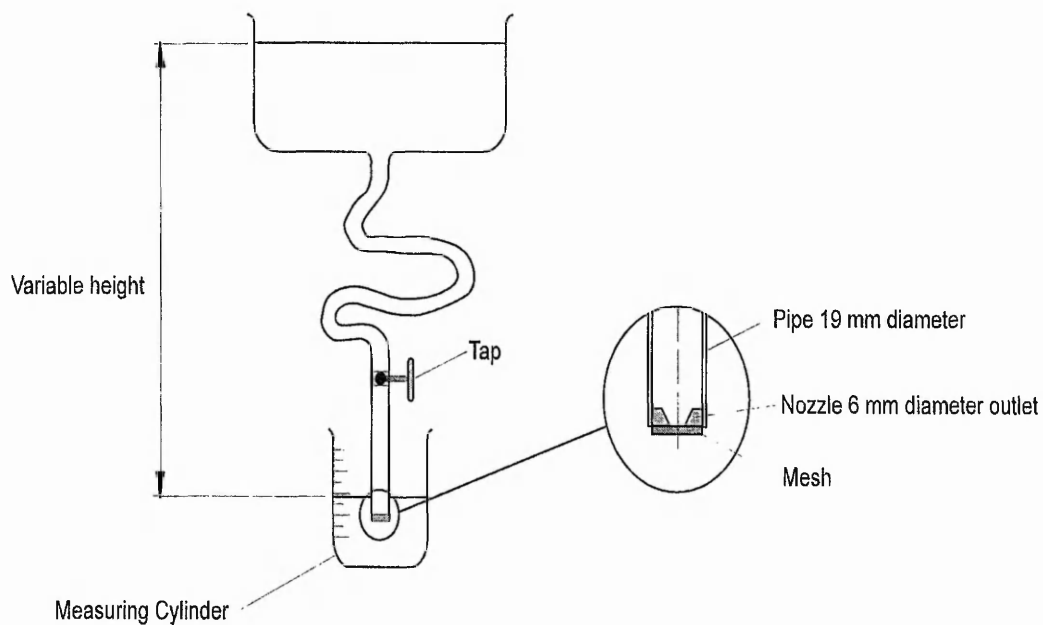


Figure 4.11 Apparatus to measure flow rate through mesh

The apparatus was set up as shown in Figure 4.11. A 120T mesh was stretched with a tensile force of 200 N per linear m across a 6 mm diameter nozzle aperture using a Harlacher screen printing stretch table. The mesh was attached using a proprietary Seri-paste adhesive. The nozzle was then connected by a long, transparent, 19 mm inner diameter pipe, to a header tank filled with glycerol. A tap was positioned at 1.5 m from ground level. After waiting for the air bubbles to escape at the top of the pipe, the tap was opened to ensure a steady pour of fluid. The average time taken to fill a known volume (200 ml) was recorded and the experiment was repeated for different header tank heights. An overhead crane was used to adjust the tank heights, and a calibrated wall chart showing 0.3 m increments was hung from the crane showing the height of the tank after adjustments. Accurate readings were possible at the higher pressure heads by standing on the third floor rear access staircase. A graph of the flow rate of the glycerol against the different pressure head readings is shown in Figure 4.12. the results are tabulated in Appendix 4.6. An error of up to 0.2 m can be expected at the higher pressure heads as the level in the tank dropped from the original point by approximately 0.05 m in total and the height readings were taken 1m away from the measuring scale.

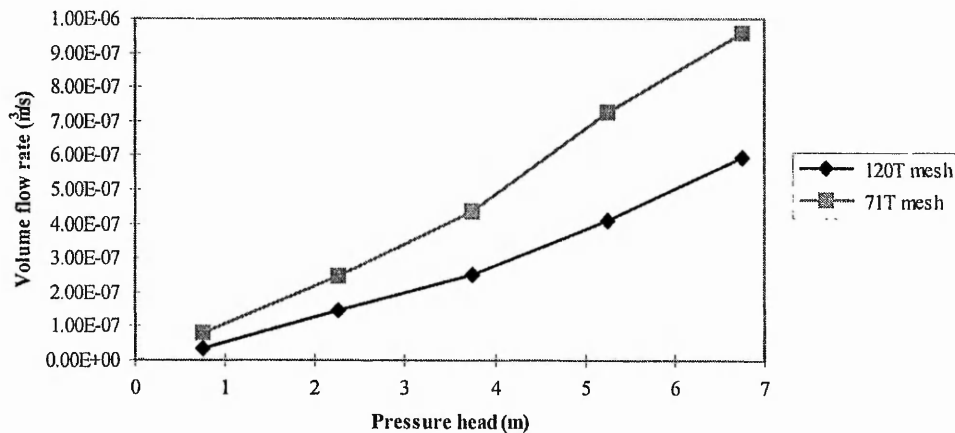


Figure 4.12 Volume flow rate against static pressure head for glycerol

The linear velocity of the glycerol through the screen, V_{scr} , can be obtained from the experimental data using the Continuity Equation:

$$Q = V_{scr} \times OA$$

which re-arranged gives

$$V_{scr} = \frac{Q}{OA}$$

where Q = volume flow rate through the screen

and OA = open area of screen in the nozzle

The theoretical squeegee speed was derived as follows. The time can be approximated by considering the time taken for the squeegee to pass from one mesh strand to the next, i.e. the thread pitch. The underlying assumption is that the ink can only be forced through a mesh opening when the squeegee blade tip is directly over that pore. Hence the time that the ink has available to pass through one pore is the same as the time it takes for the squeegee to pass over the pore, given by $V_{sq}/\text{thread pitch}$. A smaller pressure applied over a longer time, i.e., a lower squeegee velocity is not a viable alternative as screen printing requires an immediate snap off [2]. This governs the minimum speeds possible and the evidence that printing is unsatisfactory below a minimum working speed is presented in Chapter 6. Identifying the rate of snap necessary for successful screen printing is outside the scope of this project, but it is recommended as a topic for further work.

The velocity of ink flow through the screen, V_{scr} , is

$$V_{scr} = \frac{Ft}{t}$$

where Ft = Fabric thickness

and t = time.

$$V_{scr} = \frac{Ft}{\text{thread pitch}} V_{sq} \quad (4.8)$$

where V_{sq} = squeegee velocity.

Rewriting Equation (4.8) the squeegee velocity is given as

$$V_{sq} = V_{scr} \times \frac{\text{thread pitch}}{\text{fabric thickness}} = \frac{Q}{OA} \times \frac{\text{thread pitch}}{\text{fabric thickness}}$$

The experimental data of Figure 4.12 may now be interpreted in Figure 4.13 as the pressure head required in the ink under the squeegee blade to achieve successful printing at a given squeegee speed.

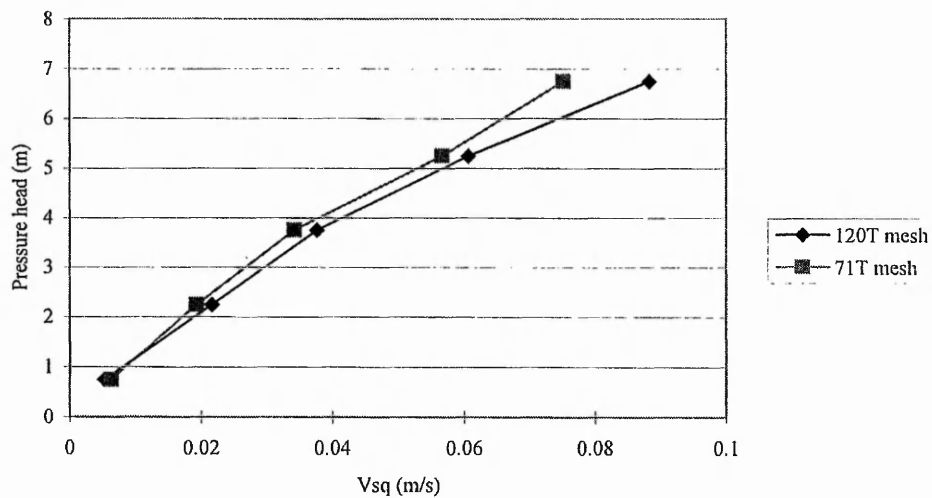


Figure 4.13 Pressure head plotted against squeegee velocity

The results show that for a squeegee speed of 0.09 m/s a pressure head of approximately 7 m would be required. This speed corresponds to that at which the maximum oil pressure head of 0.4 m was recorded using the tilting pad apparatus. A pressure head of 0.4 m in oil is equivalent to 0.28 m of glycerol, (see Appendix 4.7 for the respective densities of the oil and glycerol used) therefore the pressure required to force liquid through the screen is much higher than that obtained in the liquid roll in front of the squeegee, by a factor of about 25.

In Chapter 2 it was reported that Cropper found the pressure in the bow wave to be 10^4 N/m^2 , i.e. approximately 1m of head, and he claimed that this pressure was greater than that which was required to ensure flow through the mesh. However, this experiment showed that the pressure in the bow wave is smaller by a factor of 3, and that the pressure required for flow through the mesh to occur exceeds Cropper's value by a factor of 7.

Laminar flow was confirmed by checking that the Reynolds' number for the glycerol flowing through the pipe was below 2000.

$$\text{Re} = \frac{\rho V D}{\mu}$$

where

Re = Reynolds' number

ρ = fluid density

V = flow velocity

D = pipe diameter

μ = fluid viscosity

For glycerol flowing through a 19 mm diameter pipe, at the maximum volume flow rate, Q , achieved in this experiment, the Reynolds' number is:

$$\begin{aligned} \text{Re} &= \frac{1262 \times 3.38 \times 10^{-3} \times 0.019}{1.2649} \\ &= \mathbf{0.064} \end{aligned}$$

The flow velocity, V , using the same criteria above is calculated to be:

$$\begin{aligned} V &= \frac{Q}{A_{\text{pipe}}} \\ &= \frac{9.6 \times 10^{-7}}{\pi \times (9.5 \times 10^{-3})^2} \\ &= 3.38 \times 10^{-3} \text{ m/s} \end{aligned}$$

As the flow is laminar, Poiseuille's law can be used to determine if the pressure head lost in overcoming pipe friction is significant.

$$Q = \frac{\pi D^4 (P_2 - P_1)}{128 L \mu}$$

where

Q = Flow rate of fluid

D = Pipe diameter

$P_2 - P_1$ = Pressure loss in pipe

μ = Dynamic viscosity

L = Length of pipe

The losses in the pipe due to friction are calculated from the recorded pressure head as follows.

The greatest pressure in the experimentation is given by a pressure head of 6.75 m:

$$\begin{aligned} P &= \rho gh \\ &= 1262 \times 9.81 \times 6.75 \\ &= 83.6 \times 10^3 \text{ N/m}^2 \end{aligned}$$

The pressure losses due to friction are

$$\begin{aligned}(P_2 - P_1) &= \frac{128L\mu}{\pi D^4} \\ &= \frac{128 \times 1.2649 \times 6.75 \times 9.6 \times 10^{-7}}{\pi \times 0.019^4} \\ &= 2562 \text{ N / m}^2\end{aligned}$$

Therefore the losses due to pipe friction are less than 3% and thus can be neglected.

4.7 Conclusions

Huner's model of the squeegee as a clamped cantilevered blade is a good basis for conceptualising squeegee behaviour, provoking thought on the elastic and fluid stresses. However, on determining that the elastic stresses are dominant, the theory breaks down as it then implies that the fluid stresses have no role in the pressure build up. It has been shown by experimentation [68] that the squeegee hardness has a very significant affect on printed deposit thickness variation and it was also observed in these experiments that hydroplaning occurred, i.e. the squeegee lifted off the surface of the screen leaving a thick film of ink on the screen surface, which, theoretically, according to Huner, should not have been possible.

The calculation for pressure just ahead of the squeegee tip adapted from Huner's work shows completely the wrong result when compared to the near tip pressures measured in the modified tilting pad apparatus. Additionally, the experiment illustrating the pressure required to ensure flow through the mesh shows that the pressures recorded were a factor of twenty-five less than that which is actually required. This leads to the conclusion that the screen printing process is not governed by hydrodynamic lubrication theory as modified by Huner. Therefore, it is necessary to explore an alternative theory to explain how the fundamental screen print process is governed. The next chapter offers an analysis of EHL as a potential model for the screen print process.

Chapter 5 Analysing screen printing using elastohydrodynamic lubrication theory

5.1 Introduction

On evaluating the Huner model, the results obtained showed that the hydrodynamic pressures generated in the ink roll were insufficient to create the required ink flow through the mesh. It has been shown that the pressure head required for flow through a typical mesh (120T) is in the order of 7 m, whilst experimentally, maximum values of 0.4 m were recorded for a speed of 0.09 m/s. It can therefore be assumed that the squeegee performance is governed by a different theory, which allows higher pressures to be generated. If the assumption that the squeegee operates under fully lubricated conditions is to be upheld, then it must be that one of the other lubrication systems applies to screen printing. Boundary lubrication deals only with chemical films or physically adsorbed films: hydrodynamic lubrication, as proposed by Huner, assumes generation of moderate pressure within the ink roll but ignores elastic deformation at the tip; therefore elastohydrodynamic lubrication (EHL) theory appears most suitable as it deals with both deformation and pressure build-up in the ink roll and predicts larger pressures under the flattened tip.

This chapter gives a brief outline of EHL theory, then explores the feasibility of applying EHL to squeegee behaviour, firstly by modelling the squeegee tip using a wedge profile and then by adopting an analysis carried out using soft EHL for a tilted pad geometry.

5.2 EHL Theory

EHL theory describes the basic characteristics of the lubricating film by adapting Hertzian contact mechanics, giving a relationship between the film thickness and speed, viscosity, pressure viscosity coefficient and the deformation behaviour of the contacting surfaces.

Detailed treatments of EHL theory for line and point contacts are given by both Cameron [72] and Johnson [73] and the basic equations for elasticity, elastic pressures and deformation outside the contact area have been reproduced in Appendix 5.1.

EHL is normally applied to steel rollers or ball bearings, where the deformations are generally small and the mating materials used are similar to each other. In screen printing, however, the squeegee produces a line contact which has a relatively large deformation at the tip, in addition to the gross bending, due to the fact that it is made of polyurethane. The squeegee material is also distinctly different from that of the stencil. A further complication is that the shape of the

undeformed squeegee tip is not circular, as in rollers, but more like a wedge. Approximating a value for the radius of curvature at the contact inlet would also be difficult as the squeegee does not have a single radius (which a roller has prior to deformation) because the squeegee is initially a flat blade and its curvature depends on the applied load and the angle of attack.

5.3 Adaptation of EHL theory for use with wedge geometries

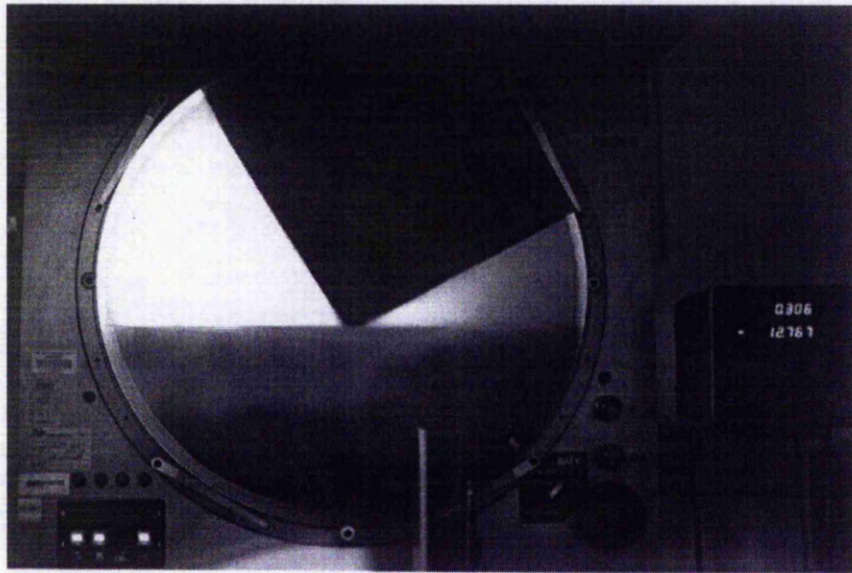


Figure 5.1 Side view of squeegee tip deformation projected through a shadowgraph

On examination of the actual tip deformation using a shadowgraph the squeegee shape appears to be that of a wedge profile, apart from the fact that it is not symmetrical (see Figure 5.1). Thus the theory has been adapted for this geometry as none of the other standard geometries seem suitable. The following analysis starts with the indented wedge model of Hills & Sackfield [74], and develops it to reflect the special conditions of squeegees moving over screens.

Figure 5.2 below depicts indentation of a surface by a wedge. The half width of the line contact, a , is given by:

$$a = \frac{P(1 - \nu^2)}{E\phi} \quad (5.1)$$

where $P =$ normal force per unit length applied

$\nu =$ Poisson's ratio

$\phi =$ angle of wedge

and the normalised pressure along the x-axis is given by:

$$p(x) = \frac{P}{\pi a} \cosh^{-1} \left(\frac{a}{|x|} \right) \quad (5.2)$$

NB. There is a restriction that the angle ϕ be kept small to minimise strains (see Hills [74]).

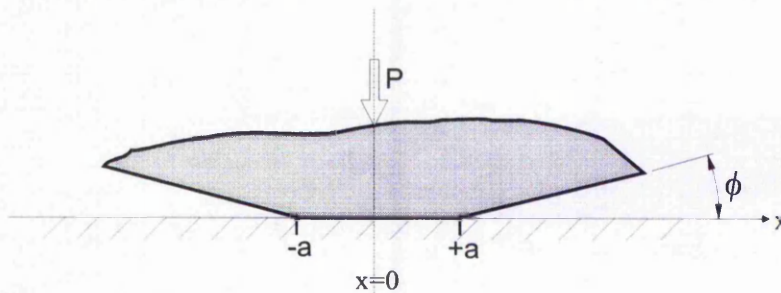


Figure 5.2 Indentation of a wedge

From Johnson (Eqn. 10.34 [73]) the film shape for elastic cylinders is given as:

$$h(x) = h_0 + \frac{x^2}{2R} + V(x) - V(0) \quad (5.3)$$

where $V(x) =$ normal surface displacement outside contact

$\frac{x^2}{2R} =$ displacement inside contact

$h_0 =$ minimum film thickness.

Figure 5.3 illustrates the case for two rotating cylinders, defining the parameters used in Equation (5.3).

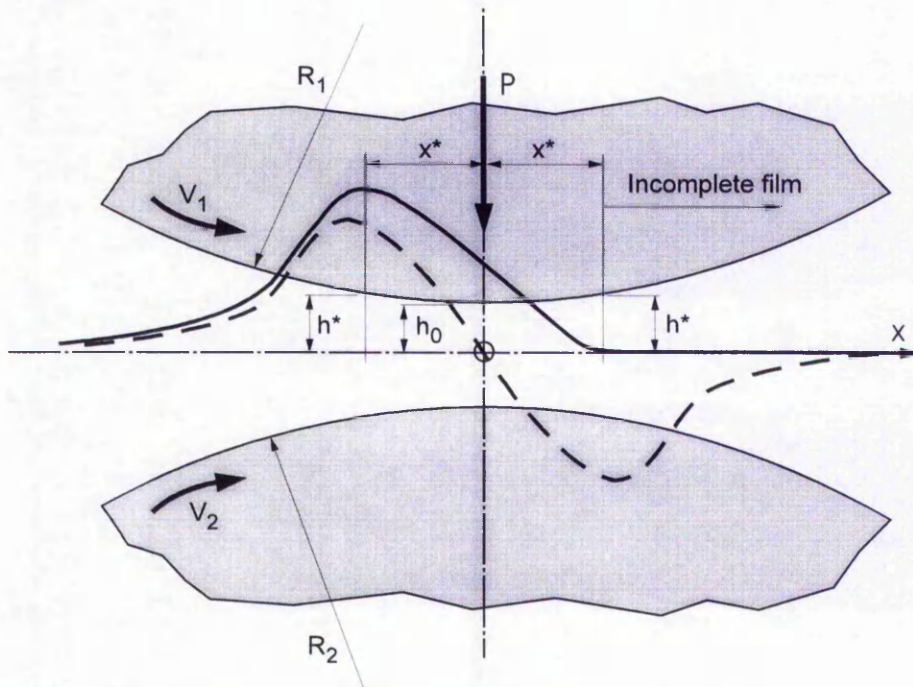


Figure 5.3 Definition of symbols for rotating rollers with predicted film pressure profiles

Adapting Equation (5.3) for the wedge geometry gives:

$$h(x) = h_0 + \phi x + V(x) - V(0) \quad (5.4)$$

differentiating this gives

$$h'(x) = \phi + V'(x) \quad (5.5)$$

but from Johnson, for an elastic contact, it can be shown that

$$V'(x) = -\frac{2}{\pi} \frac{1-\nu^2}{E} \int_{-a}^a \frac{p(s)ds}{x-s}$$

therefore, substituting into Equation (5.5):

$$h'(x) = \phi - \frac{2}{\pi} \frac{1-\nu^2}{E} \int_{-a}^a \frac{p(s)ds}{x-s} \quad (5.6)$$

but by substituting Equation (5.2), using s as the integration variable of x

$$\int_{-a}^a \frac{p(s)ds}{x-s} = \int_{-a}^a \frac{P/\pi a \cosh^{-1} \frac{1}{|s|}}{x-s} ds \quad (5.7)$$

Let $t = \frac{s}{a}$ and $x^* = \frac{x}{a}$, thus the R.H.S of Equation (5.7) becomes

$$= \frac{P}{\pi a} \int_{-1}^1 \frac{\cosh^{-1} \frac{1}{|t|}}{x^* - t} dt$$

This is the Cauchy Principal Value integral (see Johnson [73] Appendix 1) with value

$$= \frac{P}{\pi a} \pi \sin^{-1} \frac{1}{x^*}$$

$$= \frac{P}{a} \sin^{-1} \left(\frac{1}{x^*} \right)$$

where s is a point on the x axis i.e. the integration variable for a fixed point x

t is the non-dimensional form of s

x^* is the non dimensional form of x .

Equation (5.7) can now be inserted into Equation (5.6)

$$h'(x) = \phi - \frac{2}{\pi} \frac{1-v^2}{E} \cdot \frac{P}{\pi a} \pi \sin^{-1} \left(\frac{a}{x} \right)$$

but $\frac{2}{\pi} \frac{1-v^2}{E} \cdot \frac{P}{\pi a} \pi = \frac{2}{\pi} \phi$

therefore

$$h'(x) = \phi \left\{ 1 - \frac{2}{\pi} \sin^{-1} \left(\frac{a}{x} \right) \right\} \quad (5.8)$$

Integrating, gives

$$h(x) = \text{const} + \phi \left\{ |x| - \frac{2a}{\pi} \left[\frac{|x|}{a} \sin^{-1} \left(\frac{a}{x} \right) + \ln \left(\left| \frac{x}{a} \right| + \sqrt{\frac{x^2}{a^2} - 1} \right) \right] \right\}$$

where it can be assumed that the constant is h_0 .

For simplicity the film shape, h , can be rewritten as

$$h = h_0 + \phi a \delta \quad (5.9)$$

where

h_0 = minimum film thickness required to ensure separation of the surfaces

$$\delta = \left| \frac{x}{a} \right| - \frac{2}{\pi} \left[\left| \frac{x}{a} \right| \sin^{-1} \left(\frac{a}{x} \right) + \ln \left(\left| \frac{x}{a} \right| + \sqrt{\frac{x^2}{a^2} - 1} \right) \right]$$

and $\phi a \delta$ together represent the elastic deformation of the surface.

To provide a universally applicable form this must be non-dimensionalised, as set out by Cameron [72].

$$\text{Let } h_0 = \phi a H_0$$

$$h = \phi a H$$

then (5.9) reads

$$H = H_0 + \delta$$

It is shown by Cameron that Reynold's Equation can be modified to accommodate the viscosity changes due to pressure. By replacing the viscosity in the standard equation with the simple exponential viscosity equation

$$\eta_p = \eta_0 e^{\sigma p}$$

and defining

$$p_0 \equiv -\frac{1}{\alpha} \int_0^p d(e^{-\alpha p}) = \frac{1 - e^{-\alpha p}}{\alpha} \quad (5.10)$$

This gives the Reynolds equation in terms of p_0 and η_0 :

$$\frac{dp_0}{dx} = 6U\eta_0 \frac{h - \bar{h}}{h^3}$$

As also stated by Cameron, because the film is parallel $\bar{h} = h_0$, thus substituting in H and H_0 the equation becomes

$$\frac{dp_0}{dx} = 6U\eta_0 \frac{\phi a \delta}{(a\phi H)^3}$$

which can be rearranged as

$$\frac{dp_0}{dx} = \frac{6U\eta_0}{(\phi a)^2} \frac{\delta}{H^3} \quad (5.11)$$

Let $p_0 = k p_0^*$
 $x = ax^*$

Substitute into (5.11)

$$\frac{k}{a} \frac{dp_0^*}{dx^*} = \frac{6U\eta_0}{(\phi a)^2} \frac{\delta}{H^3}$$

Let $\frac{k}{a} = \frac{6U\eta_0}{(a\phi)^2}$

to get $\frac{dp_0^*}{dx^*} = \frac{\delta}{H^3}$

which is now a fully non-dimensionalised relationship between pressure and deformation.

Cameron provides a correlation of p_0^* and H_0 as follows. From (5.10) it can be seen that as p gets very large $e^{-\alpha p} \rightarrow 0, p_0 \rightarrow \frac{1}{\alpha}$. However, this is based on pressures generated for rigid surfaces e.g. steel rollers. For surfaces of low elastic moduli the generated pressures are not so high, because the material deforms more, and Cameron shows that $p_0 \rightarrow p_{\max}$ as α or $p_{\max} \rightarrow 0$.

The pressure is zero at $x = -\infty$, which would give integration limits of $x = -\infty$ and $x = -a$. Therefore, in the non-dimensionalised state $x^* = -\infty$ to $x^* = -1$ and the definite integral for p_0^* is

$$p_0^*(-1) = \int_{-\infty}^{-1} \frac{\delta}{H^3} dx^*$$

A table of values can then be obtained for the relationship of H_0 and p_0^* similar to that of Cameron's. See Table 1.

Table 1 Relationship of H_0 and p_0^*

H_0	0.20	0.50	1.00	1.30
p_0^* Wedge	4.0598	1.3592	0.6091	0.4515

The program to obtain these values, and the log plot showing the relationship for this table are given in Appendix 5.2.

Hence $p_0^* = r H_0^{-s}$

where r is the intercept and s is the gradient of the slope representing p_0^* and H_0 .

From Appendix 5.2 these values are found to be 0.969 and 1.43 respectively.

Therefore $H_0^s = \frac{r}{p_0^*}$

therefore $\left(\frac{h_0}{\phi a}\right)^s = \frac{r}{\frac{p_0}{\frac{6U\eta_0 a}{(a\phi)^2}}}$

but $p_0 = p_{\max}$ therefore $\left(\frac{h_0}{\phi a}\right)^s = \frac{r p_{\max} 6U\eta_0 a}{(a\phi)^2}$

rearranged gives

$$h_0^s = r p_{\max} 6U\eta_0 a (\phi a)^{s-2}$$

and substituting in for r and s gives

$$h_0^{1.43} = 0.969 p_{\max} 6U\eta_0 a (\phi a)^{-0.57}$$

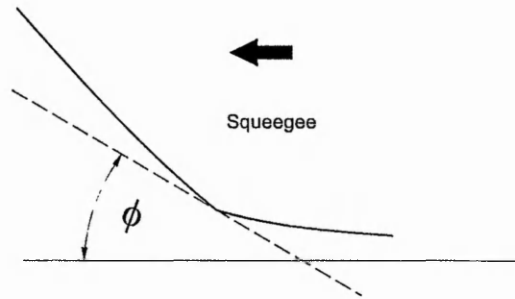
which can be rewritten as

$$h_0 = 0.80 \left(\frac{6U\eta_0 p_{\max}}{\phi} \right)^{0.7} \left(\frac{P}{E'} \right)^{0.3} \quad (5.12)$$

- where h_0 = the minimum film thickness
 p_{\max} = total applied pressure
 U = speed
 η_0 = viscosity
 ϕ = deformation angle
 P = $(aE\phi)/(1-\nu^2)$
 E' = $E/(1-\nu^2)$

The wedge geometry presents some difficulties however. The most important is that the value of ϕ must be obtained to allow its use. ϕ is the angle at the point where the squeegee meets the screen as shown in Figure 5.4. Equation (5.8) is the slope of the surface of the squeegee which is measured close to the point $x = a$, so $\sin^{-1} (a/x)$ is close to 90° i.e. $\pi/2$. Therefore

$\left\{ 1 - \frac{2}{\pi} \sin^{-1} \left(\frac{a}{x} \right) \right\}$ is close to 0 and it is difficult to get ϕ accurately. Measurements taken on the shadowgraph allow a very high proportion of error.

Figure 5.4 Squeegee deformation angle ϕ

A second problem is the calculation of p_{\max} which is given by the integration of Equation (5.2) shown below:

$$\int p(x)dx = \frac{P}{\pi a} \int_{-a}^{+a} \cosh^{-1}\left(\frac{a}{|x|}\right) dx$$

this means that at the extremes where $a = x$ the pressure is 0, which is to be expected, but also at $x = 0$, $\cosh^{-1}(a/x)$ gives a value where a is divided by 0. For steel it is simply assumed that the pressure tends to ∞ at $x = 0$.

A further problem is that the wedge elastic equations require a shallow, symmetrical profile and neither of these assumptions really hold true. Thus it must be concluded that an alternative geometry must be adopted.

5.4 EHL theory for materials of low elastic moduli

The conditions of EHL theory for hard materials differ from those of softer materials because the pressures generated are too small to increase the lubricant viscosity and therefore the deformation alone is important and not the pressure viscosity coefficient. According to Baglin & Archard [75] the point where a special case of EHL, i.e., soft EHL theory, is reached is when $p_{\max} = p_0$. p_{\max} is defined as the maximum hydrodynamic pressure calculated and p_0 is defined as the maximum Hertzian pressure for dry contact under the same load. They summarised that numerical methods up to 1972 gave no satisfactory solution similar to the Grubin type for low elastic modulus materials (see [74]). The then existing work ignored the geometry of the inlet, gave film thickness as an arbitrary constant and did not include the applied load to derive the film thickness. The latter arguably does not allow any real physical relationships to be made.

5.4.1 Elastic Equations for Soft EHL

The main assumption which Baglin & Archard use for their analytical solution is that the deformation is very large with respect to the film thickness. Thus, the pressure distribution is approximated as Hertzian, and the film thickness is assumed to be almost parallel. However because the pressure does not influence the viscosity, the required pressures must be generated from the geometry. Baglin & Archard assume the geometry can be modelled as that of a tilted pad bearing as shown in Figure 5.5.

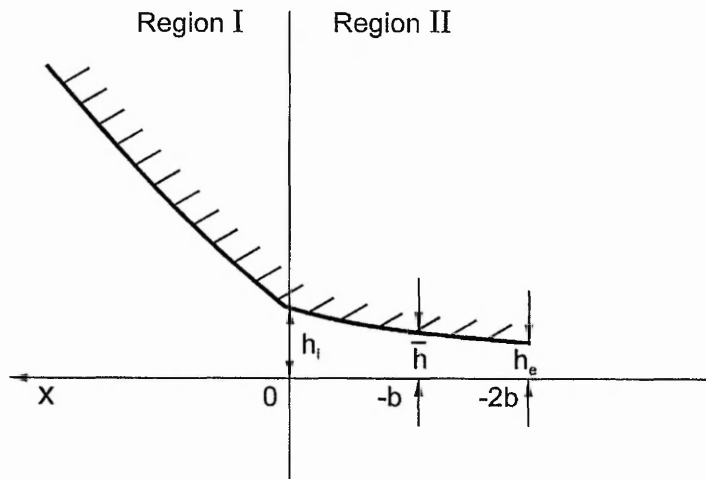


Figure 5.5 Assumed tilting pad bearing geometry

Baglin & Archard acknowledge that the tilted pad does not give the symmetrical conditions as required by Hertz theory but state a number of assumptions which allow a near symmetric pressure distribution. They also use the Crook approximation for the Hertzian shape which gives the film thickness in terms of geometry only. The geometry for region I is given as a function of b , R , h_i , and for region II, it is simply approximated as the equation for a straight line:

$$h = h_i + mx \quad (5.13)$$

where m is the gradient of the tilted pad at a point x from the origin

$$\text{and } m = \frac{h_i - h_e}{2b} \quad (5.14)$$

By applying boundary conditions, and the continuity law, the limits for p are set:

$$\begin{aligned} p &= 0 \text{ at } x = +\infty \\ p &= 0 \text{ at } x = -2b \\ p &= p_{\max} = p_0 \text{ at } x = -b \end{aligned}$$

The assumption is that the pressure distribution is symmetrical. This argument is put forward [75] because the deformation of the surface is large compared to the film thickness and the contact behaviour must therefore be close to Hertzian. It follows then, that

$$\bar{h} = \frac{h_e + h_i}{2} \text{ if } \bar{h} \text{ is at } x = -b \quad (5.15)$$

5.4.2 Pressure inside the contact region using Reynolds Equation

Now using Reynolds equation the pressure distribution under the contact, i.e. in region II, can be found as follows:

$$\frac{dp}{dx} = 6U\eta \left(\frac{h - \bar{h}}{h^3} \right)$$

In the case of steel contacts the film thickness, h , is represented by:

$$h = \text{constant} + \text{elastic deformation inside the contact region}$$

where the constant is designated to be the minimum film thickness, h_0 and because the film is parallel in the contact region $\bar{h} = h_0$. However, in the case of soft contacts i.e. materials of low elastic modulus, it is known that the contact region is more akin to a tilted pad bearing whereby it is assumed that the film thickness is given by $h = h_i + mx$ as stated above.

$$\begin{aligned} \frac{dp}{dx} &= 6U\eta \frac{h - \bar{h}}{h^3} \\ \therefore [P]_0^P &= 6U\eta \int_{x=-2b}^x \frac{h - \bar{h}}{h^3} dx \end{aligned}$$

$$\begin{aligned}
 &= 6U\eta \int_{h_c}^h \frac{h - \bar{h}}{h^3} dm \\
 &= \frac{6U\eta}{m} \left[-\frac{1}{h} + \frac{\bar{h}}{2h^2} \right]_{h_c}^h \\
 \therefore p &= \frac{6U\eta}{m} \left\{ \frac{\bar{h}}{2h^2} - \frac{1}{h} - \frac{\bar{h}}{2h_c^2} + \frac{1}{h_c} \right\} \\
 &= \frac{6U\eta}{m} \left\{ \frac{1}{hh_c} - \frac{\bar{h}(h + h_c)}{2h^2h_c^2} \right\} (h - h_c) \\
 p(x) &= \frac{6U\eta}{m} \frac{h - h_c}{2h^2h_c^2} \left\{ 2hh_c - \bar{h}(h + h_c) \right\} \quad (5.16)
 \end{aligned}$$

This can then be plotted for a series of contact widths and speeds an example of which is shown in Figure 5.6. At the inlet point $x=0$ the pressure is not 0, but at the exit point it is 0.

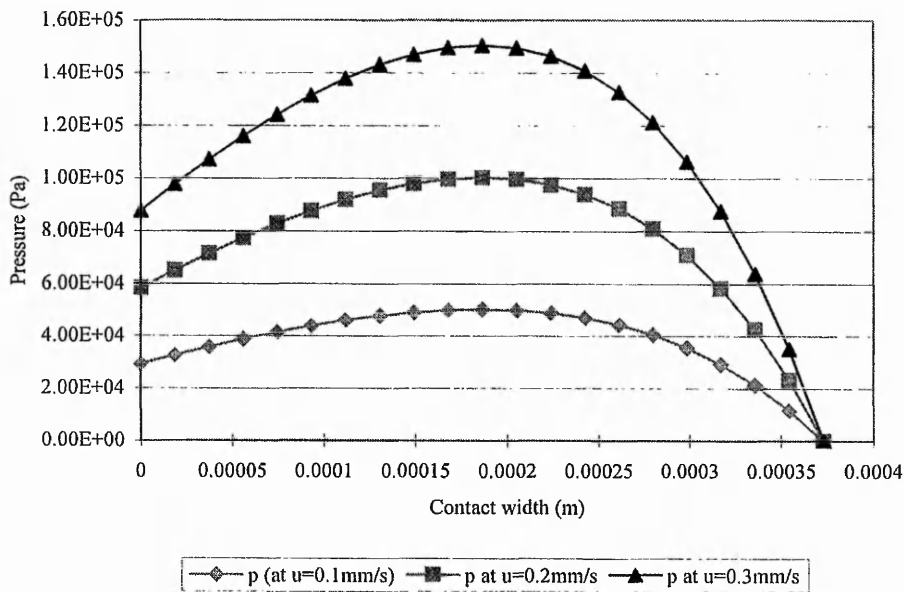


Figure 5.6 Pressure distribution plotted against contact width at a range of speeds, using 120T mesh & ink at 4 Pa.s

5.5 Derivation of equation to predict minimum squeegee speeds

To determine the condition required for the first complete print the above Equation (5.16) must be satisfied for the screen print process. To adapt this equation for screen printing parameters, it is necessary to obtain relationships for m , h , h_i and h_e in terms of squeegee and screen parameters. Squeegee speed and viscosity are already specified in the equation.

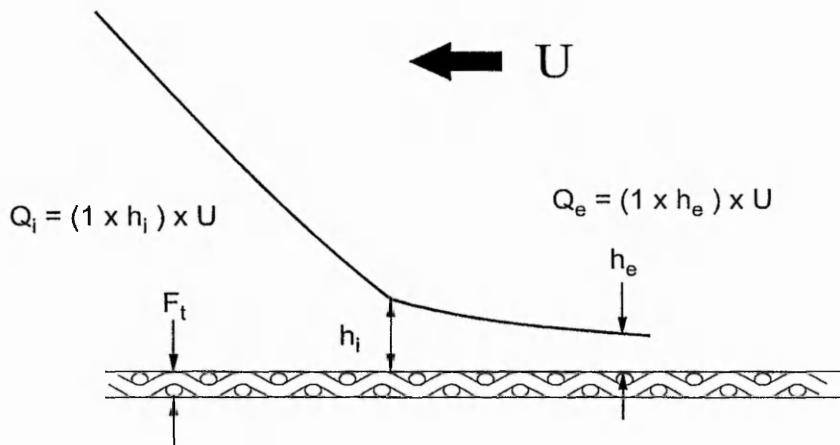


Figure 5.7 Screen parameters defined in Equations (5.17) and (5.18)

First the volume flow rate of ink through the screen, Q_{SCR} , is considered for a 1m wide screen, of which a side view is illustrated in Figure 5.7. The volume flow rate is considered to be the volume of screen filled by the passage of the squeegee in 1s. The volume filled is equal to the volume of fabric, reduced by the ratio which represents the air space between the strands of the mesh.

$$Q_{scr} = Ft \times 1m \times U \times \frac{OA}{100} \quad (5.17)$$

where

- Ft = fabric thickness
- U = squeegee speed
- $1m$ = width of screen
- OA = mesh open area %

Mesh open area expressed as a percentage is given by:

$$\frac{OA}{100} = \frac{\text{Total area of open mesh in a unit area}}{\text{Total unit area}}$$

Likewise, the volume flow rate of ink through the screen under the squeegee tip, Q_{SQ} can also be determined as being the difference between the ink flow rate into the contact area, Q_i , and the ink flow rate at the exit, Q_e . Neglecting losses due to adhesion of the ink to the mesh strands, it follows that the remainder of the ink must flow through the screen. Thus, for a 1m wide squeegee Q_{SQ} is given by

$$Q_{SQ} = Q_i - Q_e$$

where

$$Q_i = (1 \times h_i) \times U$$

$$Q_e = (1 \times h_e) \times U$$

Therefore,

$$Q_{SQ} = U(h_i - h_e) \quad (5.18)$$

By applying continuity, the volume flow rate through the screen must be equal to the volume flow rate under the squeegee tip, thus,

$$Q_{SCR} = Q_{SQ} \quad (5.19)$$

and from Equations (5.17) and (5.18), this can now be represented fully in screen printing terms as:

$$Ft \times U \times \frac{OA}{100} = U(h_i - h_e)$$

Therefore the height at the inlet of the squeegee tip region may be determined by rearranging the above equation:

$$h_i = Ft \times \frac{OA}{100} + h_e \quad (5.20)$$

Normally it is difficult to find a value for h_e as it cannot easily be measured. It is also known that the exit suffers from a constriction which is discussed in detail by Cameron [72], Johnson [73] and Baglin [75]. However to use the equation for screen printing, this work will adopt the fabric roughness, F_R as being the resulting height of h_e . Figure 5.8 illustrates how the fabric roughness is determined. This assumption is reasonable as in the application of EHL theory to rigid materials, the value of h_e is taken to be the height of the surface asperities.

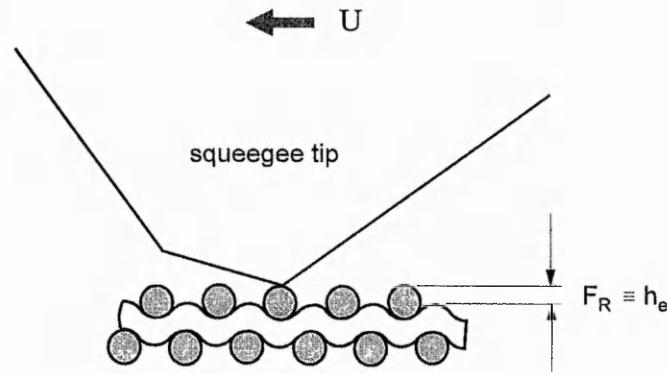


Figure 5.8 Illustration of fabric roughness

The fabric thickness, F_t , was specified from the manufacturer's data as being $66\mu\text{m}$.

Now F_R can be substituted back into Equation (5.20) to provide a value for h_i completely in screen printing parameters.

$$h_i = F_t \times \frac{OA}{100} + F_R \quad (5.21)$$

From Baglin & Archard [75] the film height under the contact region is assumed to follow the equation of a straight line as defined in Equation (5.13) and the gradient, m , was defined in Equation (5.14) as $m = \frac{h_e - h_i}{2b}$. By rearranging Equation (5.20), the gradient m can also be expressed in terms of screen printing parameters:

$$h_e - h_i = -F_t \frac{OA}{100} \quad (5.22)$$

Therefore,

$$m = \frac{-F_t \cdot OA}{200b} \quad (5.23)$$

Finally, by substituting Equations (5.15),(5.21) and (5.23) back into Equation (5.16) an equation for the actual pressure generated under the squeegee tip is derived in Equation (5.24), which has never been possible before.

$$P = \frac{-6U\eta 2b100}{F_t OA} \times \frac{h - F_R}{2h^2 F_R} \left\{ 2hF_R - \left(F_t \frac{OA}{200} + F_R \right) (h + F_R) \right\} \quad (5.24)$$

The total load on the squeegee, L_{II} , can now be obtained by integrating the pressure under the contact region II. This is a useful contribution to the work as the existing models and theory to date have not provided this information in a practically applicable form.

$$L_{II} = \int_{-2b}^0 p(x) dx$$

$$L_{II} = \int_{-2b}^0 \frac{6U\eta}{m} \cdot \frac{h-h_e}{2h^2 h_e^2} \cdot \{2hh_e - \bar{h}(h+h_e)\} dx$$

which can be rewritten as

$$L_{II} = \int_{-2b}^0 \frac{3U\eta}{mh_e^2} \cdot \left\{ (2h - \bar{h}) - \frac{2h_e^2}{h} + \frac{\bar{h}h_e^2}{h^2} \right\} dx$$

now using $h = h_i + mx$, i.e. put $x = \frac{h-h_i}{m}$

$$L_{II} = \frac{3U\eta}{m^2 h_e^2} \int_{h_e}^{h_i} \left\{ (2h - \bar{h}) - \frac{2h_e^2}{h} + \frac{\bar{h}h_e^2}{h^2} \right\} dh$$

$$= \frac{3U\eta}{m^2 h_e^2} \left[(2h_e - \bar{h})(h_i - h_e) - 2h_e^2 \ln h - \frac{\bar{h}h_e^2}{h} \right]_{h_e}^{h_i}$$

$$= \frac{3U\eta}{m^2 h_e^2} \left[(2h_e - \bar{h})(h_i - h_e) - 2h_e^2 \ln \left(\frac{h_i}{h_e} \right) - \bar{h}h_e^2 \left(\frac{1}{h_i} - \frac{1}{h_e} \right) \right] \quad (5.25)$$

Rearranging the calculation for the total squeegee load, as given in (5.25), the squeegee speed can be expressed directly in terms of L_{II} , h_e , η , and indirectly in terms of b , Ft and OA through the parameter m .

$$U = \frac{L_{II} m^2 h_e^2}{3\eta} \cdot \frac{1}{A} \quad (5.26)$$

where

$$A = \left[(2h_e - \bar{h})(h_i - h_e) - 2h_e^2 \ln \left(\frac{h_i}{h_e} \right) - \bar{h}h_e^2 \left(\frac{1}{h_i} - \frac{1}{h_e} \right) \right]$$

Due to the co-ordinate system used, as depicted in Figure 5.5, the squeegee movement from right to left is shown as being positive, but this will be converted to a negative value for the purposes of this work as the point of reference is the squeegee surface and not the x-axis surface.

Equation (5.26) is the derived equation to predict the minimum squeegee speed required to ensure a successful printed deposit is achieved for a particular squeegee type at a set angle and load. This representation of squeegee behaviour is, to the author's knowledge, entirely novel. This equation also has scope to be further examined to provide additional information regarding the screen printing process parameter relationships. These aspects will be discussed in the sections below. [Strictly speaking Equation (5.26) applies for higher speeds than the minimum: it gives the minimum only if h_c is set to the fabric roughness, as in Chapter 6.]

5.6 Screen printing parameter relationships

Equation (5.26) provides analytical information relating to the process parameter relationships which can be interpreted in a very practical way. It is difficult to use the parameter relationships from the equation to describe the process because the parameters all relate to the minimum speed required to achieve the first successful print, and not the final deposit characteristics. However a manufacturing engineer is always interested in being able to increase speed to improve productivity output. The following conditions are found to increase the required squeegee speed:

1. Decreasing the contact width. This will increase the pressure for a given load and therefore less time will be required for the same volume of ink to flow through an aperture.
2. Decreasing the viscosity. A lower viscosity will allow faster flow of ink.
3. Increasing the squeegee load. This conflicts with no. 1 above.
4. Decreasing the percentage open area of the mesh. Smaller volume of ink required to flow, therefore less time is required.
5. Decreasing the fabric thickness. Again a smaller volume of ink is required.
6. Larger values of h_c i.e., a rougher fabric surface. Higher values of h_c could be cleared at higher speeds because there will be a degree of hydroplaning.

This information could be employed as a basis for developing an intelligent system, but further work is required to correlate the resultant deposit characteristics achieved which is outside the scope of this work.

5.7 Discussion and Conclusions

Problems with the wedge geometry included: difficulties in obtaining an accurate value for ϕ ; overcoming a singularity in the pressure; and dealing with an asymmetrical profile. This geometry was thus deemed unsuitable for squeegee behaviour. The same process was then applied to obtain a tilted pad geometry solution. This solution is based on the assumption that the contact follows a Hertzian pressure distribution despite the fact that the contact boundaries are non-parallel. The boundary conditions are also assumed to follow the Hertzian principle such that \bar{h} occurs at $x = -a$.

The derived Equation (5.25) models the screen print process in terms of the ink viscosity, η , mesh parameters of: fabric thickness, F_t ; mesh open area, OA ; and fabric roughness, F_R , squeegee speed, U , and the elastic behaviour of the squeegee under load, as characterised by the half contact width, a . The mesh parameters are very well catered for as each individual aspect of the mesh is considered. The actual tension applied to the mesh and the corresponding snap heights required are not dealt with here as they are purely a function of good edge definition. The open area and the fabric thickness are however related to the tension applied (see [9]) and a relationship could be derived as further work.

The screen print parameters are discussed in terms of h_e , h_i , m and h , assuming that h_e represents the fabric roughness, and also assuming that the RMS value for the fabric roughness applies. Scooping of the squeegee inside the mesh apertures has been neglected as being improbable, particularly as the aperture sizes are approximately $80\mu\text{m}$ and the squeegee tip deformation exceeds $100\mu\text{m}$ even at the minimum possible loading, i.e., the weight of the squeegee and its holder, prior to adding any load.

Consideration of mesh tension effects regarding fabric thickness has been made, as the fabric thickness is specified at a nominal tension of 240 N/m , by the manufacturer. However, mesh tension effects on surface roughness have been neglected due to constraints of measuring techniques available. Rigorous empirical examination of this aspect would be required to validate the work if it were to be used for more than a fundamental behavioural analysis.

Rearranging Equation (5.25) in terms of squeegee speed, see Equation (5.26), allows the minimum squeegee speed to achieve an acceptable print for a set angle, load and hardness to be predicted. Despite requiring a fairly lengthy methodology, calculations to determine the minimum speeds for a range of printing conditions are possible and these can then be applied in

a practical situation. For this to hold true experimental evaluation is required whereby it should be possible to see that below the predicted speed the print will be unacceptable. The next chapter examines this in detail.

Chapter 6 Experimental Evaluation of EHL Screen Printing Model

6.1 Introduction

Chapter 5 proposed a novel model, derived from EHL theory, which provided an equation from which to predict the minimum squeegee speed required to achieve satisfactory printing for a range of set parameters. This chapter outlines the steps which must be followed in order to apply this theory in practice, whilst evaluating the validity of the model. Firstly, methodologies for obtaining values for the exit film thickness and the squeegee tip contact geometry are described. Then these values are substituted into the model to predict the minimum squeegee speed required for “successful” printing and finally a series of experiments examining the validity of the model are reported.

6.2 Exit film thickness height, h_e

This work proposes that the first successful print will occur when the exit film thickness height, h_e , is sufficient to overcome the fabric roughness. To obtain h_e for the purposes of this work, mesh samples have been viewed under a scanning electron microscope. Figure 6.1 shows a Saati Hitech 120LE mesh sample shown end on, magnified 414x. The fabric thickness was specified from the manufacturer’s data as being 66 μ m.

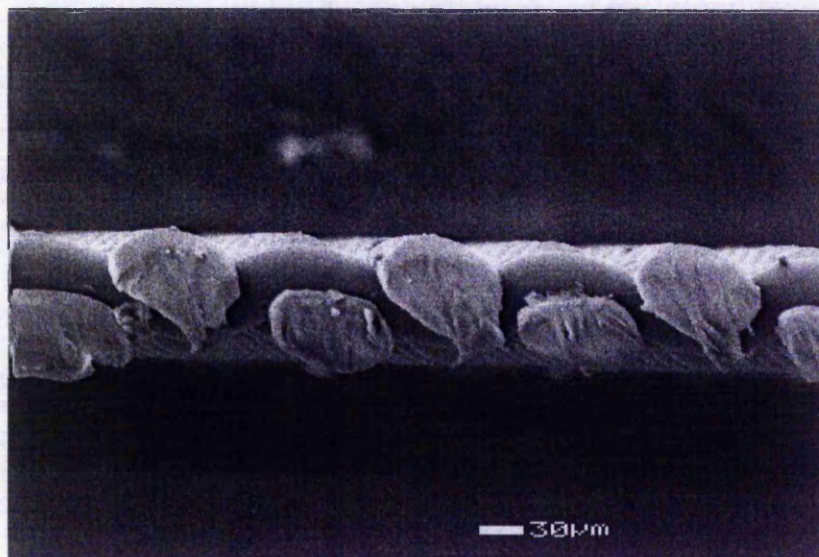


Figure 6.1 120LE mesh magnified 414x

From this image the fabric roughness was estimated as follows. It was assumed that the outline profile of the upper surface of the mesh weave represents the surface roughness of the fabric.

The root mean square (RMS) value was calculated using the formula

$$\text{RMS} = \sqrt{\frac{a^2 + b^2 + \dots + i^2}{L}} \quad (6.1)$$

The definitions of the variables in Equation (6.1) along with a schematic of how the fabric surface was interpreted for this roughness assessment is shown in Figure 6.2. The mean line is positioned so that the sum of the areas above it equates to the sum of the areas below it. For this example an RMS value of $8.6\mu\text{m}$ was obtained.

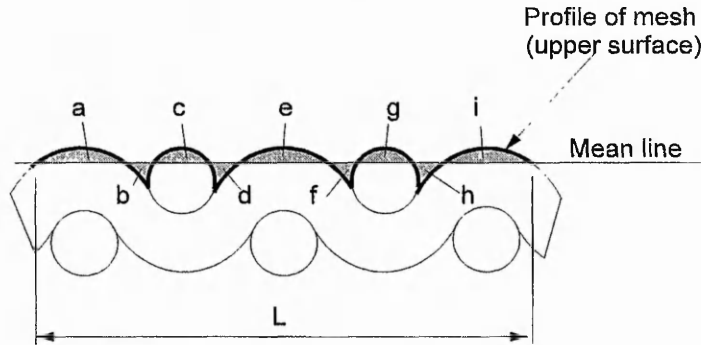


Figure 6.2 Schematic of mesh profile defining RMS equation variables

6.3 Inlet film thickness height, h_i

A relationship between the exit and inlet film thickness under the squeegee was proposed in Chapter 5 by applying the continuity law to the volume flow rates through the screen and under the squeegee tip, thus resulting in an expression for the inlet film thickness, h_i , in terms of the exit film thickness, h_e , i.e. fabric roughness, F_R , the mesh fabric thickness, F_t , and the mesh open area, OA. A worked example is given below.

Worked Example

A 120T mesh of fabric thickness $66\mu\text{m}$ has an open area of 27.04%. If the squeegee speed is 0.1 m/s then the volume flow rate through the screen using Equation (5.17) from Chapter 5 is calculated as follows:

$$\begin{aligned} Q_{\text{SCR}} &= F_t \times l_m \times U \times \text{OA} \\ &= 66.1 \times 10^{-6} \times 0.1 \times 0.2704 \\ &= \underline{1.78 \times 10^{-6} \text{ m}^3/\text{s per linear metre of squeegee}} \end{aligned}$$

Where F_t = fabric thickness as specified in the manufacturer's data i.e. 66.1×10^{-6} m
 OA = fabric open area and is given by:

$$\text{OA} = \frac{\text{Total area of open mesh in a unit area}}{\text{Total unit area}}$$

This industry formula for OA is always expressed as a percentage, %A, and is given as

$$\%A = (1 - McD)^2 \times 100$$

where Mc = Mesh count in threads per cm (T), i.e. 120T

D = thread diameter in cm, i.e. 0.004cm

therefore %A for 120T mesh is 27.04%

The squeegee is assumed to be 1 m wide and therefore the volume flow rate through the screen under the squeegee tip is calculated using Equation 5.18.

$$Q_{SQ} = U(h_i - h_e)$$

Now the total ink volume flow rate can be obtained by applying the continuity law to Equations (5.17) and (5.18), resulting in Equation (6.2)

$$Q_{SQ} = Q_{SCR} \quad (6.2)$$

Therefore,

$$u(h_i - h_e) = Ft \times 1 \times u \times \%A$$

$$h_i = h_e + (Ft \times \%A)$$

$$h_i = 31 \times 10^{-6} + (66.1 \times 10^{-6} \times 0.2704)$$

$$= 4.885 \times 10^{-5} \text{m}$$

6.4 Determining the half contact width of the squeegee tip

Normally the half contact width is easily calculated when using steel, or other such rigid material, as the deformation of the tip would be directly related to the elastic modulus.

However, having no single value for the elastic modulus for rubber, the contact width must be measured for a range of squeegee thicknesses, trailing lengths, material hardnesses, set angles and applied loads. Contact width values were obtained as follows. The squeegee was placed on a shadowgraph and the tip deformation was measured from the sideways profile, an example of which is shown in Chapter 5, Figure 5.1.

Air pressure was used to generate the squeegee load and the surface underneath the squeegee was moved to the left to simulate dynamic conditions. The tip deformations were measured for two different squeegee types at different set angles and under a range of loads. The results are plotted below in Figure 6.3, and are tabulated in Appendix 6.1.

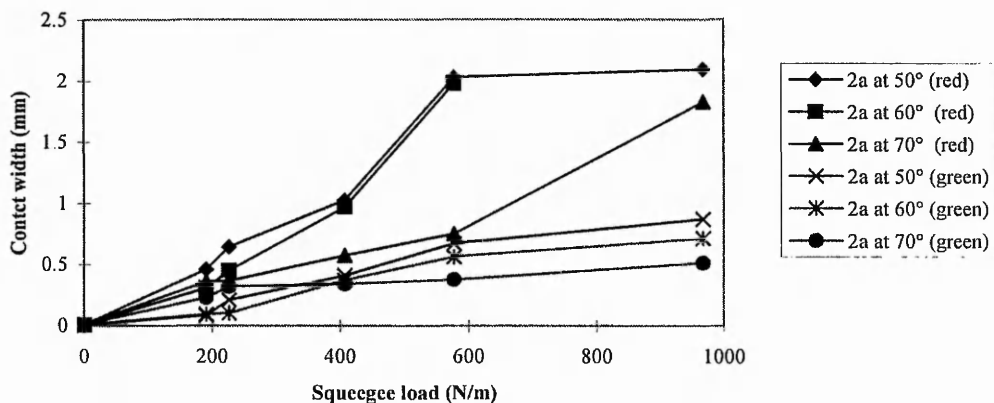


Figure 6.3 Different values of contact width (2a) for different squeegee types and set angles

6.5 Predicting the minimum squeegee speed

The equation for the predicted minimum squeegee speed as given in Chapter 5 (Equation 5.25) was

$$U = \frac{L_w m^2 h_c^2}{3\eta} \cdot \frac{1}{A}$$

Values of U were calculated for two different squeegee types over the same range of contact widths as described in section 6.3. However, to accommodate for experimental error, a straight best fit line was drawn through the points in Figure 6.3 and the rounded values for the contact width are given in Table 6.1.

Table 6.1 Rounded values for contact widths

Load (N/m)	Contact width (mm)					
	Red Squeegee at a set angle			Green Squeegee at a set angle		
	50°	60°	70°	50°	60°	70°
0	0	0	0	0	0	0
20	0.36	0.3	0.24	0.13	0.11	0.1
40	0.72	0.62	0.45	0.26	0.21	0.19
60	1.08	0.95	0.69	0.38	0.31	0.29
80	1.44	1.28	0.91	0.51	0.42	0.38
100	1.8	1.61	1.15	0.63	0.52	0.48
120	2.15	1.95	1.38	0.76	0.62	0.57

The calculated values of U are tabulated in Appendix 6.2 and the results are plotted in Figure 6.4 and Figure 6.5 for a red (60–65°A SH) and a green (80–85°A SH) squeegee respectively.

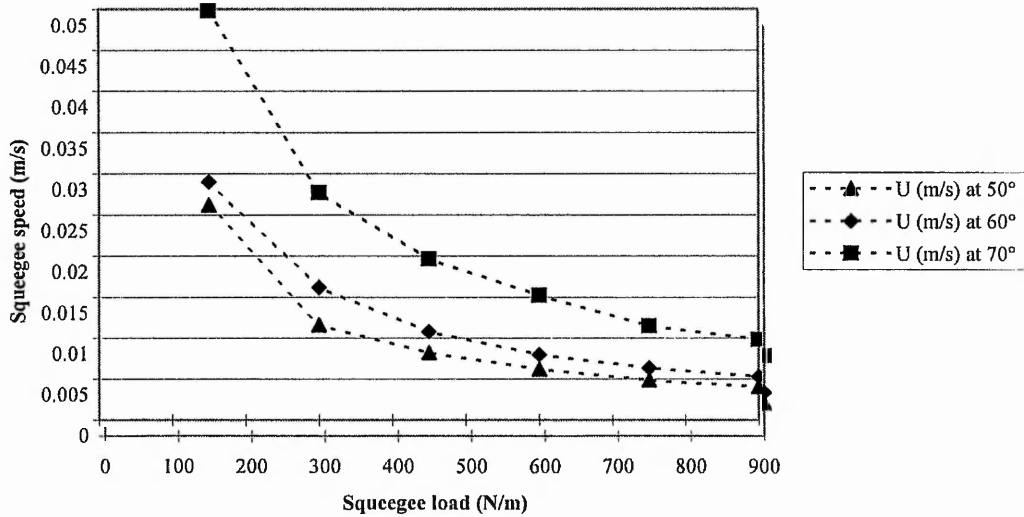


Figure 6.4 Calculated minimum speeds for a red squeegee over a range of set angles and loads

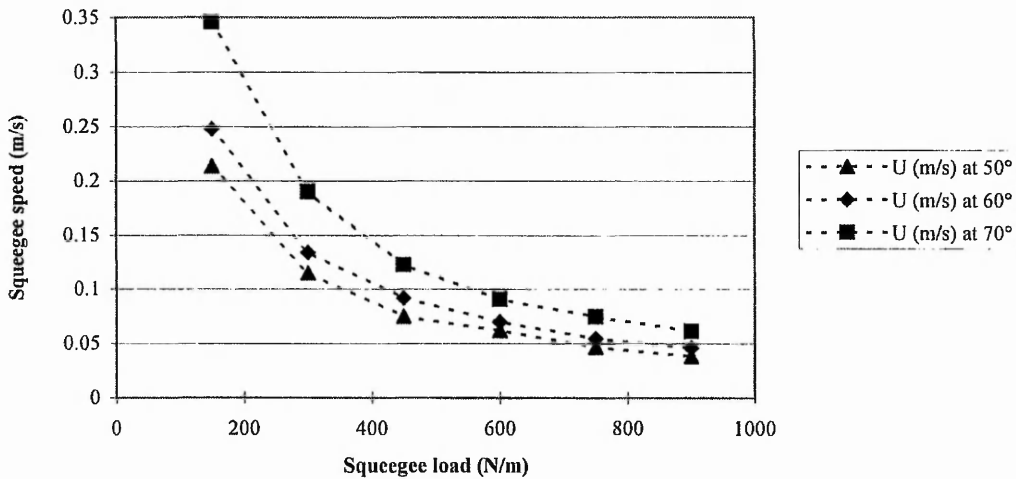


Figure 6.5 Calculated minimum speeds for a green squeegee over a range of set angles and loads

The figures show how the speed varies according to both load and angle, which is the practical interpretation of the half contact width. The general trend shows that for heavier loads a lower squeegee speed is required and, generally, for shallower angles a reduction in speed is also possible.

The squeegee speed is clearly defined in the equation and, if the theory holds true, then a full printed deposit should be achieved once some minimum speed is achieved.

6.6 Experiment to determine minimum print speeds

This experiment enabled a comparison of the predicted speeds to be made with the actual speeds required. When setting up the screen print machine there are four machine parameters to adjust: snap height and the squeegee settings of load, angle and speed. On adapting the above equation there is no information regarding the snap height, and for this work it shall be assumed that the snap height adjustment is purely there to ensure good edge definition. For practical purposes a snap height of 3mm will be set as this is an industrially recommended setting for 120T mesh. The squeegee load, angle and type have been selected to match those of the earlier work in sections 6.3 and 6.4. For each experiment, the squeegee parameters, ink and mesh type were set constant and tested over the complete range of speeds available on the Svecia screen printer. The tests were repeated for a different range of loads using two squeegee types set firstly at an angle of 60°, and then at 70°, to provide information for different contact widths. The resulting deposit profiles were measured on a UBM non-contact laser measuring device within 15 minutes of printing and the speeds were incremented positively. The equipment details, test layouts and the print deposit heights are tabulated in Appendix 6.3.

6.7 Results & Discussion

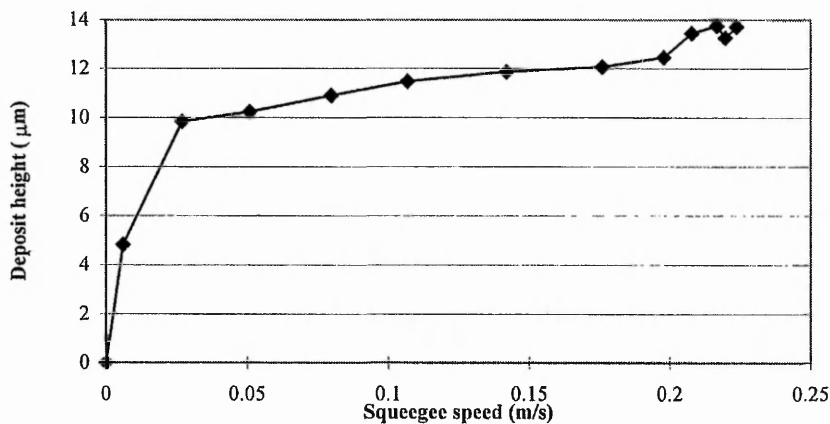


Figure 6.6 Increasing deposit thickness over a range of speeds

For each test set it was clear that the deposit heights increased with speed, a typical example of this can be seen in Figure 6.6. It can be seen that an acceptable squeegee speed range is ≈ 0.05 - 0.2 m/s. The predicted speed for this squeegee setting is ≈ 0.03 - 0.15 m/s. It is also clear that below a minimum squeegee speed a fully printed deposit will not be achieved. This data alone however, was not enough to establish the speed at which a good deposit was achieved, because it cannot be seen from this graph if the printed deposit was complete at 0.05 m/s or if it was not all there until a speed of 0.2 m/s was reached. Thus it was necessary to examine the deposit

profiles visually. As an example, a complete set of profiles for the above data set have been reproduced in Figure 6.7

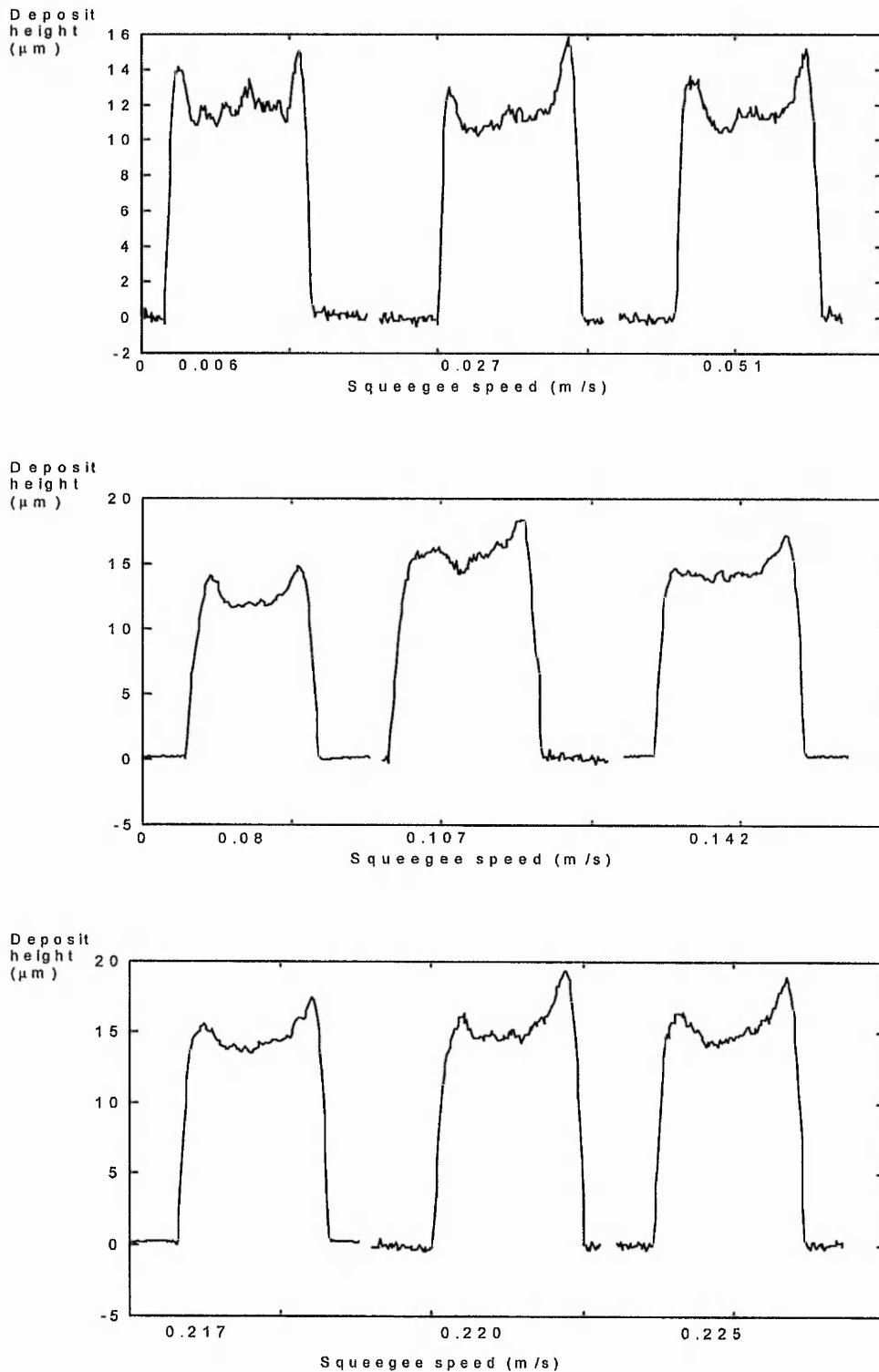


Figure 6.7 2D print deposits increasing in speed

The resulting printed deposit profiles have been assessed using the following criteria. The first criterion for a good deposit is that it must achieve a reasonable height, which for a 120T mesh is approximately $17\mu\text{m}$. The second criterion is that the profile should have a smooth surface. A statistical roughness parameter, R_q , is used in this work, which is concerned with the general waviness of the deposit rather than the classic R_a value which would see each asperity as it was created by the mesh strands and which would thus obscure the gross shape of the deposit. This method of wet deposit characterisation is described by Zhuang et al [56]. The definition for R_q is given in equation (6.3) below.

$$R_q = \sqrt{\frac{1}{N} \sum_{(x,y) \in S} \sum (\hat{Z}(x,y) - \mu)^2} \quad (6.3)$$

where

$$\mu = \frac{1}{N} \sum_{(x,y) \in S} \hat{Z}(x,y)$$

It is proposed that by dividing the deposit height by the surface roughness value an indication of a print quality can be plotted against speed for varying squeegee loads. The results are depicted in Figure 6.8 to 6.12 inclusive. It is clear to see that there is generally a steady increase in deposit quality as speed is increased until the speed exceeds a certain level. This indicates that there is only a fairly small operating window for squeegee speeds.

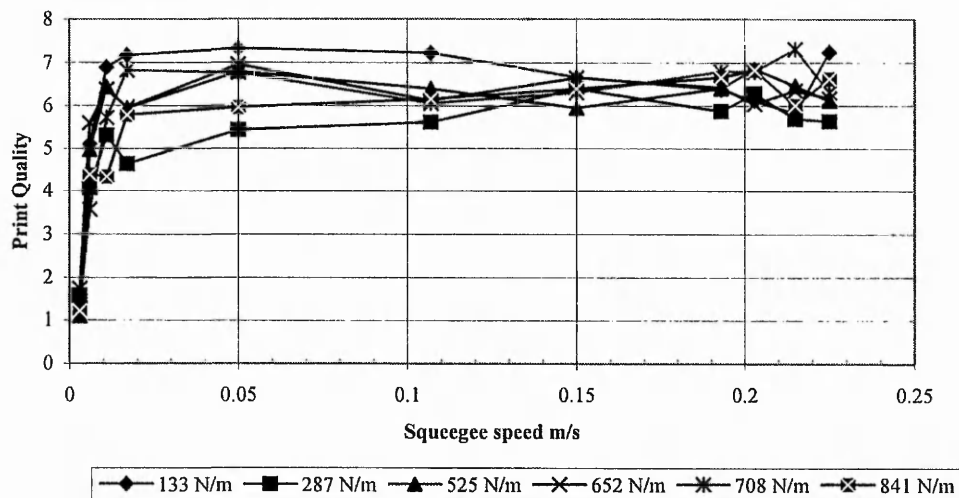


Figure 6.8 Red squeegee at 60° Print quality plotted against speed for varying loads

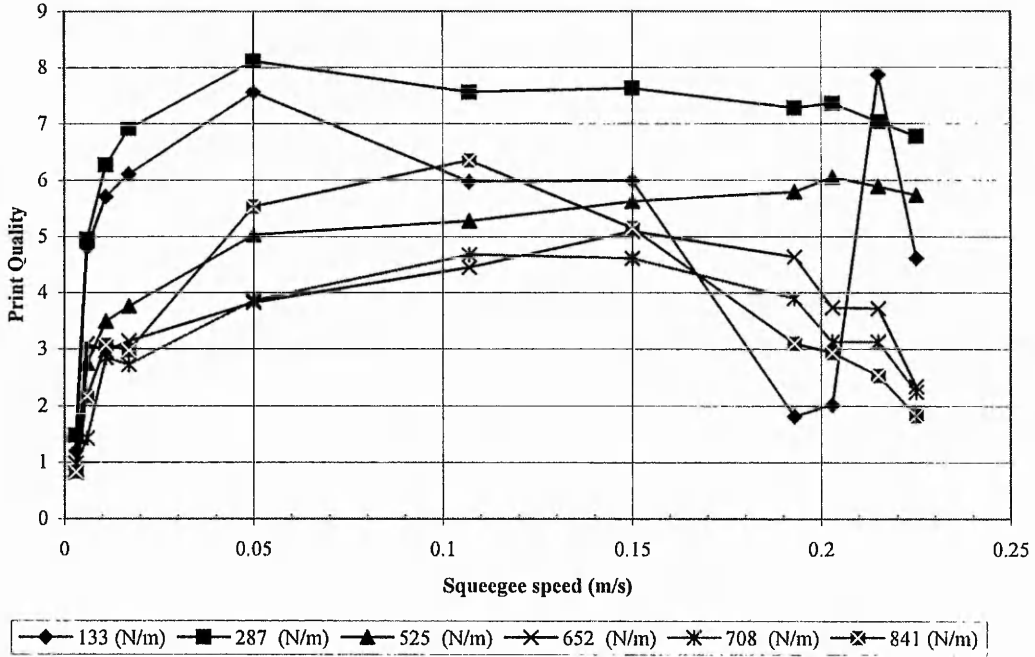


Figure 6.9 Red squeegee at 70° Print quality plotted against speed for varying loads

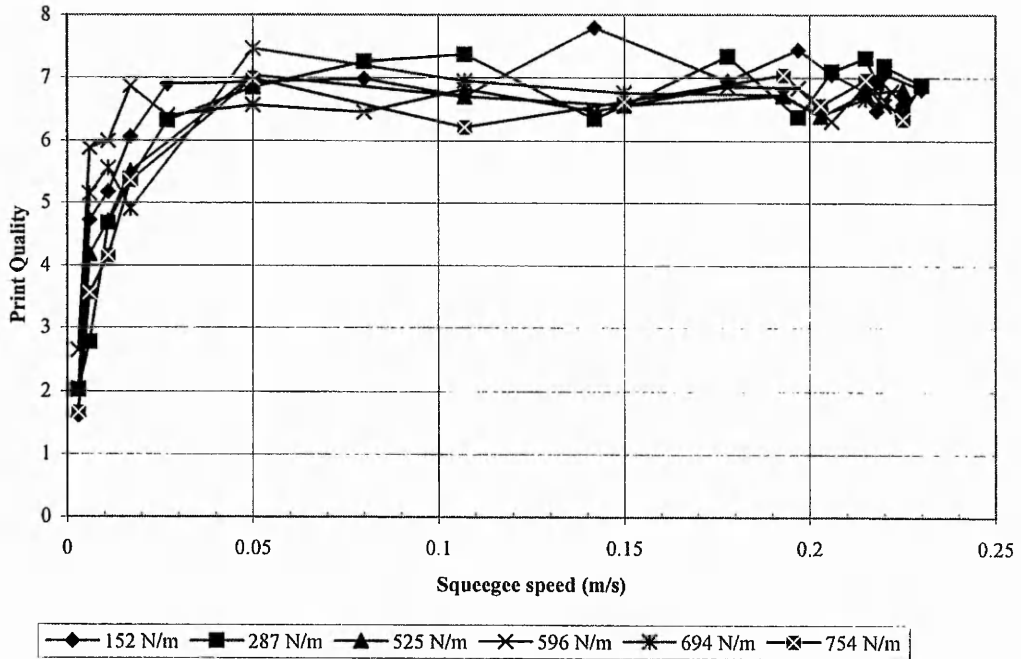


Figure 6.10 Green squeegee at 60° Print quality plotted against speed for varying loads

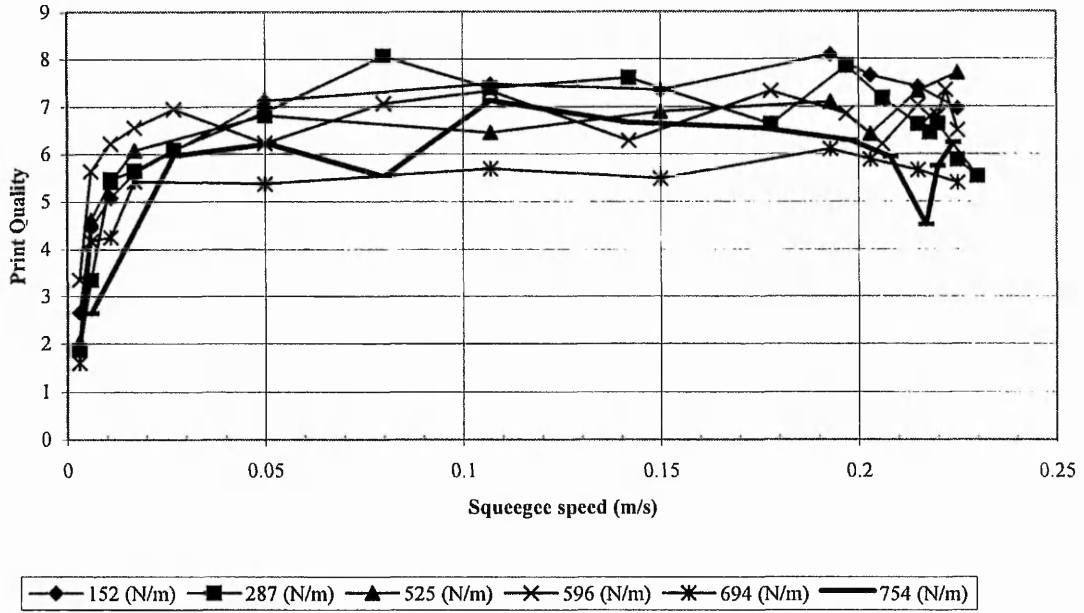


Figure 6.11 Green squeegee at 70° Print quality plotted against speed for varying loads

To interpret this information in a way which could be compared with the prediction of equation 5.26, the speed at which the first successful print from each test set was obtained by drawing two intersecting best fit lines through the data points, an example for one set of data being shown in Figure 6.12. There was a clear distinction between the deposits which were relatively smooth and of a reasonable height and those which were rough and very thin. This provided a minimum speed for each squeegee over a range of loads. The intersection points, i.e. the minimum speeds, have been plotted against the predicted speeds from the calculation in Figure 6.13 and Figure 6.14 respectively.

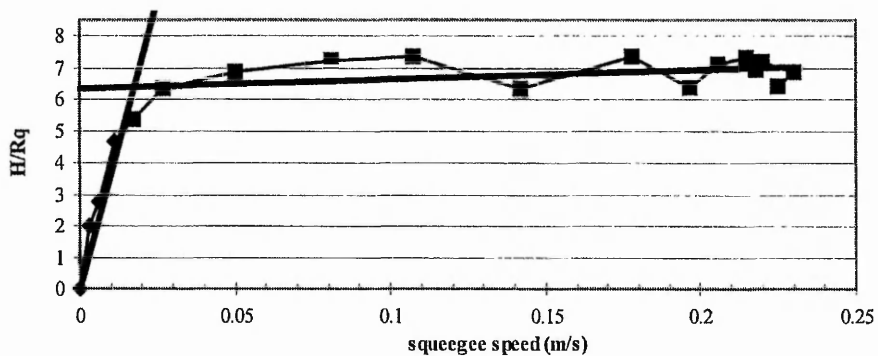


Figure 6.12 An example of best fit lines plotted for green squeegee (at 70°, load 287 N/m)

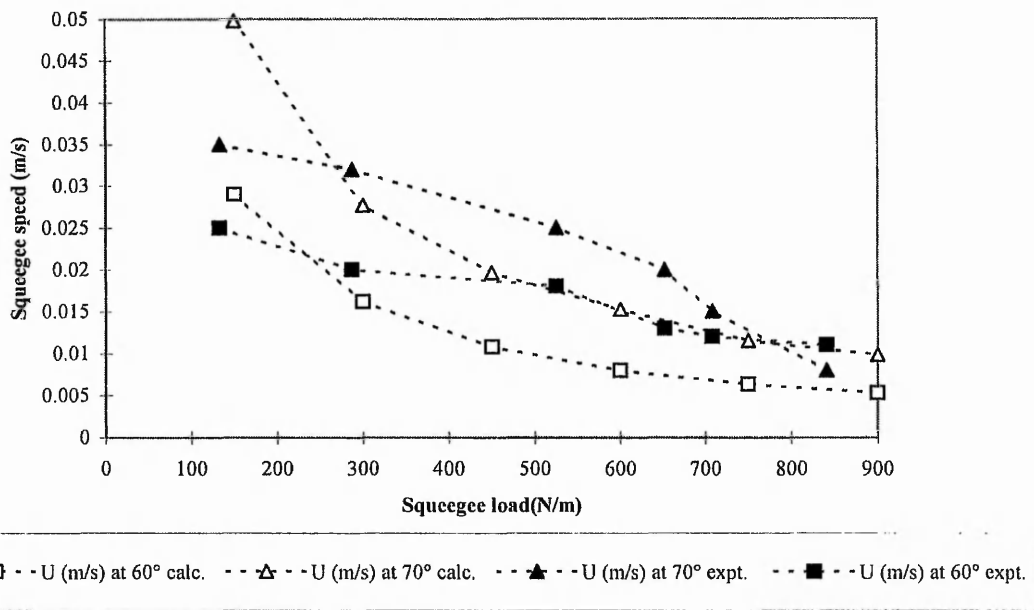


Figure 6.13 Red squeegee predicted speeds compared to experimental values

The red squeegee experimental data compares well to that of the model, until the very high loads at which point the squeegee was extremely deformed and there was severe hydroplaning, especially at the set angle of 60°. This probably accounts for the crossover of minimum speeds at 850 N/m.

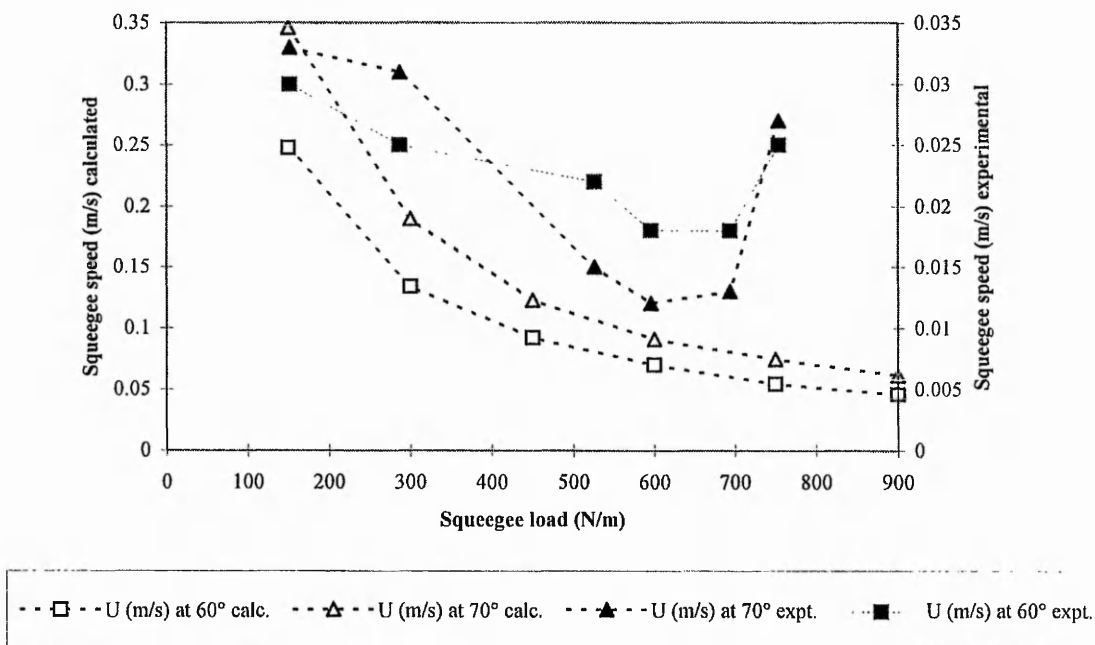


Figure 6.14 Green squeegee predicted speeds compared to experimental values

However, the results for the green squeegee were not in agreement with the model's predictions. There was a discrepancy of a factor of 10, as is shown quite clearly in Figure 6.14, because the experimental values are plotted on the secondary y-axis. The general trend of decreasing speed with a corresponding increase in load is true, as for the red squeegee, but this time only up to approximately 600 N/m after which the trend is reversed. This is explained by the fact that after this load is reached the hydroplaning became very apparent at which point the EHL theory appears to break down. The steep curve of speed against load suggests that the green squeegee is very sensitive to load.

A feasible explanation for the factor of 10 variation is that the contact widths for the green squeegee are approximately one third of those for the red squeegee. Within the calculation this figure is doubled and is a denominator. The result is then squared. This means that the model is far too sensitive to variations in the contact width.

Smaller contact widths cause the minimum required speed to be reduced in the EHL model but the deposit heights were considerably less for the green squeegee compared to the red squeegee (see Figure 6.15), so this suggests that other theories must be governing the harder squeegee.

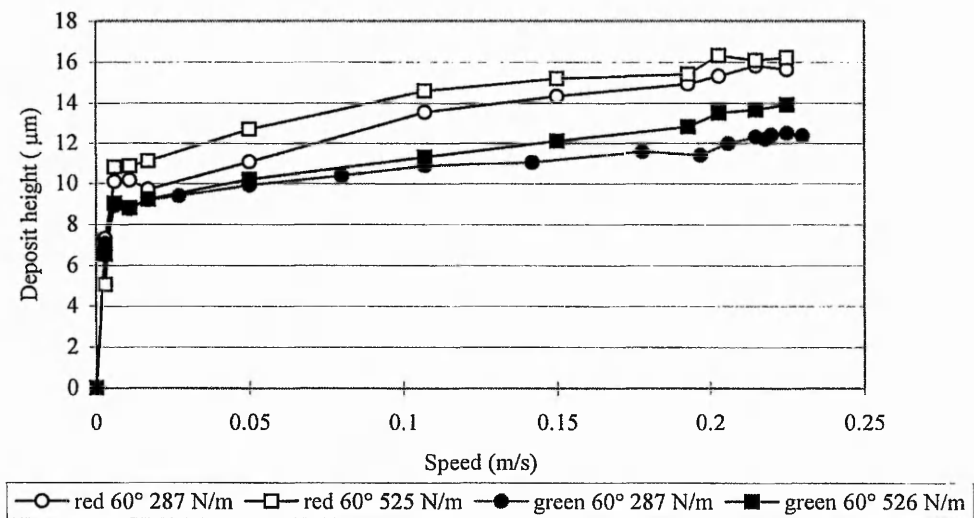


Figure 6.15 Red and green squeegee height comparison

The mesh parameters are very well catered for as each individual aspect of the mesh is considered. The actual tension applied to the mesh and the corresponding snap heights required are not dealt with here as they are purely a function of good edge definition. The open area and the fabric thickness are however related to the tension applied (see [9]) and a relationship could be derived as further work.

Unfortunately, the contact width is the only parameter which can be related to the type of squeegee used, the set angle and the applied load. Further work is required to provide a relationship between this and the set angle, load and squeegee characteristics, but there is no reason why the squeegee manufacturers could not supply this information in a tabulated format.

A limitation of the model is that it can only predict the minimum speed for the first successful print because it is only concerned with filling of the mesh and does not examine the mechanics of emptying the mesh. Surface tension effects of the mesh, non-Newtonian characteristics of the ink and the presence of a stencil on the mesh have all been ignored. Nevertheless the results for the squeegee show excellent agreement between theory and experiment and represent the best attempt to date at predicting the requirements for successful printing.

Chapter 7 - Discussions and Conclusions

The original problem statement as outlined in Chapter 1 of this work describes the fact that screen printing, as a manufacturing process, is very poorly controlled. This is because there is no complete working model at a fundamental level, nor even a rule of thumb. The literature review in Chapter 2 outlines two accepted methods of investigating the process. The first method examines the process using quite a diverse range of theories to base these models on, for example, Hagen-Poiseuille flow, permeable bearings, a cantilevered trailing blade system, and blade coating. None of these produce a satisfactory solution to describe screen printing because they contain unknown quantities or are based on false assumptions. The second approach using experimental techniques really posed more questions than were answered, and raised concerns regarding the validity of the type of experimentation being advocated by some authors. The better quality papers defined their experimental parameters specific to their end applications, and their equipment, using settings which were not in standard units. As no information was provided to convert these settings their findings could not be applied generically. This work certainly confirmed that the process was complex, and indicated that no single rule would apply for every screen printing situation. This thesis explored the screen printing process both analytically and experimentally and showed that experimentation based on factorial analysis was hopelessly longwinded and that the analytical models lacked essential fundamental knowledge of the process. Each aspect of these two approaches is discussed in greater depth below.

Chapter 3 details the dilemma faced when selecting a suitable experimental design to resolve the issue of screen printing process control. The interdependent nature of screen printing variables was confirmed by undertaking a full factorial experiment, but little information was gained about the process behaviour because the number of trials was insufficient to establish useful trends. Each test requires over 7 minutes to obtain data and for a 4 factor, 3 level full factorial experiment 81 test sets were required. These tests were only repeated once due to time constraints. At only 3 levels for each factor it is impossible to plot a meaningful graph, as at least six points are required. This would result in a total of 1296 test sets, which would all need repeating at least once, and therefore would take approximately 320 hours of experimentation prior to undertaking any analysis. It was however possible to see that certain operating windows for pressure and speed relationships were present, although it was unclear whether any particular pattern existed.

High order interactions between the snap height and the squeegee variables of pressure, speed and angle, were shown to be present, which indicates that fractional factorial experiments are seriously compromised due to confounding. This limits their use to initial process setting only. The methodology provides no process understanding and several small experiments are required to establish production capabilities depending on the operating tolerances required. The approach is extremely time consuming and severely lacking, compounded by conflicting results and poor repeatability. It was apparent that the original objectives of this work had to be abandoned and a broader knowledge of the fundamentals of screen printing was necessary, thus the leading model in screen printing research was examined.

The adaptation of Huner's model, which was tested on a modified tilting pad apparatus in Chapter 4, clearly showed that it was wrong at the most fundamental level. The whole argument that screen printing is governed by hydrodynamic lubrication theory was thus brought into debate.

The pressures required to ensure flow through a mesh at the required speed were experimentally obtained and these were found to be far in excess of those generated under the gross curvature of the squeegee. These pressures were previously undetermined, to the best of the author's knowledge. As a result of these findings Chapter 5 proposed EHL as being a suitable theory to describe the screen printing process behaviour. To date, screen printing has not been modelled in this way, although similarities exist in the model proposed by Owczarek and Howland, where the tip deformation and the flow underneath the squeegee are considered. Initially, a classic wedge indenter geometry as defined in Hills et al was adapted to provide a minimum film thickness related to squeegee and ink parameters. However, a singularity in the pressure rendered this approach unsuitable because it could only account for rigid contacts and the soft nature of the squeegee did not comply with the basic assumption of infinite pressure at the wedge tip. The wedge profile also contravened the symmetry assumptions and the deformation angle could not be accurately obtained for the soft rubber material.

Using the analytical solution from Baglin and Archard, elastic equations for soft EHL were developed to suit a squeegee profile. The key assumptions are that the contact behaviour is Hertzian, that the contact is not parallel and that the maximum pressure acts at the centre of the contact, or at a point close enough to negate the effects. An equation for pressure is thus obtained which requires a value of surface roughness for the mesh.

This equation for pressure was substituted into Reynolds' equation which was adapted by Cameron to evaluate pressure inside the contact region of two surfaces. A novel approach to obtaining the inlet film thickness was described in section 5.4 and this assumes that there is no side flow of ink and neglects losses through ink adhering to mesh strands. This work contributes to screen printing research by deriving an equation for the total load under the squeegee tip. This load could not be previously derived analytically, but having determined the relationships of h_e and h_i , the pressure is now expressed entirely in screen printing parameters. This equation was rearranged to provide a relationship of squeegee speed in terms of squeegee load, squeegee tip deformation, mesh characteristics and ink viscosity. The squeegee speed predicted is for the first successful print, as the speed is increased. This is achieved when the squeegee first clears the mesh surface, i.e. is fully lubricated. It is assumed that the maximum asperity as experienced by the squeegee tip equates to a specific value of surface roughness and that this is equivalent to the exit film thickness, h_e . For this work, the roughness of a 120T mesh was found to be $8.6\mu\text{m}$, but this value was obtained experimentally, and no account of mesh tension was made.

A major shortcoming of this work is that it only deals with filling of the mesh. The transfer of ink through the mesh, with the additional effects of acceleration created by the snap height are completely ignored. The justification for ignoring it is that not enough was known about actually filling the mesh with ink and this must come first. Furthermore the snap height's primary function has been assumed to be to ensure good edge definition. Further work to examine the snap height and mesh tension is required.

The proposed EHL model in this work provides a relationship between the print speed and the ink viscosity, mesh characteristics and the squeegee variables, but it is limited to only being able to predict the minimum speed at which the first successful print can be achieved. A separate project is required to explore the maximum possible printing speeds.

Introducing the idea of Print Quality as defined by deposit height/roughness parameter, R_q , is a convenient way of comparing these minimum speeds for different squeegee types and is an improvement on subjective methods of printed deposit characterisation. It is however not the definitive solution, as many other statistical representations are available and additional analyses should be undertaken to determine the most appropriate parameters.

Chapter 6 shows excellent agreement between the predicted and experimental values for the softer (red) squeegee and so EHL theory can be said to apply. However, for the harder (green)

squeegee the results are larger by a factor of 10. This suggests that EHL is not the only theory governing the printing process. A combination of boundary and, or, hydrodynamic, and elasto-hydrodynamic lubrication theories probably apply depending on the squeegee and ink characteristics. Further work to determine the limits of EHL and the combination of lubrication theories applicable outside of these limits is necessary. Extending the studies reported by Owczarek and Howland where the pressures within the ink roll are divided into three pressurisation regions and developing these in conjunction with the measured contact widths and the pressure equation derived in chapter 5, would perhaps be a first avenue of exploration to determine the constraints of EHL theory.

The final printed wet deposit thickness is not predicted by the EHL model at all and this is a severe limitation of the model. Investigations of print deposit features should be pursued and on determining acceptable conditions, a link establishing acceptable prints to the minimum film thickness should be made.

The aim of this work was to examine ways of improving the screen print process control from the Manufacturing Engineer's viewpoint, i.e. defining the inputs to the process required to give the desired process response. This aim has been fulfilled only for selected process parameters, i.e. squeegee variables and mesh characteristics. The deposit characterisation is recommended as a project in itself. Additional information is required to allow the Manufacturing Engineer to readily adopt it for production purposes; for example, tables of mesh roughness from cloth manufacturers, and tables of tip deformations for set angles and loads for specific squeegee types, from squeegee manufacturers.

This work has provided a further insight into screen print process behaviour and has outlined potential avenues for further exploration within the context of this thesis. Other possible areas of benefit to screen print research are CFD and application of fuzzy logic.

An experimental technique to identify the pressure required for flow through a mesh has been described which can be adapted to suit all mesh types. This can then be used to predict theoretical squeegee speeds. An equation is provided which allows the pressure generated under the squeegee tip to be calculated, which is of major importance to any control system when modelling the process, and it has been further developed in this work to provide the first successful theoretical representation of the screen printing process, within limits. This is a major advance in screen print research and continued development of this model should allow a generic model to be developed as a basis for controlling the screen printing process.

The main conclusions of this work can be summarised as:

- Experimentation using factorial analysis is excessively longwinded
- Fractional factorial experiments are misleading due to errors of confounding
- The assumption that screen printing is governed only by hydrodynamic lubrication theory is incorrect
- The author's application of elastohydrodynamic lubrication is an appropriate theory to predict minimum squeegee speeds for effective printing

From this the following further work is recommended:

- Establish limits for the EHL model
- Development of a model using both hydrodynamic and elastohydrodynamic lubrication theories to accommodate the squeegee tip deformation and gross curvature of the squeegee separately
- Review techniques to quantify print quality objectively
- Develop the ideas of Riemer to understand the emptying of mesh apertures, including the mesh effects under tension
- Produce charts to provide basic information regarding squeegee and mesh characteristics for a range of parameter settings and mesh tensions respectively

References

- 1 KOBS,D.R.,VOIGT,D.R., Parametric Dependencies in Thick Film Screening, International Society for Hybrid Microelectronics, 5.5.1-10, 1970
- 2 RIEMER,D.E, The Theoretical Fundamentals of the Screen Printing Process, Hybrid Circuits, January, 18, 8-17, 1989
- 3 ATKINSON,J., Screen Printing: The Art of Thick Film Sensors, Systems and Applications Proceedings of 5th Conference on Sensors and their Applications, Edinburgh, September, 541-46, 1991
- 4 MARKSTEIN,H.W., Hybrid Screen Printing: Art or Science, Electronic Packaging and Production, 28, 9, 28-1, 1988
- 5 CROPPER,M, Studies of Fluid Pressure in Screen Printing, Ph.D. Thesis, Watford College of Technology, England, 1973
- 6 MOLAMPHY,T.A., Application of Experimental Design to the Solder Paste Screen Printing Process, Surface Mount Int. Conf and Exposition Proc. of the Technical Program, 1, 496-502, 1991
- 7 NICKEL,J., The Way to Measure the Effective-Squeegee-Attack-Angle-Angle and its Significance for the Ink Stream, Screen Process, February, 25-27, 1993
- 8 ANDERSON, M., KIRCHNER,K., and MOLTZ, E., Development of X-Ray Laminography as a Process Control Tool, Surface Mount International Conference and Exposition of the Technical Proceedings, 2, 127-1146, 1992
- 9 HOHL, D.M., HUNT, D.D., Physical Changes In Polyester Mesh During Tensioning, SPTF Research Report, 1992
- 10 ATKINSON, W.A.,YOUNG,D.H., An Intelligent Approach to Screen Printing, International Journal of Hybrid Microelectronics, 4, 2, 385-391, 1981
- 11 YOUNG, M., Screen Process Printing Techniques, PCFab, February, 77-90, 1987
- 12 PHIPPARD, C, Screen Printing Quality Control and Faultfinding, Circuit World, 10, 1, 16- 19, 1983
- 13 BUTTARS, S.K, Parameters for Solder Paste Printing, Proceedings of the Technical Program of the National Electronic Packaging and Production Conference NEPCON West, 1, 799-806, 1990
- 14 HOHL, D.M., High Tension Effects on Ink Deposit, SPTF Research Report, March 1996
- 15 DANNER, P., Hybrid Screen printing: Art or Science? Electronic Product and Packaging, September 1988, pp.29
- 16 HOBBY, A., Practical Aspects of Printing Solder Paste, DEK Printing Machines Ltd, Albany Rd, Granby Industrial Estate, Weymouth, UK., 1992
- 17 HOBBY, A., Process Solutions for Printing Solder Paste Down to 0.3mm Pitch, DEK Printing Machines Ltd, Albany Rd, Granby Industrial Estate, Weymouth, UK., 1992

References

- 18 HOBBY, A, Printing and Firing Thick Film Hybrids., DEK Printing Machines Ltd, Albany Rd, Granby Industrial Estate, Weymouth, UK., 1989
- 19 HOBBY, A., Dispensing versus Screen Printing, *Electronic Production*, April, 29, 1988
- 20 ISMAIL, I., MANNAN, S.H., EKERE, N.N., LO, E.K., Experimental Study of the Printing of Solder Paste using the Metal Blade Squeegee System, *Proceedings 30th International MATADOR Conference, August 1992*, pp.263-266
- 21 BROWN, C.P., Process Solutions for Ultra Fine Pitch Production, *Surface Mount International Conference Proceedings of the Technical Program*, 119-126, 1993
- 22 MANNAN, S.H., EKERE, N.N., ISMAIL, I., CURRIE, M.A., Computer simulation of solder paste flow, Part II: Flow out of a stencil aperture, *Journal of Electronics Manufacturing*, 4, 1994, pp.149-154
- 23 HUNER, B., Comments on "The Function and Performance of the Stainless Steel Screen During the Screen-Print Ink Transfer Process", *ISHM*, 10, 2, 1987, pp. 6-13
- 24 HUNER, B., A Simplified Analysis of Blade Coating with Applications to the Theory of Screen Printing, *The International Journal for Hybrid Microelectronics*, 12, 2, 1988, pp.88-94
- 25 HUNER, B., A Second Look At The Printing Screen, *ISHM Journal*, 12, 1989, pp.181-187
- 26 HUNER, B., Effects of In-Plane Permeability in Printing Screens, *The International Journal for Hybrid Microelectronics*, 13, 2, 1990, pp.35-40
- 27 HUNER, B., A Note on the Estimation of the Wet Film Thickness During A Screen Print Operation, *The International Society for Hybrid Microelectronics*, 13, 1, 1990, pp.27-28
- 28 HUNER, B., Distortion of the printing screen induced by squeegee loading, *International Journal for Hybrid Microelectronics*, 14, 1, 1991, pp.23-9
- 29 HUNER, B., An Analysis of a Screen Printing System Equipped with a Trailing Blade Squeegee, *The International Journal of Microcircuits and Electronic Packaging*, 16, 1, 1993, pp. 31-40
- 30 RANGCHI, H., HUNER, B., AJMERA, P.K., A Model for Deposition of Thick Films By The Screen Printing Technique, *Proceedings, ISHM Symposium, October, 1986*, pp. 604-608
- 31 MANNAN, S.H., EKERE, N.N., LO, E.K., ISMAIL, I., Application of Ink Screening Models to Solder Paste Printing in SMT assembly, *Journal of Electronics Manufacturing*, 3, 1993, pp.113-120
- 32 OWCZAREK, J.A., HOWLAND, F.L., A Study of the Off-Contact Screen Printing Process-Part I: Model of the Printing Process and Some Results Derived From Experiments, *IEEE Transactions on Components, Hybrids, and Manufacturing Technology*, 13, 2, 1990a, pp. 358-367
- 33 OWCZAREK, J.A., HOWLAND, F.L., A Study of the Off-Contact Screen Printing Process-Part II: Analysis of the Model of the Printing Process, *IEEE Transactions on Components, Hybrids, and Manufacturing Technology*, 13, 2, 1990b, 368-375

References

- 34 BOYACIGILLER, G., Some Studies of Mechanism of Screen Printing., Ph.D. Thesis UMIST, 1970
- 35 CARLISLE ,B.H., Screen Printing Promises Smaller, Cheaper PCBs, Machine Design, December 11, 1986, pp. 101-105
- 36 RIEMER, D.E., The Direct Emulsion Screen as a Tool for High Resolution Thick Film Printing, Electronic Components Conference Proceedings, 1971, pp. 463-467
- 37 RIEMER, D.E., Deposition Weight, A Powerful Control Tool For The Thick Film Process, Proceedings of the ISHM Symposium, 1974, pp. 347-352
- 38 RIEMER, D.E., The Shear and Flow Experience of Ink During Screen Printing, Proceedings of the ISHM Symposium, 1987, pp. 335-340
- 39 RIEMER, .E., The Function and Performance of the Stainless Steel Screen During The Screen Print Ink Transfer Process, The International Journal for Hybrid Microelectronics, 10,2, 1987, pp.1-8
- 40 RIEMER, D.E, Analytical Engineering Model of the Screen Printing Process: Part I, Solid State Technology, August, 1988, pp.107-111
- 41 RIEMER, D.E, Analytical Engineering Model of the Screen Printing Process: Part II, Solid State Technology, September, 1988, pp.85-90
- 42 MITCHELL, M.C., HOWARTH, M., GENTLE, C.R., Improving Screen Printing Process Control, Advances In Manufacturing Technology VIII, Proceedings of the 10th National Conference on Manufacturing Research, Ed. Case, K. & Newman,S., September 1994. pp.562-566
- 43 HUNER, B., A cause for Patchiness in Wet Film Prints, The International Journal of Microcircuits and Electronic packaging, 15, 2, 1992. pp. 97-102
- 44 HUNER, B., A Stokes Flow Analysis of the Screen Printing Process, the International Journal of Microcircuits & Electronic Packaging, Volume 17, Number 1, First Quarter 1994, pp. 21-26
- 45 MANNAN, S.H., EKERE, N.N., LO, E.K., ISMAIL, I., Predicting Scooping and Skipping in Solder Paste printing for Reflow Soldering of SMT Devices, Soldering and Surface Mount Technology, 15, October 1993, pp. 14-17
- 46 HANRAHAN, T.F., MONAGHAN, P.F., BABIKIAN, R.D., Modelling of a solder paste flow with a free surface in stencil printing. Advances in Electronics Packaging. ASME/JSME Conference on Electronics Packaging, 2, 1992, pp.587-592
- 47 BROWN, D.O., Screen Printing - An Integrated System, International Symposium on Microelectronics, Georgia, 1986
- 48 BEHREND, G.H., Control of Ink Deposition Thickness Across a Range of Mesh Counts, Screen Process, 43, 4, 1993, pp. 36-38
- 49 HOHL, D.M., Hunt, D.D., Polyester Mesh Capability Study With UV Inks, SPTF Research Report, 1991
- 50 BERNAUER, J., Neueste Entwicklungen in der Raketentechnik, Siebdruck, 28, 4, 1982, pp.251-260

References

- 51 BUTTARS, S.K., Parameters of solder paste printing for fine pitch components, Proceedings of the Technical Program. NEPCON West '93, 3, 1993, pp. 1254-65
- 52 ANON., What Every Printer Should Know About Squeegees, Screen Process, November, 1991, pp.27-30
- 53 HOHL, D.M., Estimating Ink Deposit in Screen Printing: Improving Your Accuracy, SPTF Research Report, 1996
- 54 HOHL, D.M., Controlling Off-Contact, Screenprinting & Graphic Imaging Association International Journal, Volume 1, Fourth Quarter 1997
- 55 ZHUANG, W., HOWARTH, M., MITCHELL, M.C., Screen Print Deposit Measurement for Electronic Applications, Advances in Manufacturing Technology X, Proceedings of the 12th National Conference on Manufacturing Research, Eds. A.N. Bramley, A.R. Mileham and G.W. Owen, 1996. pp. 6-10
- 56 ZHUANG, W., HOWARTH, M., LAI, E., LOTFI, A., Wet Ink Deposit Feature Extraction for Screen Printing Process Modelling, Advances in Manufacturing Technology XI, Proceedings of the 13th National Conference on Manufacturing Research, Ed. D.K. Harrison, 1997. pp. 640-644
- 57 BOX, G.E.P., HUNTER, W.G., HUNTER, J.S., Statistics for Experimenters: An Introduction to Design, Data Analysis and Model Building, John Wiley & Sons, New York, 1978
- 58 TAGUCHI, G. System of Experimental Design, UNIPUB/Kraus International Publications (English Edition) 1987
- 59 LIN, T.E., Making Taguchi Simple, Quality Today September 1992 pp.32-34
- 60 LIN, T.E., Using Taguchi Methods in Quality Engineering, Quality Progress, September 1990
- 61 BANDUREK, G.R., DISNEY, J., BENDELL, A., Application of Taguchi Methods to Surface Mount processes, Quality and Reliability Engineering International, 1988
- 62 GREENFIEL, T., Taguchi Policy A Ridiculous and Dangerous Fashion, Royal Statistical Society News, May 1995
- 63 HEYES, G.B., Taguchi Talk - what's the message?, Quality Today, July 1990, pp.14-15
- 64 ROSS, P.J., Taguchi Techniques for Quality Engineering, McGraw Hill, 1988
- 65 HOHL, D.M., The Effects of Five Printing Variables on Resolution and Ink Deposit, Contract No. 93-F361990-000, SPTF Technical Presentation, Fespa 1996
- 66 LOTFI, A., MITCHELL, M., HOWARTH, M., THOMAS, P., Industrial Application of Fuzzy System: Part I; Fuzzy Feature Extraction and Defect Classification of Stencil Printing, Proceedings of the Third Joint Conference on Information Sciences- FTT'97, Vol. 1, March 1997, pp.299-302
- 67 STOUT, K.J., SULLIVAN, P.J., et al, The Development of Methods for the Characterisation of Roughness in Three Dimensions, published on behalf of the Commission of the European Communities, 1993.

References

- 68 SINDEN, M., The Influence of the Squeegee on the Screen Printing Process, BEng Thesis, The Nottingham Trent University, April 1995
- 69 LINDLEY, P.B., Engineering Design with Natural Rubber: NR Technical Bulletin 1970
- 70 MARTIN, G., ROTH, F.L., and STIEHLER, R.D., Behaviour of 'pure gum' rubber vulcanizates in tension. Trans. Inst. Rubber Ind., 32, 189, 1956
- 71 BROWN, R.P., Handbook of Plastic Test Methods, London: Godwin in association with the Plastics and Rubber Institute, 1981
- 72 CAMERON, A., Basic Lubrication Theory, Chapter 13, Longman Group Ltd., 1971
- 73 JOHNSON, K.L., Contact Mechanics, Chapter 10, Cambridge University Press, 1985
- 74 HILLS, D.A., NOWELL, D., SACKFIELD, A., Mechanics of Elastic Contacts, Chapter 2, Butterworth-Heinemann Ltd., 1993
- 75 BAGLIN, K.P., ARCHARD, J.F., An Analytical Solution of the Elastohydrodynamic Lubrication of Materials of Low Elastic Modulus. IMech E Conference on Elastohydrodynamics Part 72, Vol. C3 1972

Appendix 1.1 Squeegee Materials & Geometry

WATTS URETHANE PRODUCTS LTD. CHURCH ROAD,
TEL: (0594) 844090/842203 · TELEX: 43512 WATT

Plus

G1 PROFILE—LIST PRICE £ PER COIL (55-85A HARDNESSES*)										
THICKNESS (MMS)										
	5	6	6.35	7	8	9	9.5	10		
WIDTH (MMS)	20	16.12	23.36	-	26.28	28.64	32.13	34.09	35.84	-
	25	22.16	32.13	29.82	36.16	39.36	44.18	46.84	49.26	1"
	30	29.14	36.72	-	41.30	44.98	50.48	53.55	56.30	-
	32	-	-	36.75	-	-	-	57.75	-	1 1/4"
	35	31.43	39.59	-	38.78	48.54	54.48	57.75	60.76	-
	40	37.74	41.35	44.10	53.48	58.24	65.32	69.35	72.92	1 1/2"
	45/47	43.54	47.70	58.52	61.74	67.30	65.59	69.58	84.14	1 7/8"
	50/51	47.18	51.69	55.12	58.17	63.30	71.05	75.39	79.24	2"
	54	47.18	59.44	-	66.90	72.79	71.07	86.69	91.13	-
	75	70.77	89.15	-	100.31	109.20	122.60	130.02	136.72	3"
		-	-	1/4"	-	-	-	3/8"	-	
THICKNESS (INCHES)										

G2 - G15 PROFILE—LIST PRICE £ PER COIL (55-85A HARDNESSES*)				
REFER TO G1 LIST PRICE ADD % SHOWN AFTER APPLYING G1 DISCOUNTS. (G2-G15 supplements are not discountable)				
G2/G3/G4/G15	G5	G6	G7/G8/G9/G10	
+15%	+30%	+50%	+30%	
KNIFE CUT EDGES: As per above prices in pounds (£) sterling				
GROUND EDGES: Subject to £3.00 per edge surcharge				
DISCOUNTS: Quantity discounts available on application.				
COIL LENGTH: 3.0 METRES TO 3.5 METRES (standard lengths: 3.5 metres)				

ULTRATHANE HARDNESSES		
REF NO.	SHORE 'A' HARDNESS	COLOUR
5570	55 - 60 (EXTRA SOFT)	YELLOW OR RED
5620	60 - 65 (SOFT =S)	RED
5670	65 - 70 (SOFT MEDIUM)	RED
5720	70 - 75 (MEDIUM =M)	GREEN
5770	75 - 80 (HARD)	BLUE
5820	80 - 85 (EXTRA HARD)	NATURAL

Can be supplied NATURAL in all hardnesses by arrangement.

PROFILES

G1 **G2**

G3 **G4**

G5 **G6**

G7 **G8**

G9 **G10**

G15

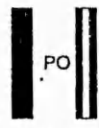
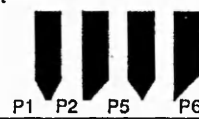
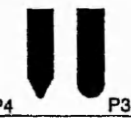
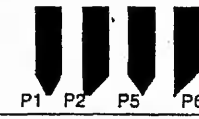
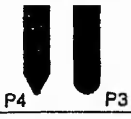
S = SOFT
M = MEDIUM
OTHER PROFILES BY ARRANGEMENT

A WATTS OF LYDNEY GROUP COMPANY



OTHER HARDNESSES AND SIZES ARE AVAILABLE BY ARRANGEMENT.
*MATERIAL 'VULKOLLAN' BASED. REG. TRADE NAME OF BAYER AG
All prices are exclusive of carriage and VAT

Choosing a serilor® squeegee accordingly to its hardness

Soft grade	Pressure, Opening, Ink Viscosity	Off-contact Setting and Screen Tension	Conformity to Print Surface	Registration and Ink Deposit
Rectangular  SR1 SR3	Medium pressure; large mesh openings and low viscosity inks.	Compatible with low tension screens or screens with minimal off-contact distance.	Use on rugged and irregular surfaces, uneven printing beds and poorly adjusted presses.	Medium control of fine details and registration. High ink deposit, heavier if edges are removed.
<div style="border: 1px solid black; padding: 5px; display: inline-block;">Noticeable improvement with serilor®3 (soft+hard+soft)</div>				
Bevelled/pointed  SR1 P1 P2 P5 P6	Medium pressure; large mesh openings and low viscosity inks.	Compatible with low tension screens or screens with minimal off-contact distance.	Use for rugged and irregular surfaces and curved surfaces (containers).	Medium control of fine details and registration. High ink deposit.
Rounded  SR1 P4 P3	Medium pressure; large mesh openings and low viscosity inks.	Compatible with low tension screens or screens with minimal off-contact distance.	Use for rugged and irregular surfaces, and for absorbant materials, especially textiles.	Little control of fine details and registration; heavy ink deposit. Use to obtain maximum ink coverage.
Medium grade	Pressure, Opening, Ink Viscosity	Off-contact Setting and Screen Tension	Conformity to Print Surface	Registration and Ink Deposit
Rectangular  SR1 SR3	For higher pressure printing; useful for a wide range of meshes and ink viscosities.	Use with high tension screen and an appropriate off-contact distance.	Moderate adaptability; may even be used on surfaces with minimal texture.	Good control of fine details and registration on well-adjusted machines. Moderate ink deposit.
<div style="border: 1px solid black; padding: 5px; display: inline-block;">serilor®3 medium+hard+medium recommended</div>				
Bevelled/pointed  SR1 P1 P2 P5 P6	For higher pressure printing; useful for a wide range of meshes and ink viscosities.	Use with high tension screen and an appropriate off-contact distance.	Excellent adaptability to a large variety of irregular surfaces.	Good control of fine details and registration on well-adjusted machines. Moderate ink deposit.
Rounded  SR1 P4 P3	For higher pressure printing; useful for a wide range of meshes and ink viscosities.	Medium tension and off-contact distance acceptable.	Little adaptability; use only on surfaces with minimal texture.	Fair to poor control of fine details and registration. Heavy ink deposit. Use to obtain thick coverage.
Hard grade	Pressure, Opening, Ink Viscosity	Off-contact Setting and Screen Tension	Conformity to Print Surface	Registration and Ink Deposit
Rectangular  SR1 SR3	Use for maximum pressure printing with all meshes and high viscosity inks.	Use for high tension meshes with little off-contact distance.	Minimal adaptability; for limp surfaces if presses well adjusted.	Excellent control of fine details and registration. Low ink deposit.
<div style="border: 1px solid black; padding: 5px; display: inline-block;">serilor®3 medium+hard+medium recommended</div>				
Bevelled/pointed  SR1 P1 P2 P5 P6	Use for maximum pressure printing with all meshes and high viscosity inks.	Use for high tension meshes with little off-contact distance.	Good adaptability; may be used on most irregular surfaces.	Good control of fine details and registration on most surfaces. Very low ink deposit.
Rounded  SR1 P4 P3	Use for maximum pressure printing with all meshes and high viscosity inks.	Use for high tension meshes with little off-contact distance.	Minimal adaptability; use on limp surfaces only if presses well aligned.	Satisfactory control of fine details and registration. High ink deposit.

IMPORTANT: This chart is a general table based on experiences with "standard" pressure, angle, medium speed. It does NOT take specific settings into account nor rubber wearing and swelling. Those will increase or compensate for the consequences of the blade choice. This chart does not take into account the improvement of serilor®com1 which will ease set-up in the future.

Appendix 1.2 Selection of Mesh Types

The **Saatilene** range of monofilament polyester screen fabrics is considered to be the best all round material for screen printing. It is available in two types, **Saatilene** and **Saatilene Hitech**.

Saatilene is available in thread counts between 15 and 77 threads per centimetre. Saatilene Hitech has thread counts of 90 to 180 per centimetre.

Saatilon monofilament nylon mesh is similar in construction to Saatilene but is less dimensionally stable.

Haver Wire Cloth is a woven stainless steel mesh. Due to its high cost it is generally only used where extremely high ink deposits or absolute dimensional stability are required. Additional information regarding Haver Wire can be found in the brochure entitled 'Haver Wire Cloth for Screen Printing Stencils'.

Type	Thread Count	Widths m	Colour	Applications
Saatilene Monofilament polyester with good dimensional stability	15 - 77	1.02 - 2.50 See current price list for details	White Ultra-Orange	All types of screen printing including posters, T Shirts and Textiles
Saatilene Hitech Hi-Modulus monofilament polyester with exceptional dimensional stability	77 - 180	1.02 - 2.50 See current price list for details	White Ultra-Orange	All types of screen printing, especially high tolerance such as circuits, credit cards, nameplates and where close registration between colours is required
Saatilon Monofilament nylon with excellent abrasion resistance but less dimensionally stable	10.5 - 180	1.02 - 2.50 See current price list for details	White. Fabric can be dyed Ultra-Orange on request, subject to minimum orders.	High elasticity and excellent abrasion resistance make it ideal for printing irregular shaped objects and ceramic colours.
Haver Wire Cloth Woven stainless steel with absolutely uniform mesh openings	32 - 160	1.02 & 1.22		Recommended for ceramic transfers and printed circuits where high ink deposits and absolute registration are essential.

Fabric Tension

To get the best possible results and optimum life from a screen it is essential that the fabric is correctly tensioned. Mesh that is too slack will give poor definition and registration. Screens that are too tight could cause the frame to distort or bow, or cause premature splitting.

Fabric should be tensioned using mechanical or pneumatic stretching devices and a Serimeter Tension Measuring Gauge to measure the tension. Recommended tensions are listed in the following tables.

Screen Making Service

Our eight regional screen making departments offer a full screen stretching service onto either new or customer's own frames.

Screen Preparation and Reclamation

Recommendations for the selection and use of screen adhesives, mesh preparation and screen reclamation chemicals can be found in the 'Screen Chemicals Application Guide'.

Appendix 1.2 Selection of Mesh Types

Operational area		Polyester fabrics (PET)				Nylon fabrics (PA)	
		Conventional inks		UV-inks		Conventional inks	
		from	to	from	to	from	to
Graphic art printing	Line work	90-40	120-34*	140-34*	165-31*		
	Varnish	90-40	120-34	140-34	180-31		
	Half tones up to 28 L/cm	120-34*	150-34*	140-34*	180-27*		
		120-31*	150-31*				
	Half tones from 28 L/cm up to 54 L/cm	150-34*		150-34*	180-31*		
		140-31*	165-31*	165-31*	180-27*		
		150-27*	165-27*				
Printed circuits	Pealable solder mask	12-140	18-250				
	Light sensitive solder mask	24-120	68-64				
	Solder Paste for SMT	32-70					
	Solder mask, 2-comp:						
	Conductor lines height up to 35 my	68-64	77-55				
	from 35 to 70 my	54-64		68-64	120-34		
	over 70 my	43-80	48-55				
	Etch resist	90-48*	120-34*	120-34*	140-34*		
	Plating resist	90-48*	120-34*	120-34*			
Legend printing	120-34*	140-31*	140-34*	150-31*			
Membrane switches	Insulation layer	36-100	68-64				
	Silver conductive paste	48-70*	68-64*				
	Adhesive	48-70	77-55				
	UV inks for textured finish			77-55	165-31		
	Graphic inks	90-48*	120-34*				
	Lacquer for clear windows	120-34					
T-shirt	Direct flocking	18-250	32-100				
	Overprint	32-100	40-80				
	Plastisol transfer	36-100	90-48				
	Pigment dye, solids, lines	40-80	68-64				
	General purpose fabric	48-55					
	Plastisol direct	54-64*	120-34*				
	Sublimating transfer ink	77-55*	120-34*				
	Half-tones	61-64	77-55				
Textile printing	Heavy decor and furnishing fabrics (turkish towel, denim)	18-250	48-70				
	Smooth fabrics (table cloths, heavy curtains)	43-80	54-64				
	Smooth and light materials (scarves, light curtains)	54-64	77-55				
	Smooth and light materials (synthetics)	68-2-40					
	Extremely light materials (special fine effects)	77-55*	120-34*				
			90/2-34				
Ceramic printing	Glass printing, coarse, embossed	10-260	21-140			10-350	21-140
	Covercoat/film solution	12-140	32-100				
	Glass printing, medium to fine	21-140	64-64			21-140	61-70
	In- and underglaze colours	43-80	100-40*			43-80	100-38*
	On glaze/Decalcomania:						
	solids/lines	77-55*	150-31*			77-50*	150-35*
	Half-tones and fine lines	100-40*	165-31*			100-30*	165-30*
Gold and lustre preparations	120-34*	165-31*			120-35*	180-30*	
Object printing	Opaque inks, solids	100-40*	120-34**	140-34*	150-31*	100-38*	150-35**
	Half-tones and fine lines	120-34*	165-27*	150-31*	180-27**	120-34*	180-30**

*) We recommend dyed fabrics.

Appendix 1.2 Selection of Mesh Types

SEFAR® PET 1000

Gewebenummer
Fabric number
Número do tecido
Número del tejido
Número del tejido

Bindung
Weave
Ligamento
Armadura
Ligamento

Fädenzahl
Density of mesh-count
Densidade de malha
Número de fios - tolerância

Maschenweite
Mesh opening
Abertura de malha
Abertura de malha

Diametromaximal
Thread diameter nominal
Diámetro nominal
Diámetro nominal

Quadratmeter
Square meter
Superficie libre
Superficie livre

Seidlichgewicht
Fabric thickness
Espaisseur du tissu
Espesor de tela
Espessura do tecido

Seidlichgewicht
Fabric thickness
Espaisseur du tissu
Espesor de tela
Espessura do tecido

Theoretisches Füllvolumen
Theoretical fill volume
Volume théorique d'ence
Volume teorico de enca

Gewebegewicht
Weave weight
Peso del tejido
Peso do tecido

enfilage
Bretzen
Ligament
Armadura
Ligamento

anforderungen
requirements
allicze disponibeli
ligature disponibeli

cm	inch		±n/cm	µm	µm	%	µm	±µm	cm ² /m ²	g/m ²	cm	inch	115	136	158	180	202	224	246	268	290	312	334	356
5-450W PW	13-450W PW	1:1	0.2	1550	450	60.1	850	43	510.5	238			115	136	158	180	202	224	246	268	290	312	334	356
6-400W PW	15-400W PW	1:1	0.2	1267	400	57.8	800	40	462.1	226			115	136	158	180	202	224	246	268	290	312	334	356
8-300W PW	20-300W PW	1:1	0.2	950	300	57.8	575	29	332.1	169			115	136	158	180	202	224	246	268	290	312	334	356
10-260W PW	25-260W PW	1:1	0.5	739	260	54.6	465	23	253.9	158			115	136	158	180	202	224	246	268	290	312	334	356
10-350W PW	25-350W PW	1:1	0.5	643	350	41.3	640	32	264.6	287			115	136	158	180	202	224	246	268	290	312	334	356
12-140W PW	30-140W PW	1:1	0.5	688	140	68.2	280	14	191.0	55			115	136	158	180	202	224	246	268	290	312	334	356
12-300W TW	30-300W TW	2:1	0.5	520	300	39.0	620	31	241.7	254			115	136	158	180	202	224	246	268	290	312	334	356
15-200W PW	40-200W PW	1:1	0.5	465	200	48.6	355	18	172.5	141			115	136	158	180	202	224	246	268	290	312	334	356
15-250W PW	40-250W PW	1:1	0.5	417	250	39.1	430	22	168.0	220			115	136	158	180	202	224	246	268	290	312	334	356
18-180W PW	45-180W PW	1:1	0.5	375	180	45.5	320	16	145.5	128			115	136	158	180	202	224	246	268	290	312	334	356
18-250W TW	45-250W TW	2:1	0.5	306	250	30.3	510	26	154.3	264			115	136	158	180	202	224	246	268	290	312	334	356
21-140W PW	54-140W PW	1:1	0.5	333	140	49.0	260	13	127.3	96			115	136	158	180	202	224	246	268	290	312	334	356
21-140Y PW	54-140Y PW	1:1	0.5	333	140	49.0	260	13	127.3	96			115	136	158	180	202	224	246	268	290	312	334	356
24-120W PW	60-120W PW	1:1	0.5	294	120	49.7	235	12	116.7	81			115	136	158	180	202	224	246	268	290	312	334	356
24-140W PW	60-140W PW	1:1	0.5	270	140	41.9	255	13	106.8	110			115	136	158	180	202	224	246	268	290	312	334	356
24-140Y PW	60-140Y PW	1:1	0.5	270	140	41.9	255	13	106.8	110			115	136	158	180	202	224	246	268	290	312	334	356
27-120W PW	70-120W PW	1:1	0.5	249	120	45.3	225	11	102.0	91			115	136	158	180	202	224	246	268	290	312	334	356
27-140W PW	70-140W PW	1:1	0.5	222	140	36.0	270	14	97.3	124			115	136	158	180	202	224	246	268	290	312	334	356
30-120W PW	76-120W PW	1:1	1.0	211	120	40.2	210	11	84.4	101			115	136	158	180	202	224	246	268	290	312	334	356
30-120Y PW	76-120Y PW	1:1	1.0	211	120	40.2	210	11	84.4	101			115	136	158	180	202	224	246	268	290	312	334	356
30-140W PW	76-140W PW	1:1	1.0	188	140	31.9	260	13	83.0	137			115	136	158	180	202	224	246	268	290	312	334	356
32-70W PW	83-70W PW	1:1	1.0	240	70	58.7	115	6	67.5	37			115	136	158	180	202	224	246	268	290	312	334	356
32-70Y PW	83-70Y PW	1:1	1.0	240	70	58.7	115	6	67.5	37			115	136	158	180	202	224	246	268	290	312	334	356
32-100W PW	83-100W PW	1:1	1.0	209	100	44.5	165	8	73.5	75			115	136	158	180	202	224	246	268	290	312	334	356
32-100Y PW	83-100Y PW	1:1	1.0	209	100	44.5	165	8	73.5	75			115	136	158	180	202	224	246	268	290	312	334	356
32-120W PW	83-120W PW	1:1	1.0	191	120	37.2	210	11	78.0	108			115	136	158	180	202	224	246	268	290	312	334	356
32-120Y PW	83-120Y PW	1:1	1.0	191	120	37.2	210	11	78.0	108			115	136	158	180	202	224	246	268	290	312	334	356
36-90W PW	92-90W PW	1:1	1.0	183	90	43.3	150	8	64.9	68			115	136	158	180	202	224	246	268	290	312	334	356
36-100W PW	92-100W PW	1:1	1.0	174	100	39.1	160	8	62.6	84			115	136	158	180	202	224	246	268	290	312	334	356
36-100Y PW	92-100Y PW	1:1	1.0	174	100	39.1	160	8	62.6	84			115	136	158	180	202	224	246	268	290	312	334	356
40-80W PW	103-80W PW	1:1	1.0	166	80	44.1	130	7	57.3	60			115	136	158	180	202	224	246	268	290	312	334	356
43-80W PW	110-80W PW	1:1	1.0	149	80	40.8	130	7	53.0	64			115	136	158	180	202	224	246	268	290	312	334	356
43-80Y PW	110-80Y PW	1:1	1.0	149	80	40.8	130	7	53.0	64			115	136	158	180	202	224	246	268	290	312	334	356
43-90W PW	110-90W PW	1:1	1.0	136	90	34.0	150	8	51.0	82			115	136	158	180	202	224	246	268	290	312	334	356
43-90Y PW	110-90Y PW	1:1	1.0	136	90	34.0	150	8	51.0	82			115	136	158	180	202	224	246	268	290	312	334	356
45-70W PW	115-70W PW	1:1	1.0	150	70	45.7	115	6	52.6	52			115	136	158	180	202	224	246	268	290	312	334	356
45-70Y PW	115-70Y PW	1:1	1.0	150	70	45.7	115	6	52.6	52			115	136	158	180	202	224	246	268	290	312	334	356
45-80W PW	115-80W	1:1	1.0	138	80	38.7	130	7	50.3	67			115	136	158	180	202	224	246	268	290	312	334	356

Appendix 1.2 Selection of Mesh Types

SEFAR® PET 1000

Gewebenummer
Fabric number
Número do tecido
Número del tessuto
Número do tecido

Bindung
Weave
Armele
Armatura
Ligamento

Scheda numerata
Znak
Libreria de nombre de file
Libreria de numero de hilo
Numero de file - Libreria
Numero de hilo - Libreria

Maschweite
Mesh-opening
Ouverture de maille
Abertura de malla
Abertura do malha

Durchmesser nominal
Nominal diameter
Diámetro nominal del hilo
Diámetro nominal del hilo
Diámetro nominal do fio

Seidofinanzgrad
Open ure
Surface libre
Superficie libre
Superfície livre

Seidofinanz
Elasticity
Elasticidad
Elasticidade
Elasticidade

Seidofinanz
Elasticidad
Elasticidade
Elasticidade

cm	inch		±n/cm	µm	µm	%	µm	±µm	cm ² /m	g/m ²	cm	inch	115	136	158	180	202	224	246	268	290	312	334	356	
											inch	inch	45	53	62	73	83	92	102	124	143	163	183	203	223
110-40W PW	280-40W PW	1 : 1	3.0	47	40	26.6	67	3	17.8	40															
110-40Y PW	280-40Y PW	1 : 1	3.0	47	40	26.6	67	3	17.8	40															
120-31W PW	305-31W PW	1 : 1	3.0	49	31	35.0	49	3	17.2	26															
120-31Y PW	305-31Y PW	1 : 1	3.0	49	31	35.0	49	3	17.2	26															
120-34W PW	305-34W PW	1 : 1	3.0	45	34	29.6	55	3	16.3	34															
120-34Y PW	305-34Y PW	1 : 1	3.0	45	34	29.6	55	3	16.3	34															
120-40W PW	305-40W PW	1 : 1	3.0	37	40	20.1	65	3	13.0	44															
120-40Y PW	305-40Y PW	1 : 1	3.0	37	40	20.1	65	3	13.0	44															
130-34W PW	330-34W PW	1 : 1	3.5	40	34	26.9	53	3	14.3	37															
130-34Y PW	330-34Y PW	1 : 1	3.5	40	34	26.9	53	3	14.3	37															
140-31W PW	355-31W PW	1 : 1	3.5	36	31	26.0	48	2	12.5	30															
140-31Y PW	355-31Y PW	1 : 1	3.5	36	31	26.0	48	2	12.5	30															
140-34W PW	355-34W PW	1 : 1	3.5	31	34	19.4	53	3	10.3	39															
140-34Y PW	355-34Y PW	1 : 1	3.5	31	34	19.4	53	3	10.3	39															
140-34W TW	355-34W TW	2 : 1	3.5	33	34	21.3	62	3	13.2	39															
140-34Y TW	355-34Y TW	2 : 1	3.5	33	34	21.3	62	3	13.2	39															
150-27Y PW	380-27Y PW	1 : 1	4.0	36	27	28.6	41	2	11.7	26															
150-31W PW	380-31W PW	1 : 1	4.0	32	31	23.3	47	2	10.9	32															
150-31Y PW	380-31Y PW	1 : 1	4.0	32	31	23.3	47	2	10.9	32															
150-34W PW	380-34W PW	1 : 1	4.0	23	34	12.1	55	3	6.6	42															
150-34Y PW	380-34Y PW	1 : 1	4.0	23	34	12.1	55	3	6.6	42															

150-34W TW	380-34W TW	2 : 1	4.0	26	34	15.4	62	3	9.6	42															
150-34Y TW	380-34Y TW	2 : 1	4.0	26	34	15.4	62	3	9.6	42															
165-27Y PW	420-27Y PW	1 : 1	4.0	29	27	22.3	43	2	9.6	29															
165-31W PW	420-31W PW	1 : 1	4.0	23	31	14.5	48	2	7.0	36															
165-31Y PW	420-31Y PW	1 : 1	4.0	23	31	14.5	48	2	7.0	36															
165-34W TW	420-34W TW	2 : 2	4.0	23	34	13.9	62	3	8.6	46															
165-34Y TW	420-34Y TW	2 : 2	4.0	23	34	13.9	62	3	8.6	46															
180-27W PW	460-27W PW	1 : 1	4.5	22	27	15.1	43	2	6.5	31															
180-27Y PW	460-27Y PW	1 : 1	4.5	22	27	15.1	43	2	6.5	31															
180-31W TW	460-31W TW	2 : 2	4.5	23	31	16.5	55	3	9.1	39															
180-31Y TW	460-31Y TW	2 : 2	4.5	23	31	16.5	55	3	9.1	39															
190-31W TW	480-31W TW	2 : 2	5.0	16	31	9.0	57	3	5.2	41															
190-31Y TW	480-31Y TW	2 : 2	5.0	16	31	9.0	57	3	5.2	41															

deutsch Legende

● = Vorrangartikel, in der Regel ab Lager lieferbar (Zwischenverkauf vorbehalten)
○ = Vorrangartikel, nur 247 cm

☒ = Artikel auf Anfrage
☒ = Artikel auf Anfrage, nur 248 cm
☒ = Artikel auf Anfrage, nur 244 cm

W = weiss
Y = gelb

PW = Bindung Taflet 1 1
TW = Bindung Köper 2 1, 2 2

Breiten ohne Webkanten, +4cm/-0cm, +2"/-0"

Alle Daten, die gegenüber der Liste mit Ausgabedatum August 97 geändert wurden, sind kursiv gedruckt

Anderungen vorbehalten

english Legend

● = Priority item, usually on stock (subject to prior sale)
○ = Priority item, only 247 cm

☒ = Item on request
☒ = Item on request, only 248 cm
☒ = Item on request, only 244 cm

W = white
Y = yellow

PW = Plain Weave 1 1
TW = Twill Weave 2 1, 2 2

Widths without selvages, +4cm/-0cm, +2"/-0"

The figures which were altered in comparison to the August 1997 list are printed in italics

Subject to change without notice

français Légende

● = Article prioritaire, normalement livrable du stock (sauf vente intermédiaire)
○ = Article prioritaire, seulement 247 cm

☒ = Article sur demande
☒ = Article sur demande, seulement 248 cm
☒ = Article sur demande, seulement 244 cm

W = blanc
Y = jaune

PW = Armure tafletas 1 1
TW = Armure serge 2 1, 2 2

Largeurs sans lisières, +4cm/-0cm, +2"/-0"

Toutes les dates qui ont été corrigées depuis la dernière édition d'août 1997 sont imprimées en caractères italiques

Sous réserve de changements

español Leyenda

● = Artículo prioritario, normalmente disponible ex-stock (salvo venta intermedia)
○ = Artículo prioritario, 247 cm solamente

☒ = Artículo a pedido
☒ = Artículo a pedido, 248 cm solamente
☒ = Artículo a pedido, 244 cm solamente

W = blanco
Y = amarillo

PW = Ligamento tafetan 1 1
TW = Ligamento sarga 2 1, 2 2

Anchos sin orillos, +4cm/-0cm, +2"/-0"

Todos los datos que fueron alterados con relación a la última lista técnica de Agosto 1997 están marcados con letra cursiva

Salvo alteraciones eventuales

italiano Leggenda

● = Articolo prioritario, disponibile normalmente da magazzino (salvo vendita intermedia)
○ = Articolo di preferenza, solo 247 cm

☒ = Articolo su richiesta
☒ = Articolo su richiesta, solo 248 cm
☒ = Articolo su richiesta, solo 244 cm

W = bianco
Y = giallo

PW = Armatura tafetà 1 1
TW = Armatura sarga 2 1, 2 2

Altezze senza cmose, +4cm/-0cm, +2"/-0"

Tutti i dati cambiati dopo l'ultima pubblicazione di agosto 1997 sono stampati in caratteri corsivi

Salvo modifiche

português Legenda

● = Item prioritário, normalmente disponível em estoque (salvo venda prévia)
○ = Tipo de prioridade, somente 247 cm

☒ = Tipo sob consulta
☒ = Tipo sob consulta, somente 248 cm
☒ = Tipo sob consulta, somente 244 cm

W = branco
Y = amarelo

PW = Ligamento tafeta 1 1
TW = Ligamento sarja 2 1, 2 2

Larguras sem aurelas, +4cm/-0cm, +2"/-0"

Todos os dados que foram alterados em relação à lista de agosto 1997 estão impressos de forma diferenciada (itálica)

Salvo eventuais alterações

Appendix 1.3 Repeatability Tests

Figure 1.3.1 is a graph showing the resulting deposit thickness heights for 10 consecutive prints at the same setting which were repeated by three different operators, i.e., the author and other research team members, at one week intervals. The maximum variation within each trial was 28.9% and the maximum variation between trials was 35.65%.

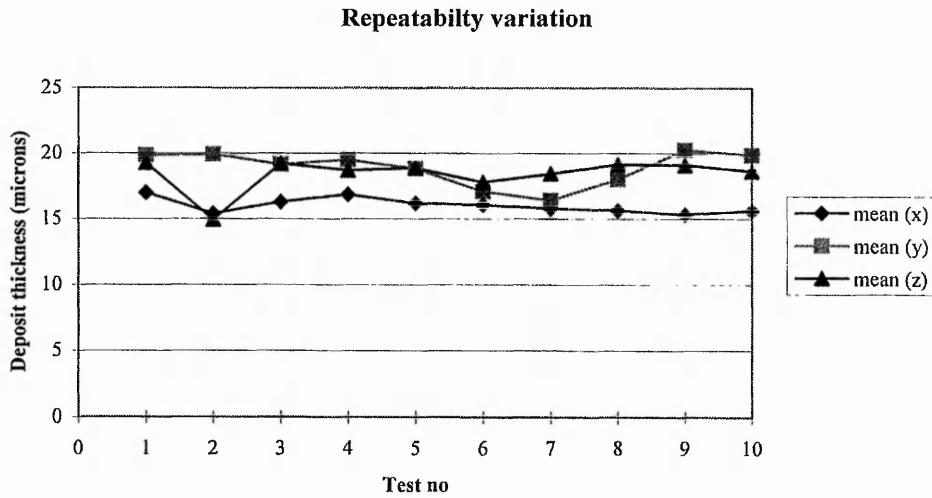


Figure 1.3.1 Plot of repeatability variation in three sets of printing

This shows that on different days with different operators the variation is high but that even with the same operator running consecutive prints the variation is only 5% lower.

Appendix 2.1 Results of Squeegee Hardness Tests

Hard squeegee deposit (μm)	Soft squeegee deposit thickness (μm)	Hard squeegee thinner
13.2	8.6	x
10.9	9.1	x
9.8	20.0	✓
10.0	20.2	x
9.0	8.4	x
9.8	10.3	✓
11.1	9.5	x
9.2	8.3	x
9.2	11.9	✓
10.5	9.2	x
9.8	22.7	✓
9.2	36.0	x
11.4	10.6	x
12.2	11.7	x
12.5	11.6	x
10.2	9.1	x

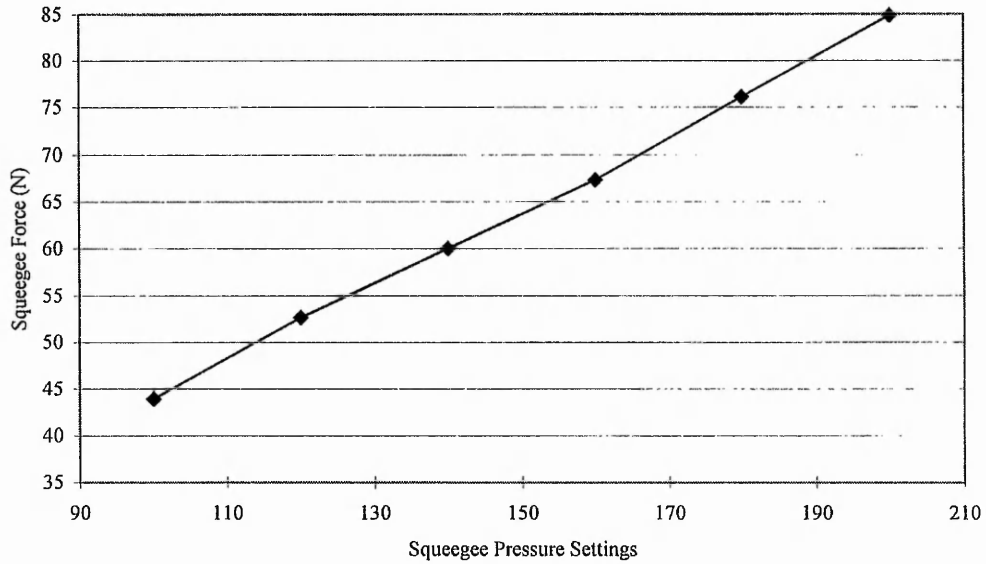
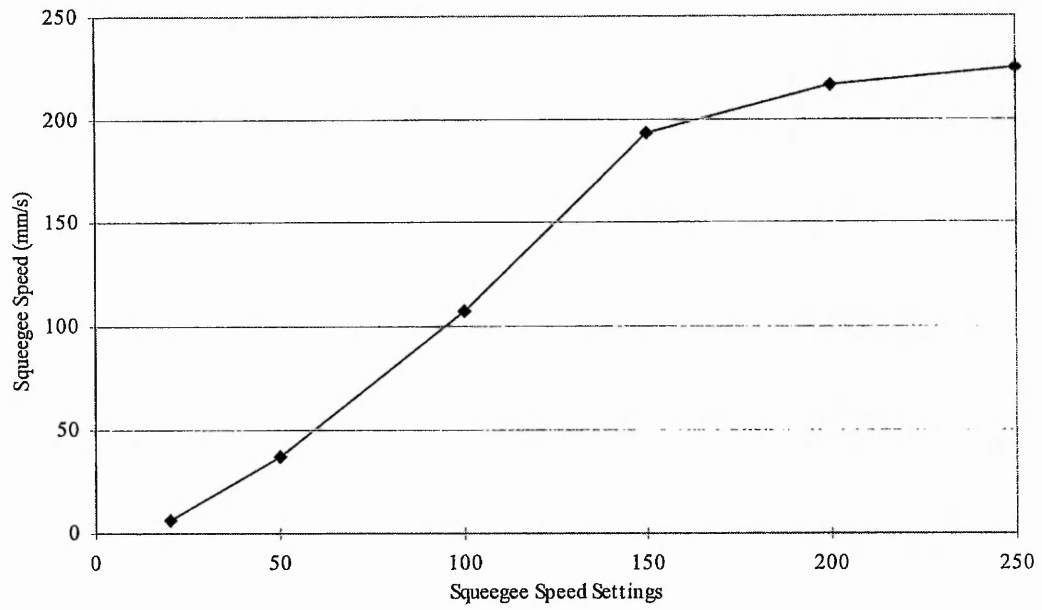
The tests showed that the softer squeegee resulted in thinner deposits for almost 69% of the trials.

Appendix 3.1 Technique Adopted for Deposit Height Measurement

The wet printed deposit was measured using a UBM 3D non contact laser profilometer. Each deposit was measured over its entire area, using a height range of $\pm 50\mu\text{m}$. Data collection in the x and y direction were typically set to 100 and 2 points per mm respectively. Data for each deposit was stored in a separate file. This information was then down loaded using MatLAB[®]. A program was developed to handle as many files as required for each set of testing. The program is listed below.

First the profile was levelled to compensate for any variation in the substrate thickness by determining the best fit datum line as a reference point. The sum of the peaks was then averaged for all the points which were substantially higher than the base reference line so that the affects of the substrate variation were ignored. Single excessive spikes were also removed as rogue data. This mean value was taken as being the wet deposit height for the purposes of this work as, although it is not a British Standard parameter, it gives a good representation of the actual deposit. Alternative parameters could have been chosen but these complicate the issue to the extent of requiring a separate research study beyond the scope of this work [67].

Appendix 3.2 Calibrations of Squeegee Speed and Pressure



Appendix 3.3 Layout and results of L81 experiment

Trial	Snap	Angle	Speed	Pressure	Av height 1	Av. Height 2	% variation (within samples)
1	1	60	40	110	18.8971685	19.7929445	4.74026572
2	1	60	40	130	18.4806305	18.351498	0.7036619
3	1	60	40	150	18.176436	18.1868585	0.05734072
4	1	60	50	110	18.609337	17.8132535	4.46905165
5	1	60	50	130	17.751686	17.3309325	2.42776031
6	1	60	50	150	16.823971	17.7970705	5.78400605
7	1	60	60	110	18.054791	19.9007845	10.2243969
8	1	60	60	130	17.9307725	18.339396	2.27889512
9	1	60	60	150	18.433141	17.1374275	7.56072345
10	1	65	40	110	17.7483335	17.7946185	0.26078505
11	1	65	40	130	17.826403	18.4759255	3.64359821
12	1	65	40	150	17.3901165	16.3189455	6.56397192
13	1	65	50	110	18.601203	17.489053	6.35912076
14	1	65	50	130	17.2089815	15.803507	8.89343422
15	1	65	50	150	17.9275695	18.5578115	3.51549049
16	1	65	60	110	17.6989335	17.418379	1.61068088
17	1	65	60	130	17.6540355	18.109279	2.57869369
18	1	65	60	150	17.5562855	16.258705	7.9808355
19	1	70	40	110	15.9683365	17.2174095	7.82218611
20	1	70	40	130	18.5218955	16.883761	9.70242649
21	1	70	40	150	15.5558155	15.1874795	2.42526089
22	1	70	50	110	16.4578135	17.6116075	7.01061535
23	1	70	50	130	18.150769	17.3176775	4.81064219
24	1	70	50	150	17.177483	15.7433535	9.10942831
25	1	70	60	110	18.9719315	17.21902	10.1800886
26	1	70	60	130	16.964619	17.344228	2.2376512
27	1	70	60	150	16.3702075	17.575622	7.363465
28	3	60	40	110	19.230284	18.135404	6.03725178
29	3	60	40	130	16.758812	17.2517805	2.941548
30	3	60	40	150	17.1639505	16.8593695	1.80659781
31	3	60	50	110	19.0775065	17.5214415	8.88091884
32	3	60	50	130	17.8853985	18.921289	5.79182231
33	3	60	50	150	19.1674835	21.0315565	9.7251838
34	3	60	60	110	19.298886	15.6040605	23.6786156
35	3	60	60	130	18.610785	17.669134	5.3293557
36	3	60	60	150	19.9712635	17.9240135	11.421828
37	3	65	40	110	17.613846	17.9446495	1.87808784
38	3	65	40	130	17.5464095	17.701004	0.8810606
39	3	65	40	150	18.277145	17.644793	3.58378815
40	3	65	50	110	16.7650915	17.453198	4.1044005
41	3	65	50	130	15.03323	17.1897995	14.3453503
42	3	65	50	150	17.865222	19.126982	7.06266063
43	3	65	60	110	19.1674835	21.0315565	9.7251838
44	3	65	60	130	17.3720905	19.1039645	9.96928953
45	3	65	60	150	18.8792915	17.561224	7.50555599

Layout and results of L81 Continued

Trial	Snap	Angle	Speed	Pressure	Average Height 1	Average Height 2	% variation (within samples)
46	3	70	40	110	16.8707825	17.422748	3.27172436
47	3	70	40	130	17.865043	15.984355	11.7658048
48	3	70	40	150	17.7994765	17.9479495	0.83414251
49	3	70	50	110	17.582501	18.8373565	7.1369568
50	3	70	50	130	18.7999325	15.8304475	18.758061
51	3	70	50	150	15.235216	17.431783	14.4176952
52	3	70	60	110	15.2273035	17.704659	16.2691674
53	3	70	60	130	17.993302	16.6976025	7.75979366
54	3	70	60	150	14.7893415	18.5739425	25.5900575
55	5	60	40	110	18.2438705	17.3416285	5.20275244
56	5	60	40	130	16.9419045	19.337721	14.1413647
57	5	60	40	150	18.4556355	18.4165785	0.21207522
58	5	60	50	110	15.8212265	19.8285855	25.3290034
59	5	60	50	130	17.3750305	15.852189	9.60650608
60	5	60	50	150	18.265645	19.1037335	4.58833236
61	5	60	60	110	19.1440075	19.887633	3.8843774
62	5	60	60	130	18.0296545	16.7788285	7.45478744
63	5	60	60	150	18.02776	18.579251	3.05912104
64	5	65	40	110	17.1541345	18.2284645	6.26280504
65	5	65	40	130	17.408529	17.167668	1.40299195
66	5	65	40	150	19.9884515	18.0188375	10.9308606
67	5	65	50	110	18.1819285	18.3007495	0.65351153
68	5	65	50	130	18.866366	18.4871475	2.0512548
69	5	65	50	150	17.8049375	18.3156205	2.86821001
70	5	65	60	110	18.763258	17.5150005	7.12679112
71	5	65	60	130	17.514766	18.1604215	3.68634956
72	5	65	60	150	18.784662	18.778177	0.03453477
73	5	70	40	110	17.715942	14.8938925	18.9476962
74	5	70	40	130	16.8573725	17.5218175	3.94156919
75	5	70	40	150	17.9718355	17.9941735	0.12429448
76	5	70	50	110	18.0828035	18.7637855	3.76590942
77	5	70	50	130	18.92851	16.5401535	14.4397481
78	5	70	50	150	14.844692	16.2643945	9.56370466
79	5	70	60	110	17.2743055	16.9915555	1.66406189
80	5	70	60	130	17.8111815	16.856588	5.6630292
81	5	70	60	150	17.3351985	15.9071275	8.97755424
				max	19.9884515	21.0315565	25.5900575
				min	14.7893415	14.8938925	0.03453477
				var	5.19911	6.137664	
				% var between samples	35.1544388	41.2092675	

Appendix 3.4 Analysis of Variance for Full Factorial Experiment (L81)

Table 3.4.1 Analysis of Variance for L81RES.response c & d - Type III Sums of Squares

Factor	SS	df	MS	F-Ratio	Sig. Level	% Contribution
A	2.600475	2	1.300237	1.406	0.251	0.389087
B	31.81196	2	15.90598	17.203***	0	15.517
AB	0.697747	2	0.348873	0.377	0.6869	-0.59629
C	3.092894	2	1.546447	1.673	0.1942	0.644099
AC	2.280335	4	0.570084	0.617	0.6519	-0.73434
BC	1.206109	4	0.301527	0.326	0.8597	-1.29066
ABC	5.72544	4	1.43136	1.548	0.1962	1.049794
D	1.414863	4	0.353716	0.383	0.8205	-1.18255
DA	8.945761	4	2.23644	2.419	0.0551	2.71752
BD	0.639225	4	0.159806	0.173	0.9517	-1.58423
ABD	16.05134	8	2.006417	2.17	0.0383	4.482052
CD	2.85591	8	0.356989	0.386	0.9251	-2.35154
ACD	8.961493	8	1.120187	1.212	0.3028	0.810395
BCD	9.948887	8	1.243611	1.345	0.2336	1.321743
ABCD	21.97309	16	1.373318	1.485	0.1257	3.718241
e1	74.89106	81	0.924581			
e2	193.0966	161				

Appendix 3.5 Percentage error attributable to measurement technique

Screen Print Deposit Measurement Accuracy

UBM Laser Sensor Measurement Capability

The UBM sensor has a linearity error of <1%, and a maximum possible resolution of the range divided by 4,096. Thus, at a range of $\pm 500 \mu\text{m}$, the linearity could be as poor as $10 \mu\text{m}$ and the maximum possible resolution would be $0.244 \mu\text{m}$. At a range of $\pm 50 \mu\text{m}$, the linearity will be better than $1 \mu\text{m}$ and the resolution will be $0.0244 \mu\text{m}$.

A slip gauge height difference of 0.02mm was repeatedly measured in both forward only and forward and backward directions, at a range of $\pm 50 \mu\text{m}$. The X and Y- directions were both recorded. The results of this are illustrated in Table 3.5.1. Clearly, it can be seen that measuring in one direction only produces much less variation: 1.13% in the Y (backward) direction and 2.6% in the X (fwd) direction.

Table 3.5.1

profile	Y-direction +/- 50			X-direction +/- 50			+/-500		
	total	fwd	bwd	total	fwd	bwd	total	fwd	bwd
pt2.pr1	15.584	15.584	16.155	16.864	16.864	16.539	17.575	17.575	17.540
pt3.pr1	15.867	15.867	16.257	16.474	16.474	16.757	17.540	17.520	17.838
ptf4.pr1	15.921	15.921	16.144	16.554	16.554	16.364	17.520	17.595	17.614
ptb5.pr1	16.155	15.999	16.075	16.539	16.438	16.887	17.838	17.569	17.536
ptf6.pr1	15.999	16.118	16.104	16.438	16.533	16.826	17.595	17.731	17.701
ptb7.pr1	16.257	16.085		16.757	16.529		17.614		
ptf8.pr1	16.118	15.973		16.533	16.733		17.569		
ptb9.pr1	16.144			16.364			17.536		
ptf10.pr1	16.085			16.529			17.731		
ptb11.pr1	16.075			16.887			17.701		
ptf12.pr1	15.973			16.733					
ptb13.pr1	16.104			16.826					
Min	15.584	15.584	16.075	16.364	16.438	16.364	17.520	17.520	17.536
Max	16.257	16.118	16.257	16.887	16.864	16.887	17.838	17.731	17.838
Var	0.673	0.534	0.182	0.523	0.427	0.523	0.318	0.211	0.302
% Var	4.319	3.429	1.132	3.195	2.596	3.195	1.817	1.205	1.725

Screen Print Deposit Measurement Variation

The deposits were screen printed onto glass slides which were $76 \text{ mm} \times 26 \text{ mm} \times 1\text{-}1.1 \text{ mm}$ thick. Five different glass slides were measured to assess the typical variation within and between slides. The results are shown in Table 3.5.2. In the worst case there is a variation of $2.06 \mu\text{m}$ (accounting for approximately 12% error at typical deposit heights of $17 \mu\text{m}$).

Table 3.5.2

	min	max	Var	% Var	angle
Glass 1	-0.490	1.280	1.770	-3.612	0.026
Glass 2	-0.820	5.580	6.400	-7.805	0.012
Glass 3	-0.260	0.240	0.500	-1.923	0.005
Glass 4	-0.980	1.110	2.090	-2.133	0.003
Glass 5	-1.130	8.840	9.970	-8.823	0.038

A printed sample was measured repeatedly to give an idea of the accuracy obtainable for a typical screen printed surface. Table 3.5.3 shows the results of consecutive scan lines taken without moving the sample at all between measurements. This shows that measuring forward only, or in both the forward and backward directions is not important. The variation accounts for 1.2% error. However just measuring backward, after measuring forward appears to reduce the variation to 0.5%. This might be explained by the fact that there are considerably fewer samples measured in the backward direction.

Table 3.5.3

profile	total	fwd	bwd
	16.483	16.483	16.396
or2.pr1	16.309	16.309	16.413
or3.pr1	16.363	16.363	16.362
or4.pr1	16.286	16.286	16.332
or5.pr1	16.337	16.337	16.360
ndr1.pr1	16.454	16.454	
ndr2.pr1	16.396	16.374	
ndr3.pr1	16.374	16.384	
ndr4.pr1	16.413	16.369	
ndr5.pr1	16.384	16.379	
ndr6.pr1	16.362		
ndr7.pr1	16.369		
ndr8.pr1	16.332		
ndr9.pr1	16.379		
ndr10.pr1	16.360		
min	16.286	16.286	16.332
max	16.483	16.483	16.413
var	0.198	0.198	0.081
% var	1.214	1.214	0.496

In Table 3.5.4 the same sample was measured but the sample was removed from the measuring table and returned to the same position each time between measurements. By moving the sample away between measurements, which is of course necessary in a real situation, the variation increases to just under 4%. Forward and backward information is not available.

Table 3.5.4

profile	mean2	profile	mean2
rep1.pr1	17.505	rep8.pr1	16.633
rep2.pr1	16.332	rep9.pr1	16.793
rep3.pr1	16.506	rep10.pr1	16.099
rep4.pr1	17.235	min	16.09857
rep5.pr1	16.469	max	17.23461
rep6.pr1	16.704	var	1.136048
rep7.pr1	16.244	% var	7.056828

The print process parameters were set up to give a good print and 100 samples were printed. To allow the ink to slump there was a time delay of 1 hour before measuring. The prints were measured using forward and reverse directions alternately on successive prints. The range was set at $\pm 500 \mu\text{m}$. The results are shown in table 3.5.5. There is a variation of 25% across this set of 100 samples, but according to the above it could be accounted for as follows:

Maximum achievable linearity (determined by slip gauges)	2%
Glass slide variation	12%
Measuring forward and backward	1%
Different glass slides	4%
Total	19%

Table 3.5.5

profile	mean	profile	mean	profile	mean	profile	mean
am1.pr1	16.74	am28.pr1	17.03	am63.pr1	16.82	am89.pr1	17.38
am2.pr1	15.74	am29.pr1	17.67	am64.pr1	16.85	am90.pr1	16.06
am3.pr1	17.71	am30.pr1	16.41	am65.pr1	16.72	am91.pr1	17.51
am4.pr1	16.37	am41.pr1	16.28	am66.pr1	16.19	am92.pr1	16.98
am5.pr1	16.17	am42.pr1	16.99	am67.pr1	16.33	am93.pr1	16.96
am6.pr1	17.86	am43.pr1	18.13	am68.pr1	16.09	am94.pr1	17.24
am7.pr1	16.95	am44.pr1	17.14	am69.pr1	15.85	am95.pr1	16.70
am8.pr1	17.16	am45.pr1	17.94	am70.pr1	18.48	am96.pr1	16.34
am9.pr1	17.56	am46.pr1	17.79	am71.pr1	18.36	am97.pr1	16.72
am10.pr1	16.24	am47.pr1	16.74	am72.pr1	17.30	am98.pr1	16.50
am11.pr1	14.84	am48.pr1	16.47	am73.pr1	17.20	am99.pr1	16.40
am12.pr1	15.79	am49.pr1	18.10	am75.pr1	15.60	am100.pr1	16.85
am13.pr1	16.23	am50.pr1	17.56	am76.pr1	17.78	am101.pr1	17.44
am15.pr1	15.96	am51.pr1	16.38	am77.pr1	16.55	am102.pr1	17.68
am16.pr1	15.67	am52.pr1	15.77	am78.pr1	16.42	am103.pr1	16.54
am17.pr1	16.84	am53.pr1	17.46	am79.pr1	17.38	am104.pr1	18.51
am18.pr1	17.05	am54.pr1	15.83	am80.pr1	17.73	max	18.51
am19.pr1	16.62	am55.pr1	17.27	am81.pr1	16.79	min	14.84
am20.pr1	17.38	am56.pr1	16.17	am82.pr1	17.15	var	3.67
am21.pr1	16.25	am57.pr1	16.13	am83.pr1	15.78	%	24.74
am22.pr1	16.62	am58.pr1	16.09	am84.pr1	17.59		
am23.pr1	16.77	am59.pr1	16.20	am85.pr1	16.91		
am24.pr1	16.35	am60.pr1	17.49	am86.pr1	16.09		
am25.pr1	15.48	am61.pr1	15.83	am87.pr1	17.01		
am27.pr1	16.38	am62.pr1	16.35	am88.pr1	16.21		

This procedure was repeated for 50 samples, as shown in table 3.5.6, but the range was set at $\pm 50 \mu\text{m}$ and the deposits were measured in the forward direction only. The variation was less than 15%, but this can only be attributed to the fact that the slides might have been more uniform across their surfaces.

Table3.5.6

profile	mean2	Ra	Rt	profile	mean2	Ra	Rt
rep1.pr1	17.34	13.12	20.81	rep23.pr1	16.70	14.90	19.41
rep2.pr1	18.02	12.22	21.56	rep24.pr1	16.68	10.95	18.48
rep3.pr1	17.19	12.23	20.74	rep25.pr1	17.86	13.82	20.66
rep4.pr1	17.28	9.79	18.64	rep26.pr1	17.01	10.12	18.65
rep5.pr1	16.48	12.07	19.25	rep27.pr1	17.17	13.30	19.22
rep6.pr1	16.98	13.63	20.51	rep28.pr1	17.59	9.89	18.88
rep7.pr1	17.04	14.11	19.61	rep29.pr1	16.76	11.86	19.48
rep8.pr1	16.90	13.95	21.37	rep30.pr1	17.21	12.08	18.98
rep9.pr1	17.28	14.37	20.07	rep41.pr1	17.19	11.50	19.16
rep10.pr1	16.21	10.85	19.09	rep42.pr1	17.63	15.79	22.73
rep11.pr1	16.77	10.12	18.19	rep43.pr1	17.27	11.64	20.10
rep12.pr1	17.42	12.72	19.82	rep44.pr1	17.61	13.17	20.07
rep13.pr1	17.05	8.71	18.52	rep45.pr1	17.73	11.26	19.84
rep14.pr1	17.44	10.24	19.80	rep46.pr1	17.21	15.41	19.79
rep15.pr1	16.83	14.04	19.09	rep47.pr1	17.11	10.81	18.92
rep16.pr1	15.73	9.95	16.12	rep48.pr1	17.34	14.39	19.89
rep17.pr1	17.01	17.16	19.29	rep49.pr1	17.01	12.11	18.72
rep18.pr1	16.72	14.25	20.65	rep50.pr1	16.57	18.75	21.93
rep19.pr1	16.35	9.86	17.08	max	18.02	18.75	22.73
rep20.pr1	17.20	9.89	18.21	min	15.73	8.11	16.12
rep21.pr1	16.81	8.11	17.17	variation	2.29	10.64	6.60
rep22.pr1	17.95	10.53	19.65	% variation	14.54	131.07	40.96

Appendix 3.6 Layout and results of an L25 experiment

Table 3.6.1

Slide #	Trial #	Snap D	angle C	pressure E	Speed F	response a	response b	response c	% variation within samples
1	1	2	50	100	40	13.74	13.09	11.85	15.95
2	11	3	74	120	115	15.44	15.15	14.97	3.14
3	21	4	70	150	65	14.51	12.99	12.45	16.55
4	6	5	65	200	135	17.27	15.66	12.7	35.98
5	16	6	60	200	90	15.51	15.01	14.59	6.31
6	23	2	65	200	115	13.49	14.11	14.65	8.60
7	8	3	60	100	65	12.67	13.34	12.88	5.29
8	18	4	50	120	135	16.96	14.38	14.39	17.94
9	3	5	74	150	90	14.91	13.36	14.58	11.60
10	13	6	70	170	40	17.05	16.52	16.37	4.15
11	20	2	74	170	65	13.58	12.22	12.87	11.13
12	5	3	70	200	135	17.26	16.61	16.29	5.95
13	15	4	65	100	90	15.57	15.57	13.98	11.37
14	25	5	60	120	40	17.57	15.27	16.08	15.06
15	10	6	50	150	115	16.13	16.75	16.75	3.84
16	12	2	60	150	135	16.65	15.09	15.24	10.34
17	22	3	50	170	90	15.03	14.58	14.88	3.09
18	7	4	74	200	40	17.5	14.98	15.62	16.82
19	17	5	70	100	115	14.88	11.61	13.87	28.17
20	2	6	65	120	65	11.89	12.28	12.46	4.79
21	9	2	70	120	90	14.41	12.95	12.92	11.53
22	19	3	65	150	40	18.09	15.91	18.06	13.70
23	4	4	60	170	115	16.6	14.84	14.78	12.31
24	14	5	50	200	65	15.71	15.71	15.71	0.00
25	24	6	74	100	135	15.13	13.88	14.94	9.01
max						18.09	16.75	18.06	35.98
min						11.89	11.61	12.45	0
var						6.2	5.14	5.61	
% variation between samples						52.14	44.27	45.06	

Appendix 3.7 Analysis of variance for L25 experiment

Table 3.7.1 ANOVA Table-Raw Data L25 first experiment, 3 replicates

Source	Pool	Df	S	V	F	S'	rho%
A	[N]	4	14.78527	3.69632			
B	[N]	4	16.76726	4.19181			
C	[N]	4	2.55029	0.63757			
D	[N]	4	22.64497	5.66124			
E	[N]	4	30.70637	7.67659			
F	[N]	4	53.63757	13.40939			
e1	[N]	0	0				
e2	[N]	50	46.82026	0.93641			
(e)		0	0				
Total (Raw)	[-]	74	187.912	2.53935			

Table 3.7.2 ANOVA Table-Raw Data L25 first experiment, 3 replicates after pooling

Source	Pool	Df	S	V	F	S'	rho%
A	[N]	4	14.78527	3.69632	5.79751	12.23499	6.51
B	[N]	4	16.76726	4.19181	6.57467	14.21698	7.57
C	[Y]	4	2.55029	0.63757			
D	[N]	4	22.64497	5.66124	8.8794	20.09469	10.69
E	[N]	4	30.70637	7.67659	12.04039	28.15609	14.98
F	[N]	4	53.63757	13.40939	21.03203	51.08729	27.19
e1	[N]	0	0				
e2	[N]	50	46.82026	0.93641	1.46872	14.94176	7.95
(e)		4	2.55029	0.63757			
Total (Raw)	[-]	74	187.912	2.53935			

To perform an F-ratio test for the L25 experiment, $v_1=4$ and $v_2=50$, therefore $F_{0.01(4,50)} = 3.72$. The F value for A is 5.79 which is greater than 3.72, and all the other F values are higher than that of A, thus it may be said that there is a confidence level of greater than 99%.

Appendix 3.8 L25t2 Repeat experiment to confirm the first outcomes

The method and apparatus are the same as that for the first L25 experiment. The deposit heights for three repetitions at each setting are given in Table 3.8.1 and Figure 3.8.1 shows the height differences both within and between trails, expressed as a percentage. This illustrates that the majority are below 10%, which is acceptable.

Table 3.8.1

filename	height t2, a	height t2, b	height t2, c	filename	height t2, a	height t2, b	height t2, c
a:\L25t21a.pr3	14.297	13.206	13.182	a:\L25t215a.pr3	16.570	15.503	14.378
a:\L25t22a.pr3	13.760	13.029	12.117	a:\L25t216d.pr3	17.173	15.007	15.196
a:\L25t23a.pr3	14.415	13.483	13.291	a:\L25t217a.pr3	17.195	15.267	15.226
a:\L25t24a.pr3	15.343	15.377	15.581	a:\L25t218a.pr3	15.355	12.824	13.159
a:\L25t25a.pr3	16.170	16.306	16.320	a:\L25t220a.pr3	15.230	14.458	14.765
a:\L25t26a.pr3	15.739	14.094	14.249	a:\L25t221a.pr3	14.808	13.557	13.513
a:\L25t27a.pr3	16.385	15.326	16.026	a:\L25t222a.pr3	15.039	13.681	13.483
a:\L25t28a.pr3	16.090	15.263	15.300	a:\L25t223a.pr3	16.133	14.850	15.165
a:\L25t29a.pr3	14.486	13.598	13.054	a:\L25t224a.pr3	18.272	15.902	15.740
a:\L25t210a.pr3	15.142	13.975	13.673	a:\L25t224b.pr3	15.902		
a:\L25t211a.pr3	13.373	11.851	11.751	max	18.272		
a:\L25t212a.pr3	16.283	13.417	14.295	min	13.373		
a:\L25t213a.pr3	18.072	16.534	16.683	var	4.899		
a:\L25t214a.pr3	16.019	14.547	14.215	%var	36.635		

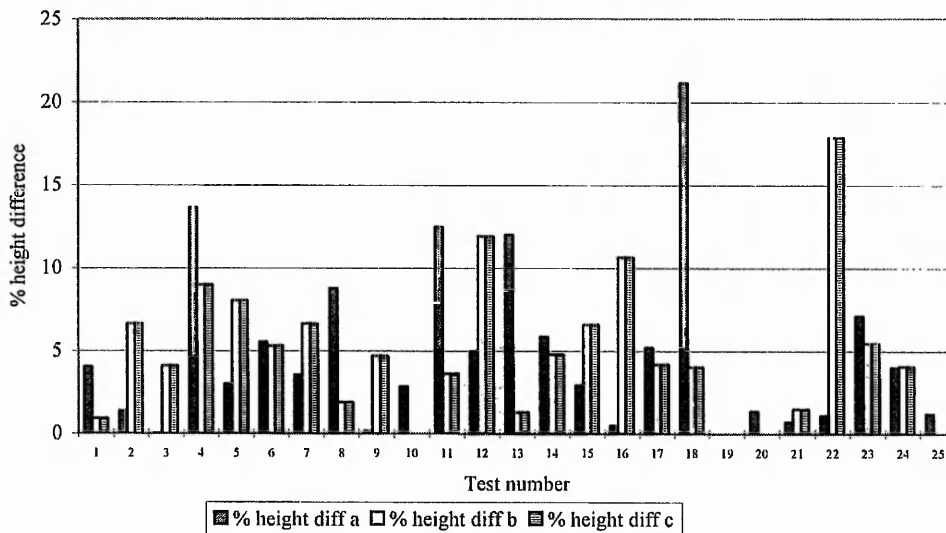


Figure 3.8.1 % Variation within and between print deposit trials

The variation between the two experiments L25t1 and L25t2 is plotted as a percentage in height difference in Figure 3.8.2. Again, it can be seen that a large proportion fall below 10%.

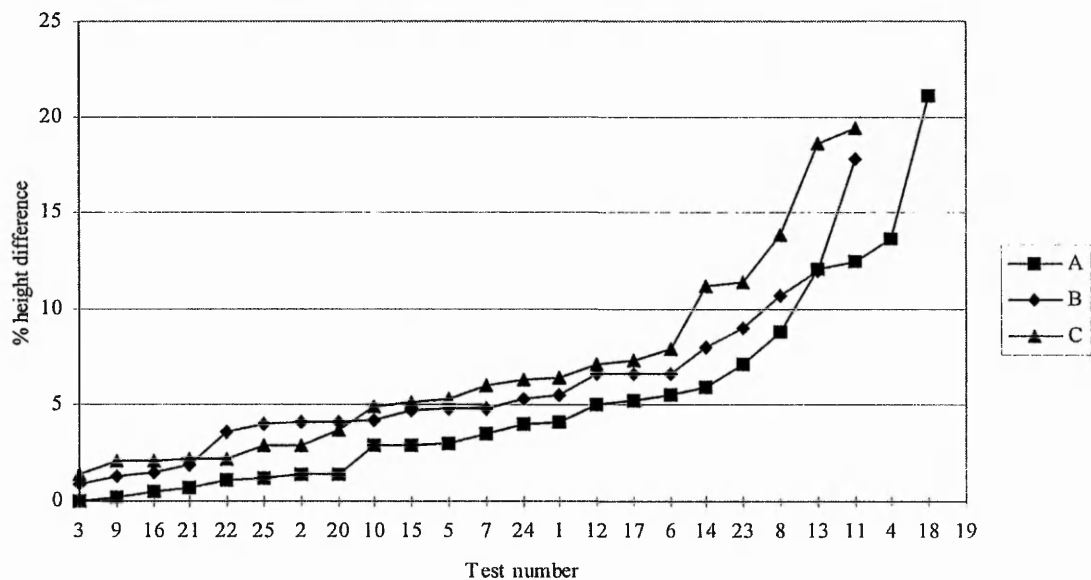


Figure 3.8.2 Variation in repeatability between L25t1 & 2 compared by % height difference

The results of conducting an analysis of variance are shown in Tables 3.8.2 and 3.8.3, but these have no significance because of the confounding effect and therefore can only be used as a basis for establishing the F-ratio.

Table 3.8.2 Repeated L25 ANOVA

	Source	Pool	Df	S	V	F	S'
A	[N]	4	7.84924	1.96231			
B	[N]	4	5.34552	1.33638			
C	[N]	4	40.08327	10.02082			
D	[N]	4	15.20035	3.80009			
E	[N]	4	11.76897	2.94224			
F	[N]	4	18.89018	4.72254			
e1	[N]	0	0				
e2	[N]	50	36.48807	0.72976			
(e)	0	0					
Total (Raw)	[-]	74	135.6256	1.83278			

Table 3.8.3 Repeated L25 ANOVA after pooling

Source	Pool	Df	S	V	F	S'	rho%
A	[N]	4	7.84924	1.96231	1.46838	2.50372	1.85
B	[Y]	4	5.34552	1.33638			
C	[N]	4	40.08327	10.02082	7.49848	34.73775	25.61
D	[N]	4	15.20035	3.80009	2.84357	9.85483	7.27
E	[N]	4	11.76897	2.94224	2.20165	6.42345	4.74
F	[N]	4	18.89018	4.72254	3.53383	13.54466	9.99
e1	[N]	0	0				
e2	[N]	50	36.48807	0.72976	0.54607	-30.3309	-22.3
(e)		4	5.34552	1.33638	98.89212	72.92	
Total (Raw)	[-]	74	135.6256	1.83278			

To perform an F-ratio test for the L25t2 experiment, $v_1=4$ and $v_2=50$, therefore $F_{0.01(4,50)} = 3.72$. However, in this repetition of the L25 the F value for A is 1.468 which means that the confidence level is less than 99%. Comparing the F ratio for a 95% confidence level gives $F_{0.05(4,50)} = 2.56$, but this is still higher than the F value for A and E, which casts doubt on the confidence of the experiment altogether.

Appendix 3.9 Layout and results of L9 experiment

Table 3.9.1

Test	Snap	Angle	Pressure	Speed	height (L9ta)	height (L9tb)	height (L9tc)
1	3	65	140	60	14.72413	13.40382	14.02145
2	3	67	150	73	14.94281	13.73245	14.53644
3	3	70	160	85	14.60315	14.53573	13.51126
4	4	65	150	85	16.3723	14.44533	15.6574
5	4	67	160	60	15.2517	14.73629	15.2672
6	4	70	140	73	15.47021	14.83514	14.62524
7	5	65	160	73	16.89496	15.44107	15.91341
8	5	67	140	85	16.42053	15.39816	15.22576
9	5	70	150	60	16.06926	15.0466	14.90429
10	4	67	150	73	15.9438	15.31354	14.43324

Table 3.9.2

ANOVA Table		Raw Data					
Source	Pool	Df	S	V	F	S'	rho%
A	[N]	2	10.12712	5.06356			
B	[N]	2	0.6007	0.30035			
C	[N]	2	0.25285	0.12642			
D	[N]	2	0.60692	0.30346			
e1	[N]	0	0				
e2	[N]	18	7.58993	0.42166			
(e)		0	0				
Total (raw)	[-]	26	19.17751	0.7376			

Table 3.9.3

ANOVA Table		Raw Data					
Source	Pool	Df	S	V	F	S'	rho%
A	[N]	2	10.12712	5.06356	40.05347	9.87428	51.49
B	[N]	2	0.6007	0.30035	2.37581	0.34786	1.81
C	[Y]	2	0.25285	0.12642			
D	[N]	2	0.60692	0.30346	2.40041	0.35408	1.85
e1	[N]	0	0				
e2	[N]	18	7.58993	0.42166	3.33539	5.31437	27.71
(e)		2	0.25285	0.12642		3.28693	17.14
Total (raw)	[-]	26	19.17751	0.7376			

Appendix 3.10 Results of repeated trials from L9 experiment

Table 3.10.1

L9 trial 7		L9 trial 8		% variation between samples
Repetition	height	Repetition	height	
1	15.984731	1	14.784167	8.120606
2	14.16853	2	14.632945	3.277792
3	15.783108	3	14.350773	9.980891
4	15.533764	4	15.027063	3.371923
5	15.78722	5	14.528674	8.662497
6	15.290875	6	14.446271	5.846519
7	15.546935	7	15.469653	0.499572
8	15.358257	8	15.805501	2.912075
9	15.770041	9	15.485169	1.839644
10	15.529236	10	15.312202	1.417392
% variation within samples	12.81856		10.13693	

Appendix 4.1 Photographs of Squeegee Curvature

Hard Squeegee Profiles

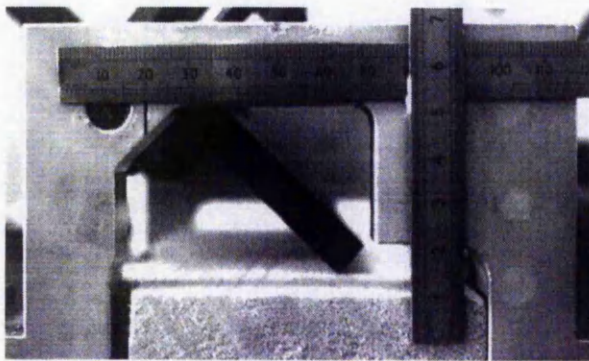


Figure 1 Hard squeegee ($u=1$)

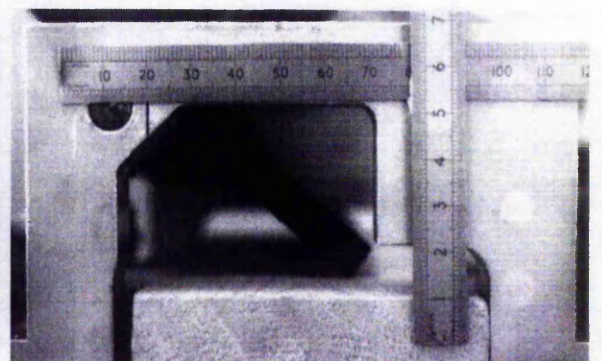


Figure 2 Hard squeegee ($u=1.2$)

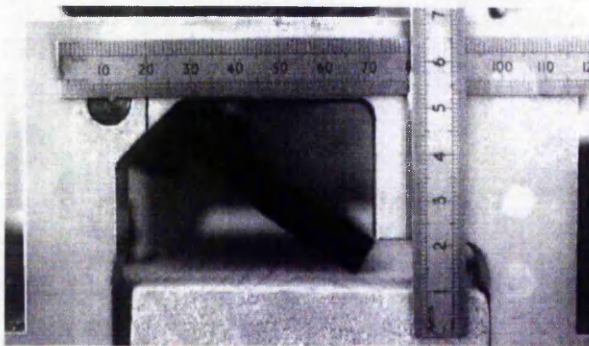


Figure 3 Hard squeegee ($u=1.6$)

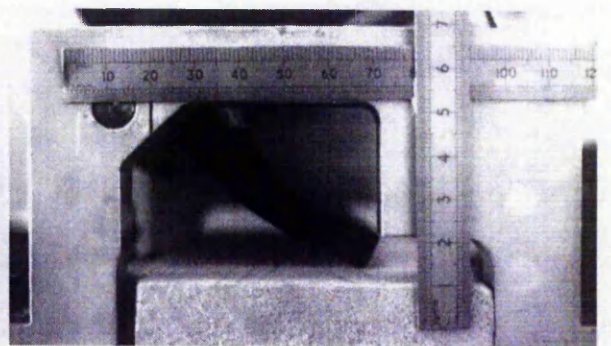


Figure 4 Hard squeegee ($u=2$)

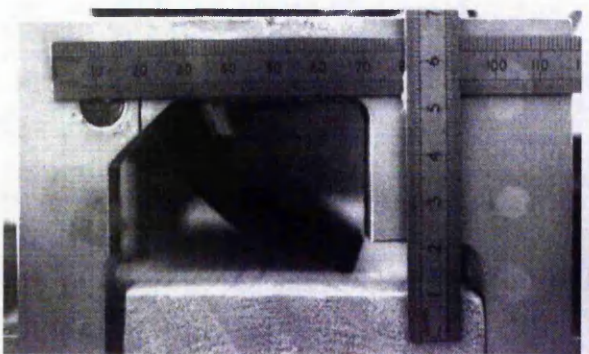


Figure 5 Hard squeegee ($u=3$)

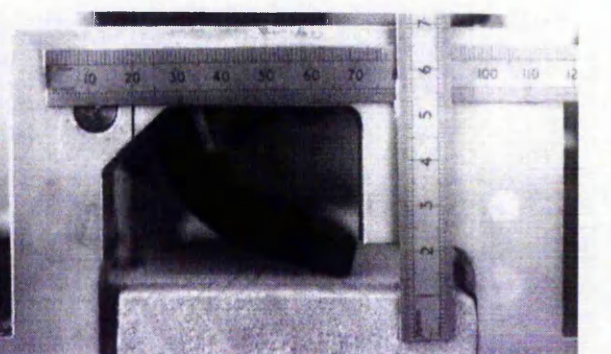


Figure 6 Hard squeegee ($u=6$)

Soft Squeegee Profiles

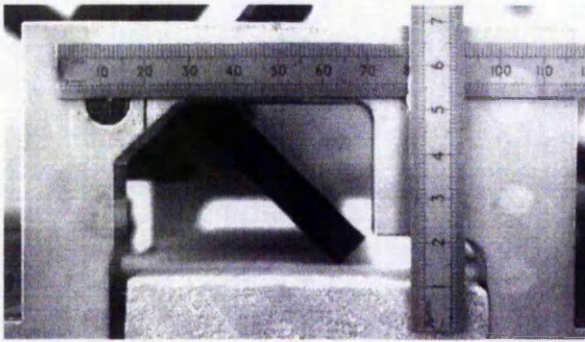


Figure 1 Soft squeegee ($u=1$)

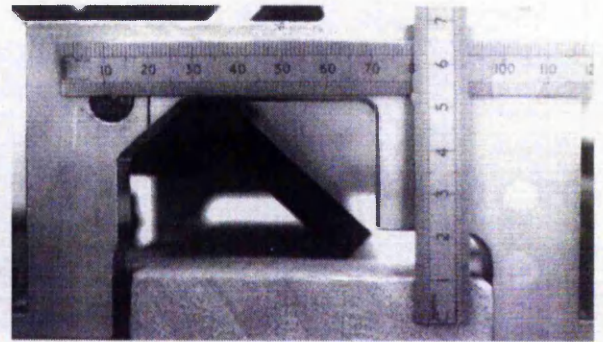


Figure 2 Soft squeegee ($u=1.2$)

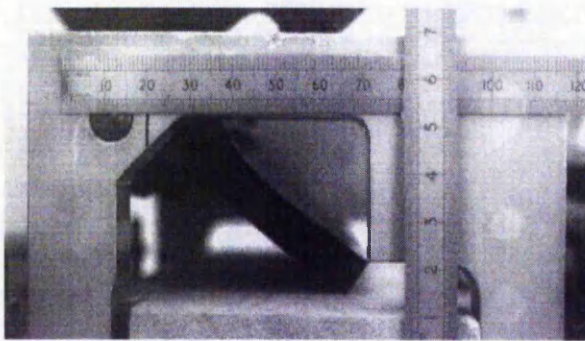


Figure 3 Soft squeegee ($u=1.6$)

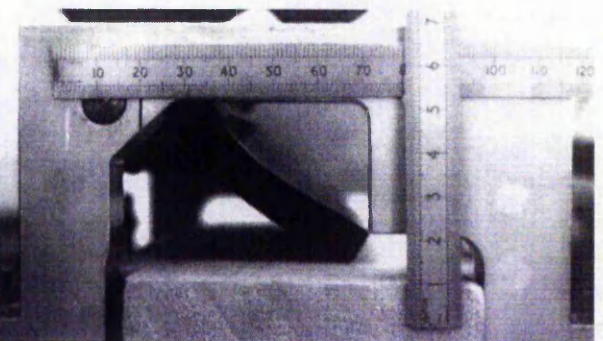


Figure 4 Soft squeegee ($u=2$)

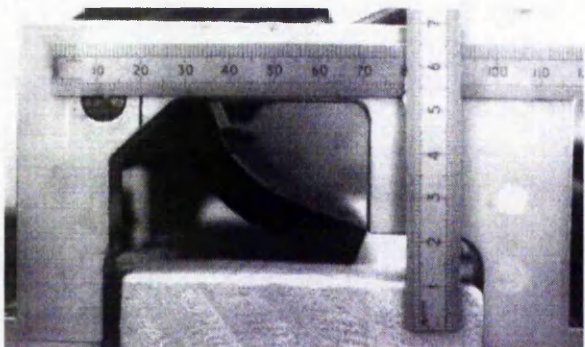


Figure 5 Soft squeegee ($u=3$)

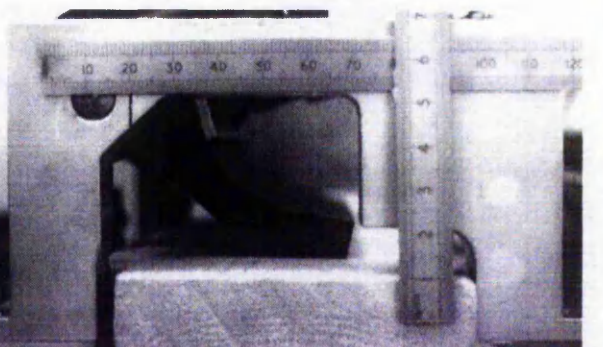


Figure 6 Soft squeegee ($u=6$)

Appendix 4.2 Estimation of flexural rigidity

The flexural rigidity is defined by Huner as:

$$D = \frac{Eh^3}{12(1 - \nu^2)}$$

where E = Young's modulus
 h = squeegee blade thickness
 ν = Poisson's ratio

Without a reliable value for Young's modulus, it is not possible to calculate the flexural rigidity, therefore it must be estimated from the load/deflection data which can be observed from the physical curvature of the squeegee, as illustrated in Figure 4.2.1.

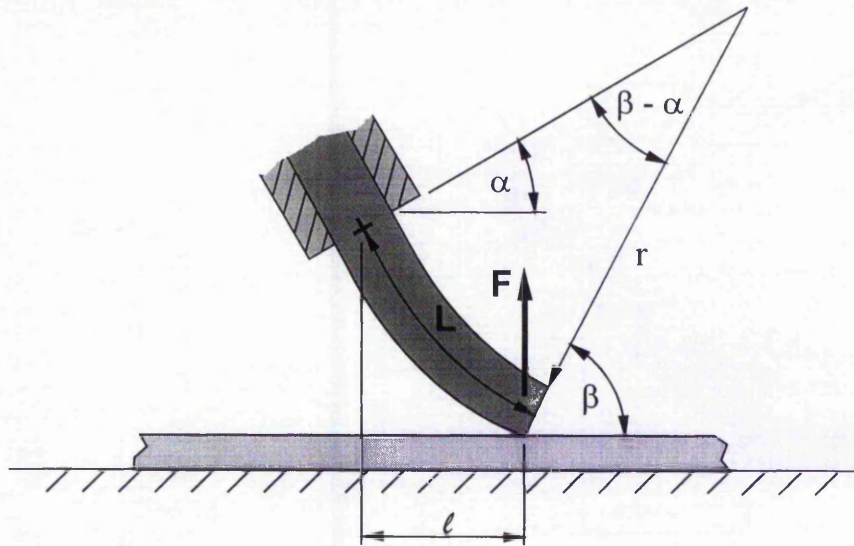


Figure 4.2.1 A typical squeegee shape under load

The squeegee, to a first approximation, takes up the shape of an arc with a radius of curvature, r . The radius of curvature is given approximately by

$$r = \frac{L}{\beta - \alpha} \quad (4.2.1)$$

The flexural rigidity, D , is given by the Bernoulli-Euler relationship:

$$D = \frac{M(x)}{k(x)} \quad (4.2.2)$$

where

$M(x)$ = bending moment per unit length of squeegee at any point x along the blade

$k(x)$ = curvature at any point x along the blade

Since we are assuming an approximate arc shape, the mean flexural rigidity can be approximated for the squeegee blade as:

$$D \approx \frac{M(\text{tip})}{k(\text{overall})} \quad (4.2.3)$$

where

$$M(\text{tip}) = \frac{F}{w} \cdot l \quad (4.2.4)$$

and F = applied squeegee force
 w = squeegee width
 $l \approx L \sin\theta_R$

Therefore, using the radius of curvature given in Equation 4.2.1 as $1/k$ (overall) and the bending moment for the squeegee tip deformation as in Equation (4.2.3) the flexural rigidity of the squeegee can be determined using Equation (4.2.5).

$$D = \frac{F/L}{w(\beta - \alpha)} \tag{4.2.5}$$

The same test rig which was used for evaluating the squeegee shape as depicted in Figure 4.3 was used for these tests. This time a spring balance was fixed onto the end of a lever at 90° , and this was used to rotate the squeegee to a known angle (θ_w) smaller than that of the initial angle at which the blade naturally rested on the horizontal surface (θ_R). Direct measurement of the force could not be obtained, therefore the distance, l , as shown in Figure , was measured at each set angle, θ_w . The force acting at the squeegee tip, F , was then determined using the relationship

$$F = \frac{fr}{l} \tag{4.2.6}$$

The set angle in each case corresponded to the same values of u which were used in section 4.3. The relationship of force to the parameter u is given below in Figure 4. The results of the calculations of force and flexural rigidity using Equations (4.2.5) and (4.2.6) at each value of u are given in Table 4.2.1 and Table 4.2.2 for a soft and hard squeegee respectively.

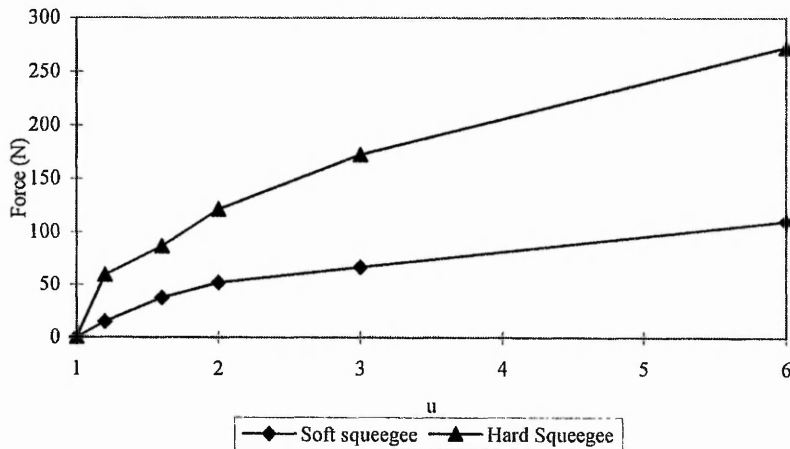


Figure 4.2.2 The relationship of u to squeegee force

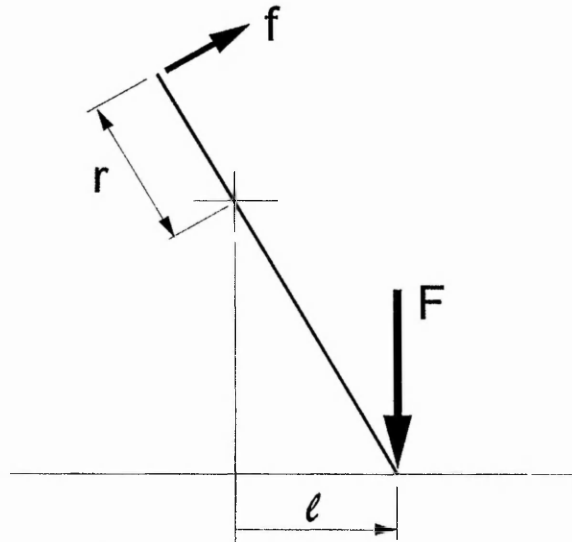


Figure 4.2.1 Indirect measurement of squeegee force

Table 4.2.1 Flexural rigidity values for a soft squeegee

u	θ_w	l (m)	$\beta-\alpha$ (radians)	f (kg)	F(N)	D (N/m)
1	45	0.0565	0.0785	0	0	*
1.2	40	0.059	0.244	0.7	23.85992	2.184132
1.6	32	0.0505	0.454	1	39.82277	1.67693
2	26	0.061	0.646	1.7	56.04566	2.00349
3	18	0.061	0.89	2.2	72.52967	1.88193
6	10	0.061	1.22	3.6	118.6849	2.246536

In all cases the value for r was 205 mm and the value for L was 53 mm.

Table 4.2.2 Flexural rigidity values for a hard squeegee

u	θ_w	l (m)	$\beta-\alpha$ (radians)	f (kg)	F (N)	D (N/m)
1	45	0.047	0.087	0	0	*
1.2	40	0.0475	0.227	1.2	50.80547	4.024631
1.6	32	0.05	0.523	2.7	108.5967	3.930364
2	26	0.0515	0.646	3.8	148.3882	4.47839
3	18	0.0515	0.951	4.4	171.8179	3.522434
6	10	0.0525	1.13	5.7	218.3426	3.840317

* No values for flexural rigidity at u=1 can be obtained as this is the position at which the squeegee just rests on the surface i.e. where the spring balance is set to zero.

The values of flexural rigidity can be taken as an average of the values for D obtained, therefore giving 1.7 Nm and 3.3 Nm for soft and hard squeegee materials respectively.

Appendix 4.3 Typical values for $\mu UI^2 / D$

Screen printing inks are available in a variety of viscosities with different binders and pigments but fairly standard products in use are UV curable dielectrics. These have approximate viscosities of 40 Poise ($4 \times 10^{-3} \text{Pa.s}$) and are printed at a speed of $\approx 50 \text{mm/s}$. Taking a typical squeegee length, L , of 25mm, the value for ℓ , the distance from the clamp pivoting point to the squeegee tip, can be approximated as $L \tan \theta_w$, where θ_w is 60° . The values for flexural rigidity, D , are assumed to be as for those in Appendix which are 1.7 and 3.3 for a soft and hard squeegee type respectively.

Therefore for a soft squeegee material:

$$\frac{\mu UI^2}{D} = \frac{4 \times 0.05 \times (0.025 \tan 60^\circ)^2}{1.7} = 2.206 \times 10^{-4}$$

and for a hard squeegee material:

$$\frac{\mu UI^2}{D} = \frac{4 \times 0.05 \times (0.025 \tan 60^\circ)^2}{3.3} = 1.136 \times 10^{-4}$$

Appendix 4.4 Calculated pressures for a range of angles and speeds

Table 4.4.1

Calculated pressure P(x) at x=5mm						
Speed (m/s)	u=1	u=1.2	u=1.6	u=2	u=3	u=6
0.014416	5478.403	3246.79	811.3359	296.5877	157.5167	70.88171
0.028016	10646.71	6309.799	1576.747	576.3875	306.1173	137.7512
0.041616	15815.01	9372.808	2342.158	856.1872	454.7179	204.6208
0.049776	18916	11210.61	2801.405	1024.067	543.8783	244.7425
0.063376	24084.3	14273.62	3566.817	1303.867	692.479	311.612
0.077248	29355.97	17397.89	4347.536	1589.263	844.0516	379.819
0.090576	34420.91	20399.64	5097.639	1863.466	989.6802	445.3511

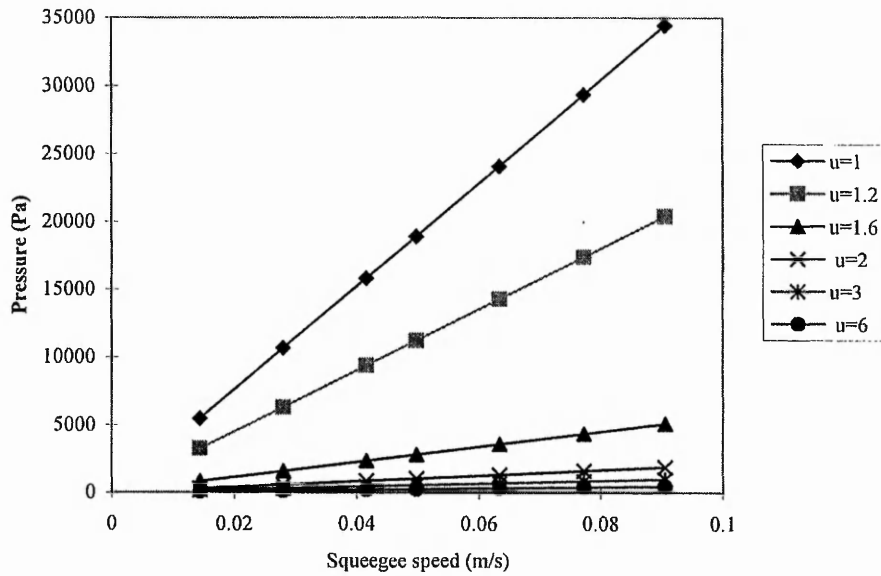


Figure 4.4.1 Calculated pressure P(x) plotted vs Squeegee speed at x=5 mm

Table 4.4.1

Calculated pressure P(x) at x=10mm						
Speed (m/s)	u=1	u=1.2	u=1.6	u=2	u=3	u=6
0.014416	684.8004	405.8487	101.417	37.07347	19.68958	8.860214
0.028016	1330.838	788.7248	197.0934	72.04843	38.26466	17.21891
0.041616	1976.877	1171.601	292.7698	107.0234	56.83974	25.5776
0.049776	2364.499	1401.327	350.1757	128.0084	67.98479	30.59281
0.063376	3010.538	1784.203	445.8521	162.9834	86.55987	38.95151
0.077248	3669.496	2174.736	543.442	198.6578	105.5065	47.47737
0.090576	4302.614	2549.955	637.2049	232.9333	123.71	55.66889

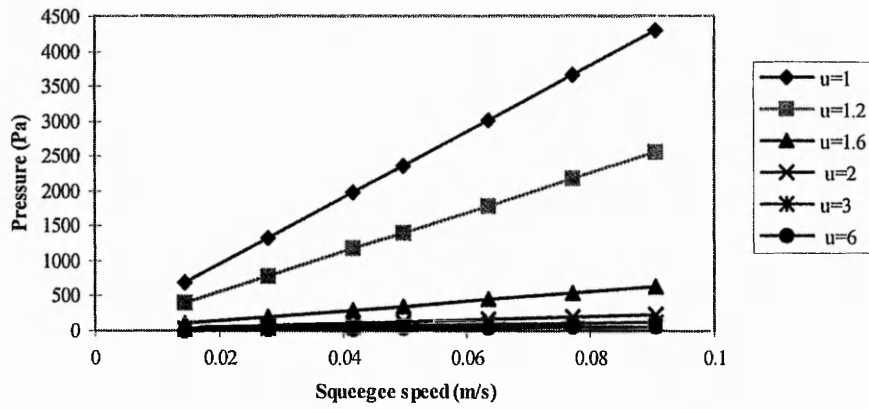


Figure 4.1.2 Calculated pressure $P(x)$ plotted vs Squeeze speed at $x=5$ mm

All pressures given in Pa

To convert to mm:

$$P = \rho gh$$

where ρ for the Tellus 68 oil used is 880 kg/m^3 at 15°C

Appendix 4.5 Pressure heads recorded from the experimental rig

Table 4.5.1

Pressure heads recorded on modified Michell Tilting Pad apparatus (mm) at x=5mm for soft squeegee						
Speed (m/s)	u=1	u=1.2	u=1.6	u=2.	u=3.	u=6
0.014416	0	0	0	0	20	40
0.028016	0	0	0	0	35	62
0.041616	0	0	0	20	45	97
0.049776	0	0	0	20	57	107
0.063376	0	0	18	28	67	137
0.077248	0	16	20	35	87	182
0.090576	0	17	22	35	97	217

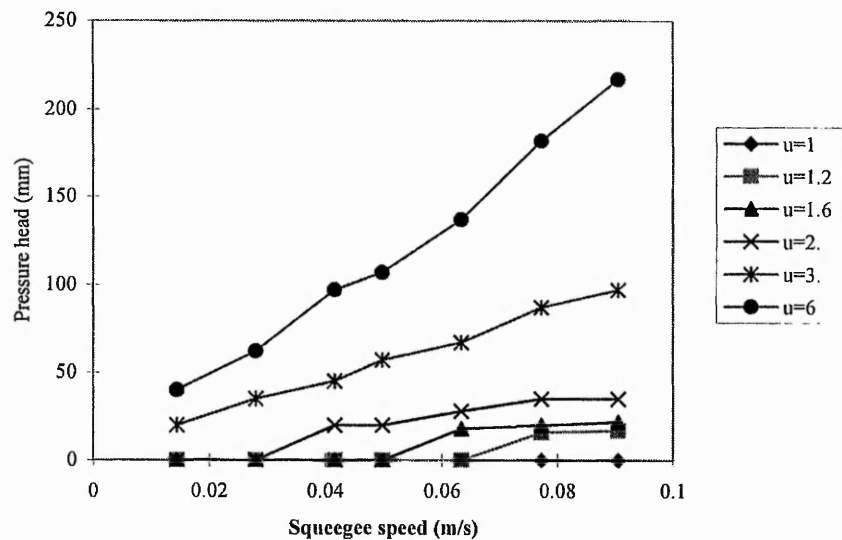


Figure 4.5.1 Recorded pressure heads at x = 5 mm for soft squeegee

Table 4.5.2

Pressure heads recorded on modified Michell Tilting Pad apparatus (mm) at x=5mm for a hard squeegee						
Speed (m/s)	u=1.	u=1.2	u=1.6	u=2	u=3	u=6
0.014416	0	0	0	0	30	70
0.028016	0	0	0	20	50	117
0.041616	0	0	15	25	70	172
0.049776	0	0	20	30	92	207
0.063376	0	0	20	35	102	267
0.077248	0	17	24	45	132	357
0.090576	0	20	30	45	152	417

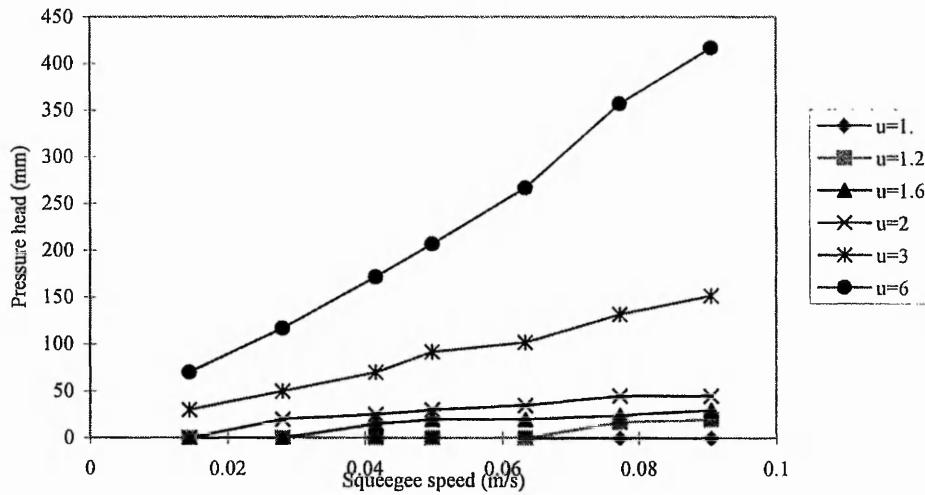


Figure 4.5.2 Recorded pressure heads at $x = 5$ mm for hard squeegee

Table 4.5.3

Pressure heads recorded on modified Michell Tilting Pad apparatus (mm) at $x=10$ mm for soft squeegee						
Speed (m/s)	$u=1$	$u=1.2$	$u=1.6$	$u=2$	$u=3$	$u=6$
0.014416	0	0	0	0	0	0
0.028016	0	0	0	0	0	28
0.041616	0	0	0	0	25	35
0.049776	0	0	0	0	25	42
0.063376	0	0	0	0	30	47
0.077248	0	0	0	0	35	67
0.090576	0	0	0	20	40	77

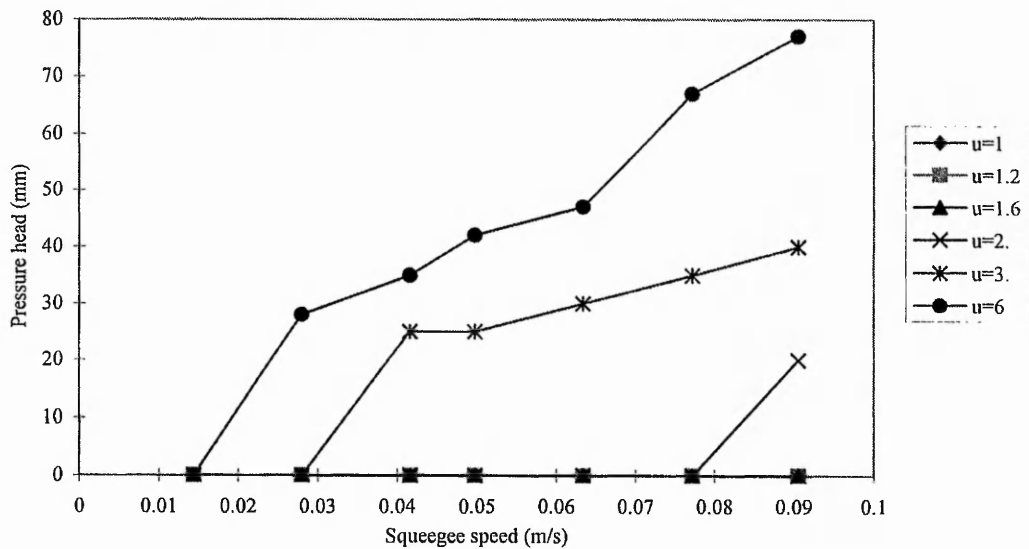


Figure 4.5.3 Recorded pressure heads at $x = 10$ mm for soft squeegee

Table 4.5.4

Pressure heads recorded on modified Michell Tilting Pad apparatus (mm) at x=10mm for hard squeegee						
Speed (m/s)	u=1	u=1.2	u=1.6	u=2.	u=3.	u=6
0.014416	0	0	0	0	0	25
0.028016	0	0	0	0	25	40
0.041616	0	0	0	0	30	55
0.049776	0	0	0	0	35	65
0.063376	0	0	0	0	40	92
0.077248	0	0	0	20	45	97
0.090576	0	0	0	25	55	122

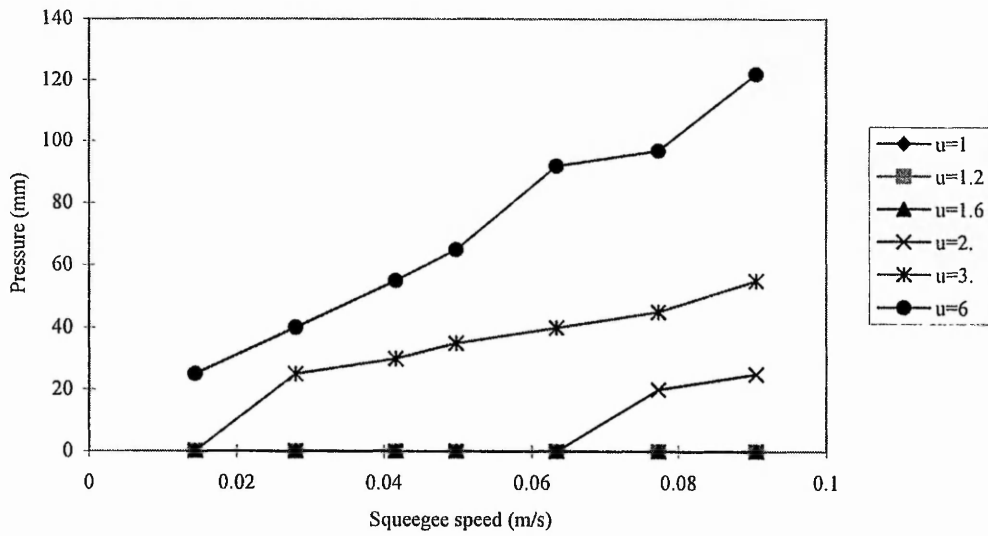


Figure 4.5.4 Recorded pressure heads at x = 10 mm for hard squeegee

Appendix 4.6 Flow rate of the ink and the pressure drop

71T 33%OA Ft=100um thread d = 55µm

Height(m)	t av (s)	Q(m ³ /s)	Vscr(m/s)	Vsq(m/s) 71T
6.75	208.34	9.6E-07	0.103	0.075
5.25	276.18	7.24E-07	0.078	0.057
3.75	457.66	4.37E-07	0.047	0.034
2.25	811.67	2.46E-07	0.026	0.019
0.75	2500.32	8E-08	0.009	0.006

120T 20%OA Ft=67um thread d= 40µm

Height(m)	t av (s)	Q(m ³ /s)	Vscr(m/s)	Vsq(m/s) 120T
6.75	336.37	5.95E-07	0.105	0.088
5.25	489.84	4.08E-07	0.072	0.061
3.75	788.90	2.54E-07	0.045	0.038
2.25	1373.45	1.46E-07	0.026	0.022
0.75	5642.63	3.54E-08	0.006	0.005

The average time, t av, taken to fill a 200 ml measuring cylinder was obtained from three separate readings at each pressure head.

Appendix 4.7 Physical properties of oil and glycerol

Tellus oil 688

Kinematic viscosity at 40°C = 68cS

Dynamic viscosity = $6.8 \times 10^{-5} \times (0.88 \times 1000)$
= 0.05984 Pa.s

At 20 °C ($\ln \mu_{20}/68 = 0.0342 \times 20$)

therefore $\mu_{20} = 68 e^{0.684}$
= 135cS or 0.12Pa.s

Density at 15°C = 880 kg/m³

Glycerol

Dynamic viscosity at 20°C = 1.49 Pa.s

Density at 20°C = 1262 kg/m³

Appendix 5.1 Basic Elasticity Equations

Elastic equations

The deflection, w , at a point (x,y) on a point load \tilde{W} is given by

$$w = \left(\frac{1 - \sigma^2}{\pi E} \right) \frac{\tilde{W}}{r}$$

where σ = Poisson's ratio

E = Young's modulus

r = the distance between (x,y) and (x_1,y_1) as shown below.

Elastic pressures

The pressure, p , at any point r is

$$p = p_{\max} \left(1 - \frac{r^2}{a^2} \right)^{\frac{1}{2}} \quad (5.1.1)$$

Elastic formulae

For a line contact Cameron integrates (5.1.1) to provide a relationship between the applied load and the respective contact width and peak pressure:

$$\frac{W}{L} = \int_{-a}^a p \, dx = \frac{\pi}{2} a p_{\max}$$

and a value for the half contact width, a , is given as

$$a^2 = \frac{4}{\pi} \left\{ \frac{1 - \sigma_1^2}{E_1} + \frac{1 - \sigma_2^2}{E_2} \right\} \frac{WR}{L}$$

Deformation outside the contact zone

$$h = \left(\frac{1 - \sigma_1^2}{E_1} + \frac{1 - \sigma_2^2}{E_2} \right) a p_{\max} x \left\{ \frac{x}{a} \sqrt{\left(\frac{x^2}{a^2} - 1 \right)} - \log_e \left[\frac{x}{a} \sqrt{\left(\frac{x^2}{a^2} - 1 \right)} \right] \right\}$$

Appendix 5.2 Correlation of H_0 and p_0^*

Program to correlate H_0 and p_0^*

```
#include <stdio.h>
#include <math.h>

int integrate(double h);
double delta(double x);
double Fx(double x, double h);

int main()
{
    double H0;

    printf("Please enter value of H0: ");
    scanf("%lf", &H0);

    integrate(H0);
    return 0;
}

int integrate(double h)
{
    double F1, F2, sum=0.0;
    double x=-1.0, dx=-0.0447; /* start limit and width of trapezium */

    printf("Please enter the LOWER limit <%lf>: ", x);
    scanf("%lf", &x);
    printf("UPPER limit is taken to be +/- inf\n");
    printf("Please enter value of trap width <%lf>", dx);
    scanf("%lf", &dx);

    F1= Fx(x, h);

    do{
        F2 = Fx(x+dx, h);
        sum += 0.5*(F1+F2)*fabs(dx); /*trapezium */
        F1=F2;
        x+=dx;
    }
    while(F2>0.0001);

    printf("ans=%lf\n", sum);
    return 0;
}

double Fx(double x, double h)
{
    double F, H, del;

    del = delta(x);
    H = h + del;
    F = del/(H*H*H);
```

```

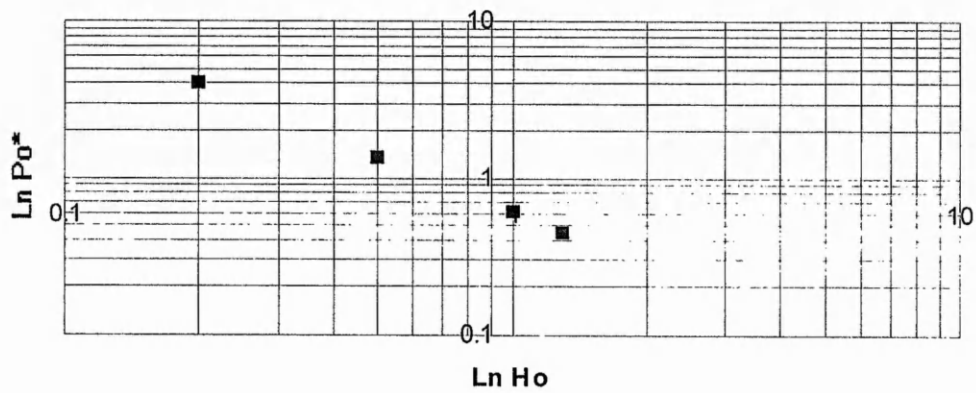
return F;
}

double delta(double x)
{
    double del;

    //printf("%lf\n", x);
    del= fabs(x) - (1.0/asin(1))*( x)*asin(1.0/x) + log( fabs(x) + sqrt(x*x - 1.0) );
    //printf("%lf\n", del);
    return(del);
}

```

Log plot of results



Appendix 6.1 Contact widths for a range of squeegee settings

The squeegee characteristics are outlined in Table 6.1.1 below.

Table 6.1.1 Squeegee characteristics

Squeegee type	Hardness (°A Shore)	Trailing length (mm)	Thickness (mm)
Red	65	21	7
Green	85	15	7

The results of the half contact widths, a , measured are in Table 6.1.2.

Table 6.1.2

Squeegee type	Load applied (N)	a at 50° (mm)	a at 60° (mm)	a at 70° (mm)
Red	0	0.004	0.004	0.0035
	15.69	0.231	0.1555	0.182
	44.04	0.3235	0.2265	0.1835
	72.39	0.513	0.4845	0.2865
	100.74	1.0165	0.9915	0.377
	129.09	1.047	2.895	0.9145
Green	0	0.004	0.005	0.0045
	15.69	0.044	0.0475	0.1155
	44.04	0.1055	0.052	0.1605
	72.39	0.2055	0.1865	0.17
	100.74	0.3365	0.282	0.1885
	129.09	0.4355	0.357	0.256

Appendix 6.2 Calculated values of U for a range of squeegee contact widths

Table 6.2.1

F (N/m)	Green Squeegee			Red Squeegee		
	U (m/s) at 50°	U (m/s) at 60°	U (m/s) at 70°	U (m/s) at 50°	U (m/s) at 60°	U (m/s) at 70°
190.59	0.68721	0.58967	0.09973	0.01518	0.05502	0.04017
226.33	0.14195	0.5843	0.06133	0.01732	0.0308	0.04692
407.33	0.06733	0.08175	0.09839	0.0108	0.01211	0.03464
577.39	0.0356	0.05068	0.11343	0.0039	0.0041	0.02836
796.71	0.02932	0.04364	0.08486	0.00507	0.00066	0.00621

Appendix 6.3 Printing performance over a range of speeds

Equipment

Mesh type 120T at 17N/cm
 Snap height set at 3mm
 Squeegee type dark green (85°A shore hardness)
 Trailing length 25mm
 Squeegee thickness 7mm
 Dielectric blue 40-516 ink

Table 6.3.1 red squeegee at 60°

Speed (m/s)	Force per unit length (N/m)					
	133	287	525	652	708	841
0.003	7.73	7.31	5.05	7.08	6.84	6.40
0.006	11.15	10.10	10.80	11.00	10.71	9.47
0.011	11.06	10.17	10.87	10.88	10.62	9.47
0.017	11.12	9.71	11.13	10.53	11.22	10.53
0.05	13.24	11.07	12.68	12.91	13.28	12.09
0.107	15.01	13.54	14.59	15.13	15.06	13.91
0.15	15.29	14.32	15.19	15.42	15.52	14.77
0.193	15.43	14.94	15.41	16.20	15.02	15.34
0.203	15.23	15.31	16.32	16.53	14.10	15.90
0.215	15.46	15.81	16.07	16.26	14.93	15.44
0.225	15.81	15.64	16.21	16.65	15.56	15.84

Table 6.3.2 red squeegee at 70°

Speed (m/s)	Force per unit length (N/m)					
	133	287	525	652	708	841
0.003	6.72	6.43	6.00	5.29	7.32	7.32
0.006	12.26	9.29	9.37	11.52	8.69	9.99
0.011	10.67	9.59	9.68	11.30	10.47	10.78
0.017	10.54	10.09	9.51	11.29	10.70	10.93
0.05	11.13	10.66	10.51	14.00	14.32	15.49
0.107	11.04	10.94	12.75	16.32	16.81	16.99
0.15	13.19	10.68	13.46	17.03	17.43	18.50
0.193	6.92	11.10	14.22	17.06	18.25	19.88
0.203	5.18	11.51	14.91	18.17	18.66	20.40
0.215	13.82	11.51	15.17	18.33	18.67	21.14
0.225	12.94	11.99	15.57	20.13	21.28	20.51

Table 6.3.3 green squeegee at 60°

Speed (m/s)	Force per unit length applied (N/m)					
	152	287	526	596	694	754
0.003	5.77	7.07	6.53	8.56	7.26	5.70
0.006	9.31	8.90	9.02	9.09	9.40	9.36
0.011	9.54	8.76	8.80	9.20	9.60	8.24
0.017	10.17	9.20	9.23	9.67	9.74	9.57
0.05	10.64	9.91	10.20	9.66	10.60	10.25
0.107	11.69	10.88	11.30	10.28	11.40	10.67
0.142	12.43	11.04	12.10	10.75	12.22	11.80
0.197	12.38	11.41	12.83	11.17	12.73	12.36
0.206	13.46	11.98	13.51	11.65	13.15	12.89
0.215	13.41	12.31	13.66	11.62	13.50	13.26
0.225	13.64	12.51	13.90	12.00	13.90	13.72

Table 6.3.4 green squeegee at 70°

Speed (m/s)	Force per unit length applied (N/m)					
	152	287	526	596	694	754
0.003	7.51	6.10	6.71	8.48	6.08	4.81
0.006	8.13	7.78	8.55	9.48	9.45	9.84
0.011	8.41	8.65	9.07	9.28	10.33	10.23
0.017	8.43	8.96	9.28	9.46	9.73	11.48
0.05	9.80	9.61	9.74	9.48	10.73	11.86
0.107	10.60	10.00	10.49	10.45	12.73	12.06
0.15	11.07	10.24	10.96	10.36	13.18	12.45
0.193	11.46	10.49	11.48	10.80	14.02	13.45
0.203	11.37	10.58	11.64	10.67	14.06	13.75
0.215	11.51	10.63	11.82	11.42	13.97	13.26
0.225	11.75	11.65	12.44	11.53	14.24	13.71

Squeegee load set at 15.59N

Squeegee angle set at 70°